Developing a full core model of the North Anna Reactor using SCALE 6.2.3, NESTLE and MCNP 6.2

TP Ringane

orcid.org/0000-0002-8370-5895

Mini-dissertation accepted in partial fulfilment of the requirements for the degree *Master of Science in Engineering Sciences with Nuclear Engineering* at the North-West University

Supervisor: Prof. VV Naicker

Graduation: November 2022

Student number: 30265169

DECLARATION

I, Tlangelani Primrose Ringane, hereby declare that the work presented in this dissertation is written and compiled by myself. I declare that the sources used in the dissertation have been referenced accordingly.

_____

Tlangelani Primrose Ringane
Date: 14 September 2022
NWU – Potchefstroom

ACKNOWLEDGEMENTS

Firstly, I would like to thank God, the Almighty, for His grace and love. He made this opportunity possible and gave me the strength, the will and perseverance to complete this master's degree.

I would like to express my gratitude to my supervisor, Professor Vishana Vivian Naicker, for her help and the guidance she has given me in this work. *I am grateful for your support, for the time, encouragement, and motivation you gave me.*

I would like to thank the DST SARChI with Grant No: 61059, for their financial assistance and support of my studies.

I want to acknowledge Dumisane Rasasemola, Duduetsang Kgomotshwane, Dr Gezekile Nyalunga, Ngoatladi Mashilangako, and Cheyeza Mulasi, for their personal and professional support in helping and mentoring me. *Your input and ideas were greatly appreciated and valued.*

Lastly and most importantly, I want to give a special thanks to my family — to my number one supporter, my mother, Khesani Ethel Ringane; my auntie Basane Ringane; my uncles, Derrick and Leonard Ringane; my grandmothers, Glady's Mahwayi and Muriel Mosipa and to my son, Tshegofatso Malwandla Ringane —Thank you for your unconditional love, patience, never-ending support and prayers, that I have continually relied upon throughout my master's degree and my life. To all my friends and cousins - *Thank you for all your support and the words of encouragement you have given to me.*

ABSTRACT

This study presents the development of the modelling for a T-NEWT/NESTLE* lattice-to-nodal diffusion calculation. The reactor selected for this study is the North-Anna (NA) Unit 1 Pressurized Water Reactor (PWR) of the Westinghouse design. Calculations are conducted at 300 K, at the beginning of Cycle (BOC).

The NEWT code of the SCALE-6.2.3 (Standard Computer Analyses for Licensing Evaluation Version 6.2.3) package, is a multi-group discrete ordinate (deterministic) neutral-particle transport code that employs the Extended Step Characteristic spatial discretization method. NEWT is used to process and generate the homogenized-multigroup macroscopic cross-sections and other group constants for the NESTLE input file. The NESTLE code, embedded within the RELAP5-3D version 4.1.3 package, is a coupled multigroup (few-group) neutron diffusion reactor core simulator code that utilizes the nodal expansion method (NEM).

The primary aim of this study was to develop a full core (FC) T-NEWT/NESTLE calculation input model for the NA PWR using the North-West University Reactor Code suite (NWURCS) developed at the North-West University, Unit for Energy and Technology Systems, as this neutronic to nodal diffusion (thermal-hydraulic) combination has not been tested at the North-West University. The verification of NWURCS was achieved as the calculations between the manually generated T-NEWT models by the user with T-NEWT models generated by NWURCS were in good agreement.

Furthermore, the results generated from the T-NEWT/NESTLE FC model were compared with a Monte Carlo full core calculation, using the Monte Carlo N-Particle radiation transport code version 6.2 (MCNP-6.2), which is equipped with a temperature-dependent ENDF/B-VII.1 cross-section library. T-NEWT was used to obtain group constants and NESTLE and MCNP-6.2 was used to obtain the multiplication factor (k_{eff}). The efficiency of the T-NEWT/NESTLE code combination was achieved, as well as ‘the results for both approaches were found to be good agreement.

* T-NEWT stands for the control module TRITON using NEWT. TRITON stands for Transport Rigor Implemented with Time-dependent Operation for Neutronic depletion code. NEWT stands for New ESC-based Weighting Transport code. NESTLE stands for Nodal Eigenvalue, Steady-State Transient, Le core Evaluator code)

Keywords: North Anna PWR, MCNP-6.2, T-NEWT, NESTLE, NWURCS

LIST OF ABBREVIATIONS

1D	One-Dimensional
2D	Two-Dimensional
3D	Three-Dimensional
AC	Active Cycles
BM	Base-model
BONAMI	BONdarenko AMPX Interpolator
BPRA	Burnable Poison Rod Assembly
CE	Continuous Energy
CENTRM	Continuous ENergy TRansport Module
CR	Control Rod
CB	Core Barrel
XSProc	Cross Section Processing
XS	Cross-Section
AMPX	Cross-section processing code
ENDF/B-VII	Evaluated Nuclear Data File
ESC	Extended Step Characteristic method
FA	Fuel Assembly
FP	Fuel Pin
FC	Full Core
IC	Inactive Cycles
INP	Input file
IP	Instrumentation Pin
k_{eff}	k-effective multiplication factor
LWR	Light Water Reactor
MCNP-6.2	Monte Carlo Neutral Particle Transport Code, version 6.2
MG	Multi-Group energy
NEWT	New ESC-based Weighting Transport code
NESTLE	Nodal Eigenvalue, Steady-State Transient, Le core Evaluator
NA	North-Anna Reactor
NWURCS	North-West University Reactor Code Suite
NPP	Nuclear Power Plant
NSRC	Number of Source Points
ppm	Parts Per Million
pcm	Per cent mile
$\% \, diff$	Percentage Difference
PWR	Pressurised Water Reactor
PMC	Produce Multigroup Cross-sections

RELAP5-3D	Reactor Excursion and Leak Analysis Program
SCALE-6.2.3	Standard Computer Analyses for Licensing Evaluation, version 6.2
RVI	Reactor Vessel Internal
std	Standard Deviation
TRITON	Transport Rigor Implemented with Time-dependent Operation for Neutronic depletion

TABLE OF CONTENTS

LIST OF TABLES

LIST OF FIGURES

CHAPTER 1: BACKGROUND AND OVERVIEW

1.1 Introduction

“The National Development Plan (NDP) 2030 of South Africa, offers a long-term plan for the country,” (IRP, 2019). The NDP plans how electricity can be distributed throughout the whole country, hence, the Integrated Resource Plan (IRP) 2010-2030 was developed by the Department of Mineral Resources and Energy (DMRE) of South Africa, to address the electrical demands of the country (IRP, 2019).

South Africa’s primary electricity supplier is Eskom. Due to economic expansion and population growth, the demand of electricity has increased, thus this results in constraints on the supply of electricity from the power systems operated by Eskom (Eskom, 2020). Eskom’s older power stations and infrastructure are being used to full capacity, hence, routine scheduling for the maintenance of plant and infrastructure is performed to prevent compromising supply capacity during periods of high demand (Eskom, 2020).

These results in load shedding of the power supply. “Load shedding is the frequent scheduled maintenance of Eskom’s power stations that lead to outages and power cuts, which is implemented throughout the country as a regulated, controlled alternative, to respond to events and to protect the electricity system from a complete blackout” (Eskom, 2020). This can occur when there is too much demand and too little supply, resulting in an imbalance in the power system, which can disrupt the entire power system.

Eskom therefore needs to increase its power capacity. In this regard, nuclear power is still considered a viable option in the energy mix, hence the South African government has decided to extend the design life and operational licence of Koeberg’s two reactor units for another 20 years, to the year 2044, as Eskom estimated that the Koeberg reactors were to reach their 40-year end of design life around 2024 (IRP, 2019).

With nuclear still being considered a viable option in South Africa, the National Research Foundation (NRF) and the Department of Science and Technology (DST) established the South African Research Chairs Initiative (SARChI) (NRF, 2022). It was designed to strengthen and improve research and innovation at South African public universities, such as research based in nuclear engineering. At the North-West University (NWU), this was set up within the Unit for Energy and Technology Systems at the Potchefstroom Campus. Therefore, with regards to the ‘New Nuclear Build programme’ and the extension of the Koeberg’s operating life, research at NWU is being conducted, ‘focusing on various nuclear technologies and

principles' (Maretele, 2016). The 'New Nuclear Build programme' means the building of further nuclear power plants to assist in addressing the increasing electricity demands in South Africa and to also assist in replacing the power plants that will be decommissioned.

Nuclear engineering is a type of engineering that deals with the science and application of nuclear and radiation processes (Bornstein & Martin, 2016), such as fission or fusion, as it is based on the fundamental principles of neutronics (nuclear physics) and mathematics at a sub-atomic level. Neutronics is the study of neutron paths and the neutron interaction within the reactor. Hence it is of importance to evaluate the nuclear chain reaction and the number of neutrons travelling throughout the reactor system. Some of this is done through reactor analysis using multigroup and continuous-energy physics with deterministic, nodal-diffusion and Monte Carlo methods (ORNL, 2021).

The reactor neutronic calculations include multigroup cross-section processing, neutron transport and diffusion analysis. In this study, the neutronic analysis was done by using lattice physics and nodal diffusion codes, to develop a full core (FC) input model of the North Anna Pressurised Water Reactor.

The North Anna (NA) reactor is a Pressurized Water Reactor (PWR) designed by Westinghouse and installed at the North Anna Nuclear Power Station in Louisa County, Virginia, USA (VEPCO, 2016). The North Anna reactor was chosen for this research as it is similar in design to the Koeberg reactor and is used as a reference design for comparison purposes in their neutronic behaviour. More details regarding the geometry specification of the NA reactor are given in Chapter 2.

1.2 Research methodology overview

Figure 1-1 provides a brief description of how this study was conducted.

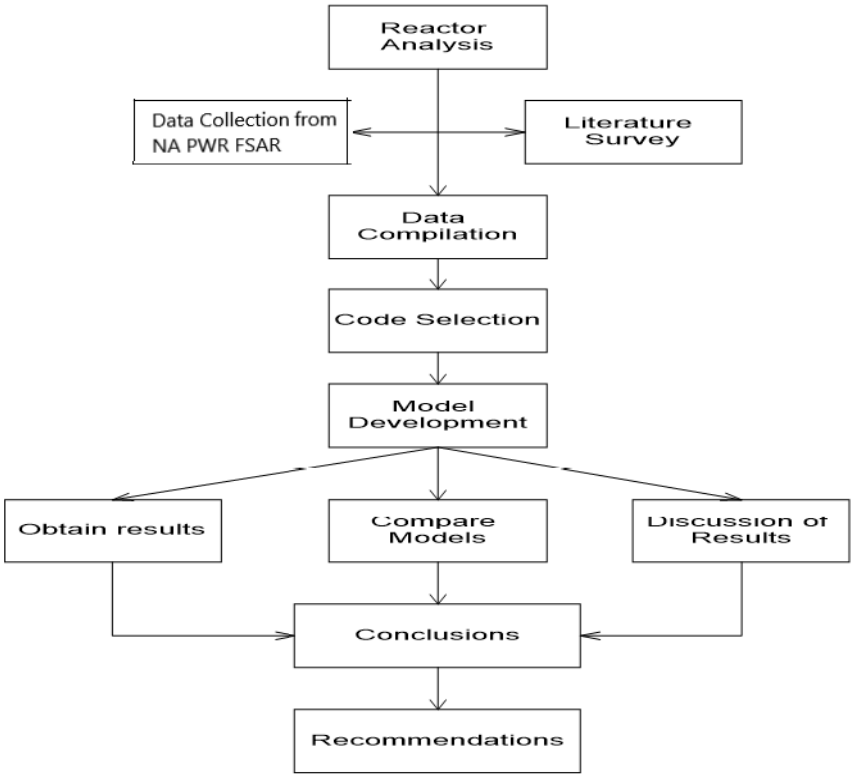

Figure 1-1: Research methodology overview

Data collection from North Anna Reactor Final Safety Analysis Report (FSAR)

Relevant data and information for model development, such as reactor dimensions, process parameters, and technical and design information required to model the North Anna Reactor, were obtained from the United States Nuclear Regulatory Commission (US-NRC) North Anna Final Safety Analysis Report (FSAR) (VEPCO, 2016). The report was submitted by Virginia Electric and Power Company (VEPCO) to the NRC for licencing of the North Anna Reactor.

Literature Survey

A literature survey was conducted to investigate and evaluate the methodologies conducted in past North-West University reactor analysis studies, as well as outside literature. This aid in determining the tasks to be conducted to advance the methodologies already set up at the NWU. This also serves as a guide for code selection.

Data Compilation

Data was gathered and compiled. Necessary conversion calculations of design measurements from British units to System International (SI) units are performed to aid with the modelling of the codes.

Codes Selection

To conduct this study, lattice physics and nodal diffusion codes are selected to calculate and obtain neutron flux distributions and criticality parameters.

The lattice-physics and nodal diffusion calculations are two important tasks in simulating the reactor core, as the outputs from the lattice code will serve as inputs to the nodal diffusion code. For this study, the following codes have been selected.

I. **Standard Computer Analyses for Licencing Evaluation (SCALE-6.2.3)** (Rearden & Jessee, 2018) - The SCALE Code System is a modelling and simulation suite for nuclear safety analysis and design that is developed, maintained, tested, and managed by the Reactor and Nuclear Systems Division (RNSD) of Oak Ridge National Laboratory (ORNL) (Rearden & Jessee, 2018). It has a wide number of applications and capabilities in nuclear safety and design and can be used for criticality calculations and uncertainty analysis in continuous energy (CE) and multigroup energy (MG) applications. The following is a list of the codes within SCALE-6.2.3 that were used in the study:

- **TRITON (Transport Rigour Implemented with Time-dependent Operation for Neutronic depletion**) (Jessee, et al., 2018) - The TRITON computer code is a multipurpose SCALE control module for lattice physics. It provides multigroup neutron transport calculations (Jessee, et al., 2018). It can also be used for uncertainty and sensitivity analysis and depletion analysis. The main functional modules that it calls are XSProc and NEWT.

- **XSProc** (**C**ross **S**ection **P**rocessing) (Williams, et al., 2018) – This is a material specification and cross-section processing code. It provides material input and multigroup cross-section preparation for most SCALE sequences (Williams, et al., 2018).

- **NEWT** (**N**ew **E**SC-based **W**eighting **T**ransport code) (Jessee & DeHart, 2018) is the Two-Dimensional (2D) extended step characteristic (discrete ordinates deterministic) transport code with flexible geometry applied to neutronics analysis.

II. **Monte Carlo Neutral Particle Transport Code MCNP 6.2** (Werner, 20217)

MCNP 6.2 is a general-purpose continuous energy-generalized-geometry, time-independent, coupled neutron/photon/electron Monte Carlo transport code.

III. **RELAP5-3D** (RELAP5-3D_Team, 2013) **-** RELAP5-3D (Reactor Excursion and Leak Analysis Programme) is primarily used as a thermal-hydraulic code. However, in terms of this study, the thermal-hydraulic part is not used, rather the NESTLE code, which is embedded in RELAP5-3D, is used.

- **NESTLE (Nodal Eigenvalue, Steady-State Transient, Le core Evaluator) – This** is a deterministic nodal diffusion code that solves the few-group neutron diffusion equation using the Nodal Expansion Method (NEM) (Turinsky, et al., 1994). The NESTLE code can solve eigenvalue (criticality) and external fixed-source steady-state problems. The code calculates various scenarios including full 3D core models (Turinsky, et al., 1994).

IV. **North-West University Reactor Code Suite (NWURCS)**

- NWURCS is a suite of codes written in Fortran, which was developed at the Unit for Energy and Technology Systems (UETS), NWU. It has the capability of generating input files for a few reactor systems. It generates input for KENO-VI, NEWT, MCNP, SERPENT and RELAP5 and it is currently on its third version. The second version is referenced in (Sihlangu, 2019). The verification of NWURCS initiated in earlier studies such as (Nyalunga, 2016; Nyalunga, 2019; Sihlangu, 2016) and (Sihlangu, 2019), is continued in this study.

Model Development

A detailed structural methodology outlining the development of the reactor full core (FC) is presented in Chapter 4.

Results and Conclusion

Once the results were produced, a comparison amongst the codes was conducted, and the results were analysed.

Conclusions and recommendations were made, based on the obtained results.

1.3 Problem statement

Previous studies carried out in the neutronic analysis of nuclear reactors at the North-West University focused on the full core methodology development based on the Monte Carlo methods (stochastic methods). Whilst Monte-Carlo methods can model the geometry to a high degree of precision, running the code becomes time-consuming and large computer memory is required for large models.

For this study, neutronic modelling is conducted using a deterministic method code sequence (utilized in the T-NEWT/NESTLE code combination), which has faster time-iterations and has considerably more computational efficiency when compared to the Monte Carlo methods (utilized in MCNP-6.2).

Although the lattice physics and nodal-diffusion method (T-NEWT/NESTLE) combination are used for light water reactor calculations internationally, it has not yet been implemented at the NWU or at any other South African academic institution, to the knowledge of the author.

Given also that South Africa already has two light water reactors, and there is an intention by the South African government to build further nuclear reactors, it is therefore important that such further development of expertise in neutronic calculations be continued.

The current study focuses on the methodology development of the full core model of the NA PWR using the deterministic lattice method and nodal diffusion method combination. Given the computational resources at the North-West University, a calculation chain using the code wrapper NWURCS is used to build lattice and nodal diffusion input (INP) models for the fresh core state of the NA reactor. The codes that are used to carry out this study are T-NEWT of SCALE 6.2.3 and NESTLE of the package RELAP5-3D. The MCNP 6.2 models are built and used for comparison purposes.

1.4 Research aim

This study aims to develop a calculation chain of a full core T-NEWT/NESTLE model for the North-Anna PWR and an equivalent full core MCNP-6.2 input model, both using NWURCS. This is done to verify the in-house code, NWURCS.

1.5 Research objectives

The objectives of this study are elaborated below:

- Build XSProc/T-NEWT fuel assembly input calculation models using NWURCS. These are 17 × 17 FA lattices with and without water nodes, with corresponding multigroup homogenised macroscopic cross-sections, assembly discontinuity factors, and k_{inf} results;
- Critically evaluate and verify NWURCS capability of generating a water node input for T-NEWT;
- Extract the homogenised macroscopic cross-sections generated from the XSProc\T-NEWT output using NWURCS, which is then used for the NESTLE input model;
- Build an FC NESTLE input model and carry out criticality calculations, with and without water nodes and calculate the k_{eff} and neutron flux;
- Critically evaluate and verify NWURCS capability of generating a T-NEWT\NESTLE lattice-to-diffusion combination input file;
- Build an equivalent full core MCNP-6.2 input model using NWURCS and calculate the k_{eff} and neutron flux using tallies;
- Verify and compare the results (k_{eff}) of the T-NEWT\NESTLE and MCNP FC models.

1.6 Outline of the dissertation

The dissertation contains six chapters, with this current first chapter giving an overview and the scope of the study.

Chapter 2 - Reactor System Specifications

This chapter provides a brief description of the Koeberg and NA PWRs.

Chapter 3 - Reactor Theory and Literature Review

This chapter presents a literature review, together with a rationale and description of why certain codes are used. Aspects of neutronics calculations and formulas related to the study are described.

Chapter 4 – Methodology

This chapter focuses on the methods used to carry out the calculations using T-NEWT, NESTLE and MCNP-6.2. Data propagation i.e., the transferring of output results from one code, for the use as inputs in another code is also described.

Chapter 5 - Results and Discussion

The results of the required parameters are presented, evaluated, and analysed. The discussions thereof are further provided.

Chapter 6 - Conclusion and Recommendations

Conclusions are made on the results obtained and recommendations for future work are discussed in the spirit of continuous research and development.

CHAPTER 2: REACTOR SYSTEM SPECIFICATIONS

This chapter aims to provide a general design description of the North-Anna Pressurised Water Reactor.

2.1 The Koeberg pressurized water reactor

The Franco-Américaine de Constructions Atomiques (Framatome) is a French nuclear reactor company, which is owned by Électricité de France (EDF) (Framatome, 2019). The company was formed with the sole purpose to license Westinghouse's pressurized water reactor (PWR) designs for use in France in 1958 (Wikipedia Contributors, 2021). Framatome has provided valuable state-of-the-art support, components, and services to Westinghouse (now Toshiba-Westinghouse) plants for decades (Framatome, 2019). Over 25 years, the EDF is now equipped with 58 pressurized water reactors. In 1976, the SOFINEL (Société française d'ingénierie électronucléaire et d'assistance à l'exportation) was formed as a subsidiary of EDF and Framatome (Framatome, 2019), with the goal of expanding and developing the Nuclear Power Plant construction business internationally. The plants that were developed included: **Koeberg** in **South Africa (1976)**, Ulchin in South Korea (1983), Daya Bay and Ling-Ao in China (1987 and 1995) (Framatome, 2019).

The Koeberg Nuclear Power Station, which is owned by ESKOM, is a Generation II plant with two reactor units that operate adjacent to each other, near Cape Town, in South Africa. Each unit is a 3 loop Framatome PWR design which produces a net output rated at 920 Mwe (ESKOM, 2021). The Framatome units are the French version of the Westinghouse PWR (Framatome, 2019). Each of the three cooling loops contains a reactor coolant pump and an inverted U-bend steam generator, which circulate pressurized water around the reactor core. The facility produces 2785 MWth of thermal electricity.

The Koeberg NPP has the following characteristics (Pelo, 2013):

- A nuclear island with two reactor buildings, each with a Nuclear Steam Supply System;
- Two fuel buildings, with a nuclear auxiliary building shared by both units;
- A shared turbine building with turbine generators and auxiliaries;
- There are five diesel generator buildings, each with one emergency diesel generator. Each unit has two of these buildings while the last one can be allocated to either unit;
- The units share an electrical building;

- Two pumping stations; one is the conventional island cooling water station, and the other is for the nuclear island cooling water station;
- A water treatment building and two condensate polishing units;
- Workshops and service structures and structures for auxiliary equipment; and
- Uses water as a coolant and moderator.

More details regarding Koeberg's characteristics and design specifications are given in (ESKOM, 2021). Table 2-1 provides a summary of some of the reactor specifications.

Table 2-1: Koeberg reactor specifications (ESKOM, 2021)

Technical details for Koeberg reactor	
Two Operational Units, each net output (MWe)	970
Installed Capacity (MW)	1 940
Average Availability over the last 3 years	79.7%
Average Production over the last 3 years (GWh)	12 715
Reactor Coolant Pressure (MPa)	15,5
Pressure in the Secondary Side of the Steam Generator (MPa)	5.8

The Westinghouse Combustion Engineering, Inc., Babcock & Wilcox Company, Mitsubishi Heavy Industries, Ltd., Framatome, and Siemens/KWU designed and constructed the majority of today's running PWR Reactor Vessel Internals (RVI) (IAEA, 1999). Figure 2-1 shows the structural assembly grouping of a PWR Reactor Vessel Internals (RVI) system which is more or less the same for Westinghouse and Framatome reactor designs (IAEA, 1999).

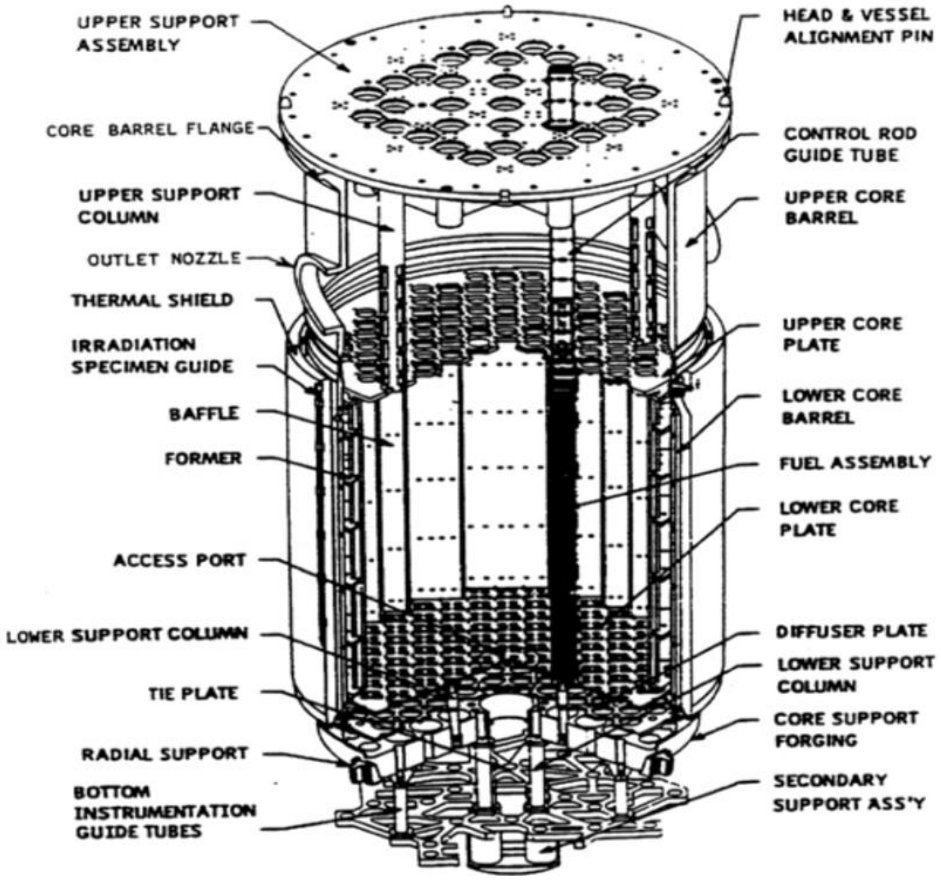

Figure 2-1: Structural assembly grouping of PWR RVI (VEPCO, 2016)

2.2 North-Anna pressurized water reactor

According to section 2.1, it was stated that the Framatome Reactors, such as the Koeberg PWRs, are the French version of the Westinghouse PWR. The North-Anna (NA) reactor was chosen for this study as it best meets the specifications of the Koeberg PWRs, with the specifications available in the open literature. The NA PWR is designed by the Westinghouse Electric Corporation company. It is noted that the Koeberg PWRs could not be studied since the Safety Analysis Report is not available in the open-source literature. A pilot study at the NWU has already been conducted on aspects of the North-Anna reactor core using the neutronic analysis codes Dragon and Donjon (Thokwane, 2020).

2.2.1 Reactor description

The NA PWR - Units 1 and 2 are sited on the southern shore of Lake Anna in Louisa County, Richmond, Virginia (VEPCO, 2016). Each unit has a 3-looped pressurized light-water nuclear

steam-supply reactor system, and the reactor cores of each unit are made up of 157 fuel assemblies. The core layout is similar to that of the Koeberg PWR.

Each reactor unit was designed to produce a core power output of 2775 $MW_{th)}$. This core power results in a gross electrical output of approximately 947 MWe (VEPCO, 2016).

The primary reactor coolant system moderates and cools the core at a pressure of 2250 psia (15.5 MPa). During normal operation, an electrical pressurizer attached to one of the coolant loops maintains coolant pressure by changing pressure during load transients and keeping the system pressure within design limits during abnormal situations (VEPCO, 2016).

2.2.2 Reactor core system

The reactor core is of the multi-region (consists of different regions such as fuel, moderator, and reflector) type. The batches of fuel assemblies are mechanically identical, although the fuel enrichment is typically not the same in all the assemblies (VEPCO, 2016). To maximise the radial power distribution, three fuel enrichments are used during the first core loading cycle. FAs with enrichments of 2.1 wt% and 2.6 wt% are arranged in a selected pattern in the central region of the core while the FAs with the highest enrichment of 3.1 wt% are arranged around the periphery of the core. Figure 2-2 shows the fuel-loading pattern used in the first core.

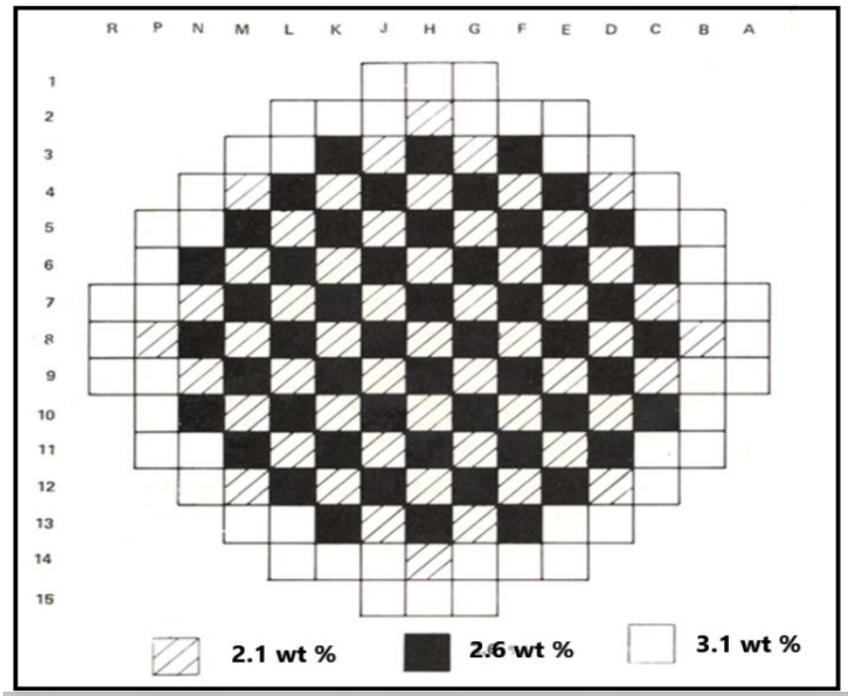

Figure 2-2: Core Fuel Distribution in NA Westinghouse PWR (VEPCO, 2016)

To control the reactor, strong neutron absorbing materials such as control rods and burnable poisons are used which move within guide tubes in certain fuel assemblies (VEPCO, 2016).

Table 2-2 below provides reactor core properties and the design parameters of the North-Anna Reactor.

Table 2-2: Reactor core properties of the North-Anna reactor (VEPCO, 2016)

Core Description	**Data**
Reactor Power (Thermal) (MW_{th})	2775
Vessel Pressure (MPa)	15.513
Mass Flow Rate (kg/m^2s)	3282.1
Equivalent Core Diameter (cm)	304.0380
Core Average Active Fuel Height (cm)	364.9980
Core Barrel Outer Diameter (cm)	350.3651
Core Barrel Inner Diameter (cm)	340.0425
Fuel Assembly Lattice	17 x 17
Number of Fuel Assemblies in Core	157
Number of Fuel Rods per Fuel Assembly	264
Number of Guide Thimbles Per Assembly	24
Number of Instrumentation Pins	1
Fuel Assembly (Lattice) Pitch Incl. Gap (cm)	21.50364
Gap between Fuel Assemblies (cm)	0.1016
Rod Pitch (cm)	1.259840
Inlet Temperature (K)	559.15
Outlet Temperature (K)	596.37
Reactor Power (Thermal) (MW_{th})	2775

Fuel Assembly (FA) Description

Each fuel assembly is a 17×17 lattice (array) and has 289 rods and thimbles, which consists of 264 fuel rods, 24 guide thimbles (for control rod insertion) and one instrumentation thimble. Grid structures support the fuel rods and thimbles at intervals along their length, ensuring that the lateral spacing between the rods and thimbles is maintained throughout the assembly's design life (VEPCO, 2016). Figure 2-3 provides a cross-sectional view of the North-Anna fuel assembly.

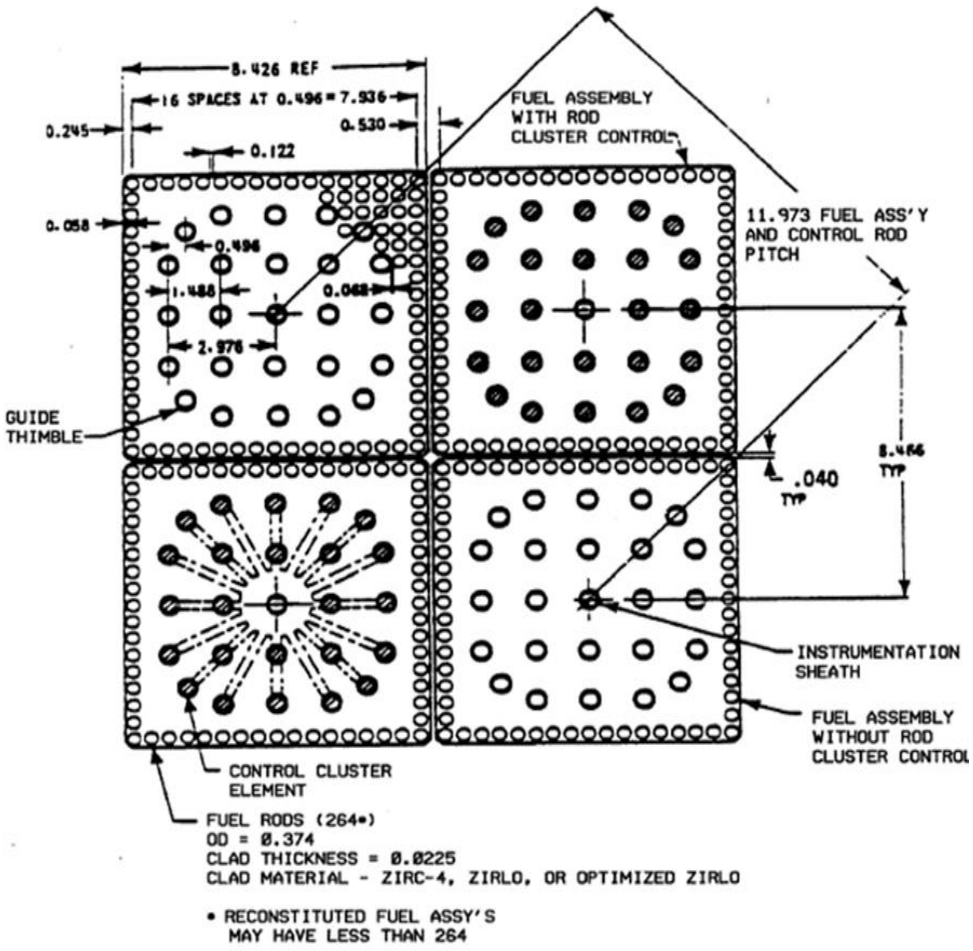

Figure 2-3: 17 x 17 Fuel assembly cross-section (VEPCO, 2016)

Fuel Rods

The fuel rods consist of slightly enriched uranium dioxide ceramic cylindrical pellets, which are pressurized with helium. The pellet is surrounded by a helium layer, which is contained in Zircaloy-4 tubing, that encapsulates the fuel. The fuel pellets consist of uranium dioxide in three enrichments: 3.1 w/o, 2.6 w/o and 2.1 w/o (weight percent) (VEPCO, 2016).

Fuel Cladding Material

The Zircaloy-4 fuel rod cladding material being used has a low absorption cross-section, and a high strength. The high strength resists deformation due to differential pressures (VEPCO, 2016). Figure 2-4 illustrates a cross-sectional view of a fuel pin cell while Table 2-3 provides detailed material dimensions of the NA PWR.

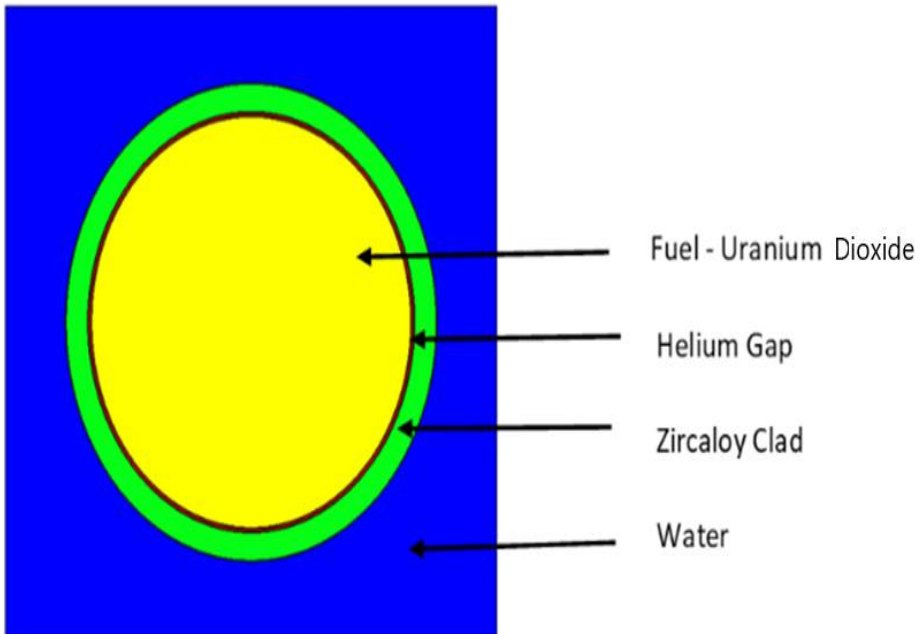

Figure 2-4: North-Anna fuel pin

Guide and Instrumentation Thimbles

The instrumentation pin (thimble) is positioned at the centre of the fuel assembly. The guide thimbles (having identical dimensions as the instrumentation thimble), serve as passages that allow the insertion for the rod cluster control assembly and the burnable poison assembly to be inserted (VEPCO, 2016).

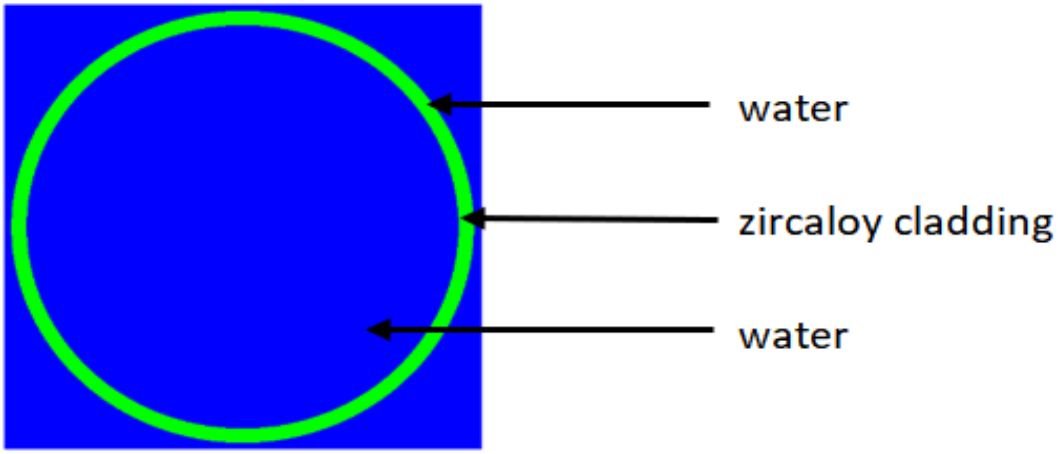

Figure 2-5: North-Anna instrumentation pin and guide tube

Rod Cluster Control Assemblies

A rod cluster control assembly comprises of a group of individual neutron absorber rods. The composition of the absorbing material is a silver-indium-cadmium alloy: 80% Ag, 15% In and 5% Cd (VEPCO, 2016). The rod is contained in zircaloy cladding. The guide tube thimbles, mentioned in the previous section, shield, and guide the control rods within the assembly.

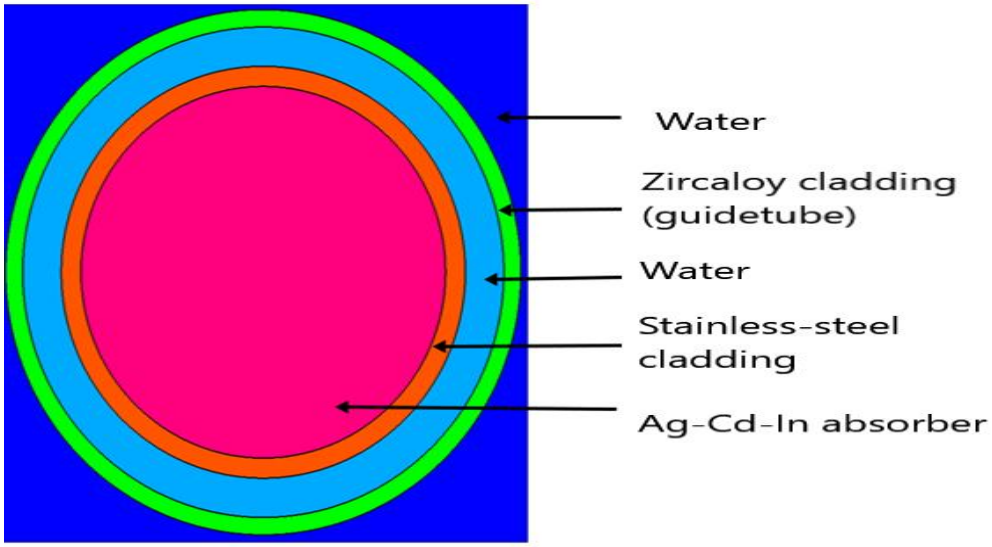

Figure 2-6: North-Anna guide-tube with control rod insertion

Burnable Poison Rods (BPR)

The burnable poison rods (BPR) consist of Al_2O_3-B_4C pellets (a borosilicate glass absorber) encapsulated in stainless steel cladding, as shown in Figure 2-7. Helium is in the void region. This structure is then contained within a Zircaloy-4 tubular cladding.

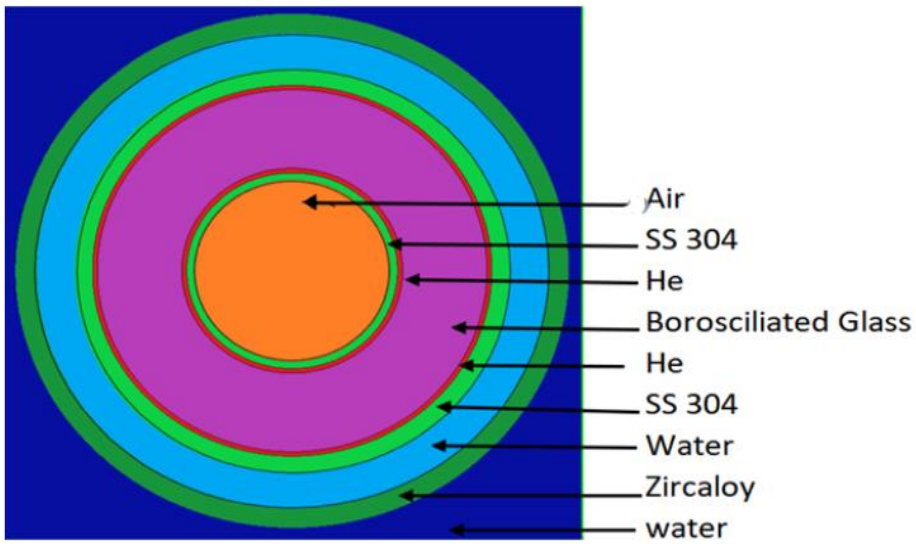

Figure 2-7: Modelled North-Anna Burnable Poison Rod (Horelik, et al., 2018)

Table 2-3: Fuel assembly description (Horelik, et al., 2018) (VEPCO, 2016) (ATI, 2015)

Fuel Rods	
Pellet Pitch (cm)	1.25984
Water Density (g/cm^3)	0.64990
Cladding Outside Diameter (cm)	0.94996
Cladding Density (g/cm^3)	6.55
Cladding Material and Its Composition (wt.%)	Zircaloy - 4. Zr - 98.2 %; Sn-1.5 %; Fe - 0.2 %; Cr - 0.1 %
Helium Gap Outside Diameter (cm)	0.83566
Helium Density in Helium Gap(g/cc)	0.0015981
Fuel Pellet	
Fuel Pellet Diameter (cm)	0.81916
Fuel Pellet Density (g/cc)	10.412
Fuel Pellet Height (cm)	1.3462
Fuel Pin Uranium Enrichments	2.1 w/o; 2.6 w/o; 3.1 w/o
Guide Tube and Instrumentation Pin	
Guide-Tube Material and Instrumentation Pin Inner Material	Zircaloy
Guide-Tube and Instrumentation Pin Inner Diameter (cm)	0.61214
Guide-Tube and Instrumentation Pin Outside Diameter (cm)	0.57150
Guide-Tube and Instrumentation Pin Density (g/cc)	6.55
Rod Cluster Control Assemblies	
Neutron Absorber	Ag (80%) - Cd (15%) – In (5%)
Neutron Absorber Diameter (cm)	0.43307
Neutron Absorber Density (g/cc)	10.1585
Cladding Material	Stainless-Steel 304
Cladding Diameter (cm)	0.48006
Cladding Density (g/cc)	8.00
Burnable Poison Rods	
Number	1072

Material	Borosilicate glass
Stainless Steel Cladding Outside Diameter (cm)	0.96774
Stainless Steel Inner Tube Diameter (cm)	0.46101
Boron Loading (wt% B_2O_3 In Glass Rod)	12.5

CHAPTER 3: REACTOR THEORY AND LITERATURE REVIEW

This chapter aims to provide the background theory and an overview of the numerical methods that are used to solve the neutron transport, as implemented in XSProc, T-NEWT, MCNP-6.2, and NESTLE. A description of the input generator, NWURCS, is given and discussed. Fundamental to this chapter are explanations of nuclear data, cross-sections, resonance self-shielding, reflected reactor systems, homogenisation, boundary conditions, the multiplication factor and multigroup generalisation.
In the theory regarding the codes described in this chapter, the definitions, cases and uses for the codes were taken directly from the respective code manuals and other sources so that the essence of the definitions and descriptions would not be lost. The source for each such occurrence has been duly noted.

3.1 The nuclear transport equation

In reactor analysis, the number of neutrons, for criticality in a given reactor system, needs to be constant and sustained at a steady state. Hence, the neutron distribution within the reactor needs to be determined.

In a fission reactor, the neutrons are either produced by nuclear fission or by a neutron source Q. They are then removed by absorption or by leaking out of the bounds of the reactor. The neutron's energy and direction are thus altered due to their interactions with the fuel and reactor materials.

The neutron transport equation is an integro-differential equation that describes the macroscopic behaviour of neutrons in a reactor. This integro-differential equation is described in seven variables: neutron energy, the two-dimensional neutron current density, the three-dimensional neutron flux and time. Various forms of this equation are given in the sections below in terms of the way the equation is used in the relevant computer codes.

3.2 Summary of calculation methods

The neutron transport can be solved using various numerical methods. Therefore, in this study, the neutron transport is solved using two methods:

- the deterministic method; and
- the Monte Carlo method.

The deterministic method is carried out using the T-NEWT control module within the SCALE-6.2.3 package. The results of these calculations are coupled with the NESTLE code of the Relap5-3D package. However, the Monte Carlo method is conducted using MCNP-6.2.

The KENO-VI code is not used in this study to produce results or perform certain tests; instead, the KENO-VI input file was used to verify whether the MNCP model was correct. A detailed explanation is presented in section 3.8.

The codes used in this study all obtain their cross-section data for neutron interactions from the Evaluated Nuclear Data File (ENDF/B-VII.1) nuclear data libraries. Both MCNP and SCALE utilise Continuous Energy (CE) atomic and nuclear data libraries. However, SCALE can also utilise Multi-Group Energy (MG) nuclear data libraries in some of its modules.

3.3 Deterministic methods

The SCALE (Standard Computer Analyses for Licensing Evaluation) deterministic transport capabilities enable criticality safety, sensitivity, and uncertainty analysis (Rearden & Jessee, 2018). In this study, T-NEWT of the SCALE-6.2.3 package and Nestle of the RELAP5-3D package (see section 3.4) are used to solve neutron transport calculations using the deterministic methods.

The SCALE-6.2.3 code system is a widely used modelling and simulation suite for nuclear safety analysis and design that is developed, maintained, tested, and managed by the Reactor and Nuclear Systems Division (RNSD) of Oak Ridge National Laboratory (ORNL) (Rearden & Jessee, 2018).

SCALE-6.2.3 has built-in module codes, of which some are stand-alone codes. This study uses the T-NEWT code (which is called a control module), which calls a sequence of codes, such as:

- XSProc which is a driver module of SCALE-6.2.3, that calls the functional modules BONAMI and CENTRM; and
- the functional module NEWT

A summary of the module codes, which were used to conduct this study, is given in the subsections below.

3.3.1 The Transport Rigor Implemented with Time-dependent Operation for Neutronic Depletion (TRITON)

TRITON/NEWT (T-NEWT) is a 2D lattice physics sequence code (a control module using SCALE-6.2.3 terminology), that provides maximum modelling flexibility, supporting the full range of cross-section processing options in XSProc, along with support for the multigroup transport NEWT module, which is a flexible mesh discrete ordinates code (Jessee, et al., 2018). TRITON/NEWT executes the XSProc module to calculate the self-shielding of multigroup cross-sections. It is noted that TRITON and TRITON/NEWT both define the same control module and can be used interchangeably.

3.3.2 Cross-Section Processing (XSProc)

XSProc (Cross-Section Processing) provides problem-dependent self-shielded multigroup cross-sections. This includes temperature correction, resonance treatment, flux weighting, as well as energy group collapsing and spatial homogenization (Williams, et al., 2018).

The cross-section data in SCALE-6.2.3 are taken from the ENDF/B-VII.1 data files. The calculated cross-section data is large and needs to be compressed (collapsed) into a finite number of groups. In this study, the cross-sections were collapsed into 252 groups. To compress these cross-sections, the XSProc module is called, which first reads the cross-section data from the ENDF/B-VII.1 data files. It then calls BONAMI (BONdarenko AMPX Interpolator) and CENTRM (Continuous Energy Transport Module) to calculate the flux distribution in the geometry of the pin cell. Once this is completed, PMC (Produce Multigroup Cross-sections) is then called to compress the cross-sections into 252 energy groups.

BONAMI processes the multi-group library specified in the input file before the CENTRM calculations during the XSProc execution. This is done so that BONAMI provides self-shielded data for the multi-group components not considered in the CENTRM solution.

3.3.2.1 BONAMI

BONAMI is used to perform resonance self-shielding calculations, which are performed for all SCALE sequences. BONAMI uses the Bondarenko factors for self-shielding treatment (Sihlangu, 2019). Bondarenko factors are multiplicative correction factors that convert the generic unshielded data into problem-dependent self-shielded values (Mertyurek & Williams, 2018).

The neutron distribution equation that is used in BONMAMI is presented in Eq. (3-1) (Mertyurek & Williams, 2018):

$$\left(\Sigma_t^{(r)}(E,T) + \sum_{j\neq r}\Sigma_t^{(j)}(E,T)\right)\Phi(E,T) + \sum_{j\neq r} S^{(j)}(E,T) = S^{(r)}(E,T) + \sum_{j\neq r} S^{j}(E,T) \quad (3\text{-}1)$$

Where

$\Sigma_t^{(r)}(E,T)$ and $S^{(r)}(E,T)$ are the macroscopic total cross-section and elastic scattering source for r, the resonance absorber, respectively; and

$\Sigma_t^{(j)}(E,T)$ and $S^{(j)}(E,T)$ are the macroscopic total cross-section and elastic source, respectively, for a nuclide *j*.

The nuclides in the summations (i.e., all nuclides except *r*) are called background nuclides for the resonance absorber *r*.

The collapsed cross-sections are calculated using the formula (Rearden & Jessee, 2018):

$$\sigma_{X,g}^{(r)} = \frac{\int_g \sigma_X^{(r)}(E)\Phi(E)dE}{\int_g \Phi(E)dE} \quad (3\text{-}2)$$

Where:

$\sigma_{X,g}^{(r)}$ is the shielded multi-group cross-section for reaction type X of resonance nuclide *r* in group g;

$\sigma_X^{(r)}$ is a pointwise (PW) cross-section; and

$\Phi(E)$ is the PW weighting function, which approximates the flux spectrum per unit of energy for the system of interest.

The integrals are taken over the limits of the energy group.

3.3.2.2 CENTRM/PMC

The CENTRM/PMC method is a more rigorous approach to the self-shielding treatment of the MG cross-sections and replaces the BONAMI results over the resolved resonance ranges of important absorber nuclides. Shielded cross-sections processed with CENTRM/PMC are

usually more accurate than the BONAMI cross-sections (Rearden & Jessee, 2018; Jessee, et al., 2018).

CENTRM calculates the pointwise flux spectra by solving the neutron transport equation for all unit cells described in the input. The energy group collapsing is carried out by PMC once the fluxes have been determined by CENTRM (Rearden & Jessee, 2018). The neutron transport equation is based on the following form (Williams, 2018):

$$\Omega \cdot \nabla\psi(\rho) + \Sigma_t(r,u)\psi(\rho) = \int_0^{\infty}\int_0^{4\pi} \Sigma(u' \to u; \mu_0)\, \psi(u', \Omega')du' + Q_{ext}(\rho) \quad (3\text{-}3)$$

Where:

$u = \ln\left(\frac{E_{ref}}{E}\right)$ is the lethargy, defined at an energy E, relative to a reference energy E_{ref};$\psi(\rho)$ is the angular flux (per lethargy) at phase space co-ordinate ρ;

$\rho(r, u, \Omega)$ is the phase space point defined by the six independent variables;

$r = (x_1, x_2, x_3)$ are the space co-ordinates;

$\Omega = (\mu, \zeta)$ is the neutron direction which is defined by the polar cosine μ and azimuthal angle ζ;

$\Sigma_t(r, u)$ is the total macroscopic cross-section;

$\Sigma(u' \to u; \mu_0)$ is the double differential scatter cross-section;

μ_0 is the cosine of scattering angle, which is measured in a laboratory co-ordinate system; and

$Q_{ext}(\rho)$ is the external source term, which includes the fission source.

The multigroup form of the transport equation is derived by integrating the above equation over the lethargy intervals defined by the group structure in the multi-group library. The multi-group transport equation is solved using the discrete ordinates method.

3.3.3 The New ESC-based Weighting Transport code (NEWT)

NEWT is a multigroup discrete-ordinates radiation transport computer code with flexible meshing capabilities that allow 2D lattice physics and neutron transport calculations, including multigroup flux spectrum calculations, collapse weighted cross-section calculations,

homogenization, calculation of assembly discontinuity factors, diffusion coefficients, and group form factors (Jessee & DeHart, 2018). The Extended Step Characteristic approach is employed in NEWT.

In this study, NEWT is used to generate the collapsed weighted cross-sections required for NESTLE.

3.3.4 Neutron transport equation

The neutron equation is often written in terms of the angular neutron flux as the dependent variable. The angular neutron flux is defined as the product of the angular neutron density and the neutron velocity. The time-independent form of the linear transport equation is then expressed as (Jessee & DeHart, 2018):

$$\hat{\Omega} \cdot \vec{\nabla}\psi\left(\vec{r}, \hat{\Omega}, E\right) + \sigma_t(\vec{r}, E)\psi(\vec{r}, \hat{\Omega}, E) = Q(\vec{r}, \hat{\Omega}, E) \quad (3\text{-}4)$$

Where:

$\psi(\vec{r}, \hat{\Omega}, E)$ is the angular flux at position $\vec{r}$ per unit volume, in direction $\hat{\Omega}$ per unit solid angle and at energy E per unit of energy;

$\sigma_t(\vec{r}, E)$ is the total macroscopic cross-section at position $\vec{r}$ and energy E; and

$Q(\vec{r}, \hat{\Omega}, E)$ is the source at position $\vec{r}$ per unit volume, in direction $\hat{\Omega}$ per unit solid angle and at energy E per unit energy (Jessee & DeHart, 2018).

The first term is losses due to leakage, the second term is the collisions term, and the last term is the source.

The source $Q(\vec{r}, \hat{\Omega}, E)$ is generally composed of three terms:

1. a scattering source (Jessee & DeHart, 2018);

$$S\left(\vec{r}, \hat{\Omega}, E\right) = \int_0^{4\pi} d\hat{\Omega} \int_0^{\infty} dE' \sigma_s(\vec{r}, \hat{\Omega}' \rightarrow \hat{\Omega}, E' \rightarrow E)\psi(\vec{r}, \hat{\Omega}', E') \quad (3\text{-}5)$$

Where:

$\sigma_s(\vec{r}, \hat{\Omega}' \rightarrow \hat{\Omega}, E' \rightarrow E)$ is the macroscopic scattering cross-section at position $\vec{r}$ from initial energy E' and direction $\hat{\Omega}$' to final energy E and direction $\hat{\Omega}$,

2. a fission source (Jessee & DeHart, 2018),

$$F(\vec{r},\hat{\Omega},E) = \chi(\vec{r},E)\int_0^\infty dE'\nu(\vec{r},E')\sigma_f(\vec{r},E')\psi(\vec{r},\hat{\Omega}',E') \tag{3-6}$$

Where:

$\sigma_f(\vec{r},E')$ is the macroscopic fission cross-section at position $\vec{r}$ and energy E' (assumed to be isotropic);

$\nu(\vec{r},E')$ is the number of neutrons released per fission event at position $\vec{r}$ and energy E'; and

$\chi(\vec{r},E)$ is the fraction of neutrons that are born at energy E; and

3. an external fixed source, $S(\vec{\boldsymbol{r}},\boldsymbol{E})$**,** such as a spontaneous fission source, a natural radioactive source, and others.

When energy is discretized into energy groups using the multi-group approach, the transport equation Eq. (3-4) becomes Eq. (3-7) (Jessee & DeHart, 2018):

$$\hat{\Omega}\cdot\vec{\nabla}\psi_g(\vec{r},\hat{\Omega}) + \sigma_t(\vec{r},\hat{\Omega})\psi_g(\vec{r},\hat{\Omega},E) = Q_g(\vec{r},\hat{\Omega},E) \tag{3-7}$$

Where the group-wise angular flux $\psi_g(\vec{r},\hat{\Omega})$ and source $Q_g(\vec{r},\hat{\Omega})$ are integrated across each energy group *g*. (The groups are numbered from 1 to *G*, with 1 being the highest energy and *G* being the lowest).

A group-specific scattering cross-section manages the coupling between energy groups, as given in Eq. (3-8) (Nyalunga, 2019).

$$\Sigma_s(\vec{r},g'\to g,\hat{\Omega}'\cdot\hat{\Omega}) = \frac{\int_{E_{g+1}}^{E_g} dE \int_{E_g'+1}^{E_{g'}} \Sigma_s(\vec{r},E'\to E,\hat{\Omega}'\cdot\hat{\Omega})\,\phi(\vec{r},E')dE'}{\int_{E_g+1}^{E_g} dE\ \phi(\vec{r},E)} \tag{3-8}$$

Spatial discretization is the process of discretizing the simulation geometry in space so that the simulation is made up of N_v volumes with homogenized material attributes inside each volume (Nyalunga, 2019). The discretization of the angular distributions of the particle interactions is conducted for the angular variables. As a result, the angular distributions are reduced to a set of directions, $\hat{\Omega}_n$, where $n = 1,\dots,N$, and N is the number of directions selected (Nyalunga, 2019).

3.3.4.1 Step Characteristic Approximation

Based on the discrete-ordinate methods, the flux streaming term is solved using finite-difference approximation. Thus, the method of characteristics is utilized to solve the transport equation analytically along characteristic directions within a computational cell (Jessee & DeHart, 2018).

To solve for the angular flux $\psi(\vec{r}, \widehat{\Omega}, \mathrm{E})$ in direction $\widehat{\Omega}$. from Eq.(3-4), the streaming term is rewritten along the s-axis, which is parallel to the characteristic direction $\widehat{\Omega}$, which yields Eq. (3-9) (Jessee & DeHart, 2018):

$$\widehat{\Omega} \cdot \widehat{\nabla}\psi\left(\vec{r}, \widehat{\Omega}, \mathrm{E}\right) = \frac{d\psi(s, E)}{d_s} \tag{3-9}$$

Eq. (3-9) substituted in Eq. (3-4) can be written in the characteristic form as seen in Eq. (3-10) (*E* is not shown explicitly) (Jessee & DeHart, 2018)

$$\frac{d\psi(s)}{d_s} + \sigma_t(s)\psi(s) = Q(s) \tag{3-10}$$

Eq. (3-10) then has a solution of the form (Jessee & DeHart, 2018):

$$\psi(s) = \psi_0 e^{-\sigma_i s} + \ e^{-\sigma_i s} \int_0^s Q \ e^{-\sigma_i s'} . ds' \tag{3-11}$$

Where:

s is the distance along the characteristic direction $\widehat{\Omega}$; and

ψ_0 is the known angular flux at $s = 0$.

Lathrop developed the Step Characteristic (SC) method which is a scheme that employs the Method of Characteristics (Lathrop, 1969) & (Jessee & DeHart, 2018). The SC approach assumes that within a computational cell, the source *Q* and macroscopic total cross-section σ_t are constant, while the angular flux is constant on the cell boundaries of the incoming direction (Jessee & DeHart, 2018)). Therefore, employing the SC approach and integrating Eq. (3-11) will thus yield Eq. (3-12) (Jessee & DeHart, 2018):

$$\psi(s) = \psi_0 e^{-\sigma_t s} + \frac{Q}{\sigma_t}(1 - e^{-\sigma_t s}) \quad (3\text{-}12)$$

3.3.4.2 Assembly discontinuity factors

The lattice transport solutions from NEWT are used to generate few-group (homogenized) cross-sections and discontinuity factors. The assembly discontinuity factors are used to preserve both reaction rates and the interface currents in the homogenization process (Jessee & DeHart, 2018). These crosss-sections are obtained from single-assembly transport calculations with zero-current boundary conditions. Figure 3-1 demonstrates the discontinuity of the flux at the assembly interface due to the use of homogenized XS. Although the homogenized flux is discontinuous at the assembly interface, the heterogeneous flux is continuous at the assembly interface.

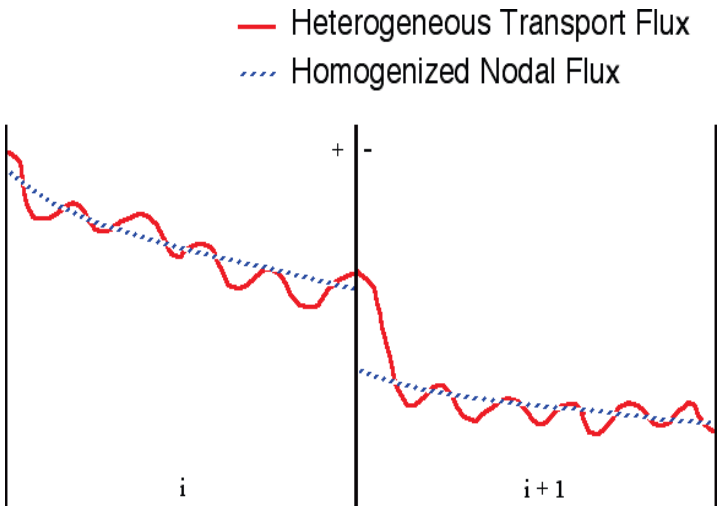

Figure 3-1: Heterogeneous vs homogeneous fluxes in a multi-assembly solution (Jessee & DeHart, 2018)

The interfaces condition which is used in nodal calculations between two assemblies (nodes) *i* and *i*+1 is as follows (Jessee & DeHart, 2018): differently,

$$\phi^{+}_{i,homogeneous} \cdot F^{+}_{i} = \phi^{-}_{i+1,homogeneous} \cdot F^{-}_{i+1} \quad (3\text{-}13)$$

Where:

F^{+}_{i} and F^{-}_{i+1} are assembly discontinuity factors (ADFs) on each side of the interface between assemblies *i* and *i+1*.

$\phi^{+}_{i,homogeneous}$ (or $\phi^{-}_{i+1,homogeneous}$) is the ADF at the assembly interface, defined as the ratio of the heterogeneous flux $\phi_{\text{heterogeneous}}$ at that assembly interface to the homogeneous flux evaluated at that interface (Jessee & DeHart, 2018):

$$F_i^{+} = \frac{\phi_{\text{heterogeneous}}}{\phi^{+}_{i,homogeneous}}; \qquad (3\text{-}14)$$

$$F_{i+1}^{-} = \frac{\phi_{\text{heterogeneous}}}{\phi^{-}_{i+1,homogeneous}}$$

Few-group homogenized cross-sections are always accompanied by equivalent few-group ADFs since fluxes and ADFs change with energy (Jessee & DeHart, 2018).T-NEWT is used to calculate single assembly lattice physics data and homogenized few-group XSs.

3.4 NESTLE

The Reactor Excursion and Leak Analysis Programme (RELAP5-3D) code has been developed at the Idaho National Laboratory under the sponsorship of the U. S. Department of Energy (Riemke, et al., 2009). This code has an integrated multidimensional 3D thermal-hydraulic and a 3D neutronic (neutron kinetics) capability, the latter is the NESTLE code.

The NESTLE (Nodal Eigenvalue, Steady-State Transient, Le core Evaluator) programme is a few-group neutron diffusion reactor core simulator code within the Relap5-3D package, which employs the Nodal Expansion Method (NEM). NESTLE can solve both steady-state and transient problems, using three-dimensions with either cartesian, cylindrical or hexagonal geometry (Kirkland, 2017). It also can apply thermal-hydraulic feedback, where the thermohydraulic solution is also calculated in RELAP5-3D and fed to the NESTLE calculation.

3.4.1 Nodal Expansion Method (NEM)

The NESTLE code solves 2 or 4 group neutron diffusion equations presented in Eq. (3-15) utilizing the Nodal Expansion Method (Turinsky, et al., 2003).

$$\overline{\nabla}^2 D_g \phi_g + \Sigma_{tg} \phi_g = \sum_{g'=1}^{G} \Sigma_{sgg'} \phi_{g'} + \frac{\chi_g}{k} \sum_{g'=1}^{G} \nu_{g'} \Sigma_{fg'} \phi'_g \qquad (3\text{-}15)$$

$$(g = 1, 2 \ldots, G)$$

Where:

The dependence of each quantity on the spatial co-ordinate $\hat{r}$ has been suppressed, and,

D_g is the diffusion coefficient [cm];

ϕ_g is the neutron flux in group *g* [cm^{-2}·sec^{-1}];

Σ_{tg} is the total macroscopic cross section [cm^{-1}];

$\Sigma_{sgg'}$ is the group-to-group scattering cross section [cm^{-1}];

χ_g is the fraction of fission neutrons entering group *g*;

$v_{g'}$ is the average number of neutrons created per fission;

$\Sigma_{fg'}$ is the macroscopic fission cross-section [cm^{-1}]; and

k is the multiplication factor (i.e. critical eigenvalue).

Integration of Eq.(3-15) over the volume of node *l* generates a local neutron balance equation shown in Eq.(3-16) in terms of the face-averaged net currents and the node volume average flux. This is known as the nodal balance equation (Turinsky, et al., 2003).

$$\frac{1}{\Delta x^l}\left(\bar{L}_{gx}^l\right)+\frac{1}{\Delta y^l}\left(\bar{L}_{gy}^l\right)+\frac{1}{\Delta z^l}\left(\bar{L}_{gz}^l\right)+A_g^l\bar{\phi}_g^l=\bar{Q}_g^l \tag{3-16}$$

Where:

assuming node l is centred around the co-ordinate's origin, the volume integrated quantities are defined below (Turinsky, et al., 2003):

$$\bar{\phi}_g^l=\frac{1}{V^l}\int_{-\frac{\Delta x^l}{2}}^{\frac{\Delta x^l}{2}}\int_{-\frac{\Delta y^l}{2}}^{\frac{\Delta y^l}{2}}\int_{-\frac{\Delta z^l}{2}}^{\frac{\Delta z^l}{2}}\bar{\phi}_g^l(\bar{r})dxdydz\equiv\text{Node volume average flux}; \tag{3-17}$$

$$\bar{Q}_g^{\,l} = \frac{1}{V^l} \int_{-\frac{\Delta x^l}{2}}^{\frac{\Delta x^l}{2}} \int_{-\frac{\Delta y^l}{2}}^{\frac{\Delta y^l}{2}} \int_{-\frac{\Delta z^l}{2}}^{\frac{\Delta z^l}{2}} \bar{Q}_g^{\,l}(\bar{r}) dx dy dz \equiv \text{Node volume average source;} \tag{3-18}$$

Where:

$(\hat{r}) \equiv (x, y, z) \epsilon V^l = \Delta\text{x}, \Delta\text{y}, \Delta\text{z} \equiv$ Volume of node $l, g = 1,2$;

$\bar{L}_{gx}^{\,l}$ is the x transverse leakage term;

$\bar{L}_{gy}^{\,l}$is the y transverse leakage term;

$\bar{L}_{gz}^{\,l}$ is the z transverse leakage term.

$$A_g^l = \Sigma_{tg}^l - \Sigma_{sgg}^l - \frac{\chi_g^l}{k} v_g \Sigma_{fg}^l; \tag{3-19}$$

And,

$$\frac{1}{\Delta x^l} \bar{L}_{gx}^{\,l} = \frac{1}{\Delta x^l} \left(\bar{J}_{gx+}^{\,l} - \bar{J}_{gx-}^{\,l} \right) = \frac{1}{V^l} \int_{-\frac{\Delta x^l}{2}}^{\frac{\Delta x^l}{2}} \int_{-\frac{\Delta y^l}{2}}^{\frac{\Delta y^l}{2}} \int_{-\frac{\Delta z^l}{2}}^{\frac{\Delta z^l}{2}} \frac{\partial}{\partial x} \bar{J}_{gx}^{\,l}(\bar{r}) dx dy dz \tag{3-20}$$

Where:

$\bar{J}_{gx\pm}^{\,l}$ ≡Average x-directed net current on node faces $\pm\frac{\Delta x^l}{2}$.

In carrying out the derivation, the equation is written in Cartesian geometry and Fick's law is used in each of the x, y and z directions (Turinsky, et al., 2003).

3.4.2 The transverse-integration method

In order to solve the nodal balance Eq.(3-16), a relationship between the node average flux and the face-averaged net currents is required. The method of transverse integration is used, where the 3D diffusion equation is integrated over the two directions transverse to each axis. This generates three one-dimensional equations, one for each direction in Cartesian co-ordinates, of the following form (Turinsky, et al., 2003),

$$\frac{d}{dx}\bar{J}_{gx}^{l}(x) + A_g^l \bar{\phi}_{gx}^{l}(x) = \bar{Q}_{gx}^{l}(x) - \frac{1}{\Delta y^l}\bar{L}_{gy}^{l}(x) - \frac{1}{\Delta z^l}\bar{L}_{gz}^{l}(x) \tag{3-21}$$

Where from Eq.(3-21):

$$Q_{gx}^{l}(x) = \frac{1}{\Delta y \Delta z}\int_{-\Delta y/2}^{\Delta y/2}\int_{-\Delta z/2}^{\Delta z/2} Q_g^l(\hat{r})\, dzdy \tag{3-22}$$

In Eq.(3-22), for a two group formulation is Eq.(3-22) and Eq.(3-23) (Bandini, 1990):

$$Q_1^l(\hat{r}) = \frac{1}{K}\nu\Sigma_{f2}^{l}\phi_2^l(\hat{r}) \tag{3-23}$$

And;

$$Q_2^l(\hat{r}) = \Sigma_{12}^{l}\phi_1^l(\hat{r}) \tag{3-24}$$

And from Eq.(3-21):

$$\bar{L}_{gy}^{l}(x) = \frac{1}{\Delta z^l}\int_{-\frac{\Delta z^l}{2}}^{\frac{\Delta z^l}{2}}\int_{-\frac{\Delta y^l}{2}}^{\frac{\Delta y^l}{2}} \frac{\partial}{\partial y} j_{gy}^{l}(\bar{r})dydz \tag{3-25}$$

$$\equiv \text{Average y direction transverse leakage}$$

And (Turinsky, et al., 2003):

$$\bar{L}_{gz}^{l}(x) = \frac{1}{\Delta y^l}\int_{-\frac{\Delta y^l}{2}}^{\frac{\Delta y^l}{2}}\int_{-\frac{\Delta z^l}{2}}^{\frac{\Delta z^l}{2}} \frac{\partial}{\partial z}\, j_{gz}^{l}(\hat{r})dzdy \tag{3-26}$$

$$\equiv \text{Average z direction transverse leakage}$$

The one-dimensional averaged flux in Eq.(3-21), is expanded as a general polynomial, given in Eq. (3-27) (Turinsky, et al., 2003):

$$\bar{\phi}_{gx}^{l}(x) = \bar{\phi}_{g}^{l} + \sum_{n=1}^{N} a_{gxn}^{l}\ f_n(x) \tag{3-27}$$

where $\bar{\phi}_g^{\ l}$ is the node average flux.

$f_n(x)$ must be chosen so that the functions satisfy (Turinsky, et al., 2003):

$$\int_{-\frac{\Delta x^l}{2}}^{\frac{\Delta x^l}{2}} f_n(x)dx = 0 \text{ for } n = 1, \dots, N \tag{3-28}$$

Given these equations, the final partial current equation set for each node can be produced, which is a 6×6 matrix of equations.

Written in matrix form, the equation set for each node is (Bandini, 1990):

$$[A] \cdot J_g^{out,l} = [C] \cdot J_g^{in,l} + [B_1] \cdot Q_g^l + [B_2] \cdot L_g^l \tag{3-29}$$

Where

$J_g^{in,l}$ and $J_g^{out,l}$ are the incoming and outgoing partial currents as defined in (3-20),

Q_g^l is the weighted average of $\bar{Q}_{gx}^l$ defined with Eq.(3-21); and

L_g^l is the weighted average of $\bar{L}_{gx}^l$ defined with Eq.(3-21)

$[A]$, $[C]$, $[B_1]$ and $[B_2]$ are matrices of constants, which depend on the constants of the system. (For the interested reader, the formula are given in (Bandini, 1990)).

The full derivation is given in (Bandini, 1990). In the derivation, the order of the function defined in Eq.(3-27) is set at 4, and the solution is known at the quartic NEM.

These equations are a response matrix set of equations, since the outgoing partial currents in each node can be expressed as a function of incoming partial currents and intra-node sources/sinks (Bandini, 1990).

In the interior of the medium, neighbouring nodes are coupled together by assuming that the partial currents are continuous across nodal interfaces. This means that the outgoing surface averaged partial current of one node is the incoming averaged partial current of an adjacent node which share a common face with each other (Bandini, 1990).

The surfaces of the nodes which form the outer boundary will have incoming partial currents defined as appropriate boundary conditions.

Details regarding the numerical solutions of these equations are given in (Bandini, 1990) together with the acceleration schemes used in obtaining the solutions.

3.5 Stochastic methods

Unlike the deterministic method that solves the integro-differential transport equation for the average particle behaviour, the Monte Carlo method solves neutron transport by simulating individual particles and recording some aspects of the average behaviour (X-5 Monte Carlo Team., 2003).

The Monte Carlo codes use continuous energy (CE) cross-section data, as they provide accurate and precise solutions. Monte Carlo methods are statistical in nature, and hence, require extensive calculation time with regard to a slow convergence rate and also require large computational memory.

An advantage of the Monte Carlo methods over the deterministic methods is that the geometry of the nuclear reactor does not need to be discretized and homogenized, thus a variety of nuclear reactors may be simulated by a single Monte Carlo criticality code.

Monte Carlo based computer codes includes Serpent (Leppänen, 2015), KENO-VI in SCALE-6.2.3 (Petrie, et al., 2018), McCard (Shim & Kim, 2016), MASTER (Cho, 1999), and MCNP (Werner, 20217) Monte Carlo N-Particle (MCNP) version 6, release 2 and KENO-VI within the SCALE-6.2.3 package code are used in this study. KENO-VI is discussed in section 3.8.

MCNP-6.2 is a general-purpose, continuous-energy, generalized-geometry, coupled neutron/photon/electron transport code (X-5 Monte Carlo Team., 2003). MCNP-6.2 is developed at the Los Alamos National Laboratory and distributed by the Radiation Safety Information Computational Centre (RSICC) (http://www-rsicc.ornl.gov/rsic.html).

MCNP-6.2.3 is used in this study to calculate the neutron flux and k_{eff} in the core.

Three processes are involved in solving the neutron transport problem (Wu, 2017).

1. Source sampling from its probability distribution;
2. Tracking (tracking of the neutrons' locations, energies, and directions); and
3. Contribution recording and result analysis.

3.5.1 Source sampling

MCNP's user-input source capability allows the user to choose from a variety of source conditions without changing the code. For the source variables of energy, time, location, and direction, the independent probability distributions are specified, as well as information on the source's geometrical extent (Sihlangu, 2016).

3.5.1.1 Probability distribution functions

To execute Monte Carlo calculations, one would have to provide the probability density functions (PDFs) that describe various processes of the system and the simulation proceeds by random sampling from the PDFs (Sihlangu, 2016).

Consider a continuous random variable, defined by x over the interval $a \leq x \leq b$. If a probability density function (PDF) $f(x)$ exists, then $f(x)dx$ is the probability that a variable takes on a value within dx about x (Stacey, 2007). The normalisation is given as:

$$\int_a^b f(x)dx = 1, f(x) \geq 0 \ ; \ \text{therefore:} \ \ F(x) = \int_a^x f(x')dx' \tag{3-30}$$

Where:

$F(x)$, is the cumulative probability distribution function (CDF), which is defined as the probability that the variable x takes on a value less than or equal to x.

3.5.1.2 Analogue Monte Carlo sampling

The Monte Carlo method simulates the stochastic nature of the neutron transport through matter by tracking the path of an individual neutron as it passes through matter and considering the various processes that may determine its history (Stacey, 2007).

The various aspects of the processes of the individual neutron history are (Stacey, 2007):

- Determining the parameters defining its source which are position, direction and energy;
- Determining the distance that the neutron will travel before a reaction occurs. In this regard, the neutron is allowed to leak out of the system without experiencing a reaction;
- Determining the type of reaction which can be scattering or absorption;

- If scattered, determining the scattering angle and direction of the scattered neutron. The neutron in then further tracked, starting with determining the distance that the neutron will travel before a reaction occurs;
- If the absorption event is fission, then the fissile neutrons are banked for use as source neutrons for further histories.

The parameters defined above are determined by sampling appropriate PDFs and CDFs using random numbers.

3.5.2 Recording and result analysis

Physical quantities such as neutron flux, energy deposition, reaction rates, and eigenvalues can be obtained using statistical methods by tracking a large number of neutron histories and recording the contribution of each neutron (Wu, 2017). The statistical errors on these quantities can also be determined.

For the interested reader, detailed descriptions of the different statistical concepts used in MCNP, such as error estimations; the central limit theorem; the mean behaviour; relative error; figure of merit and variance reduction techniques are found in (Stacey, 2007) and (Shultis & Faw, 2011). The tallies and the estimation of the neutron flux and multiplication factor (k_{eff}) are presented in following sections.

3.5.2.1 Tallies

As mentioned above, the Monte Carlo method directly simulates neutron transport as a stochastic process, by considering a series of the interactions a neutron undergoes and using random numbers to present the types of these interactions and their probabilities of occurrence along the neutron trajectory. These are added to characterize their entire behaviour in the reactor system (Maretele, 2016). The average behaviour of these particles is then recorded and tallied. This is a process that can be visualized as consisting of a series of steps, at each of which the movement made is random in direction (Oxford, 2020).

The calculation of reaction rates in various regions, over various energies, and by various nuclides is accomplished by tallying each collision event (Stacey, 2007). A tally refers to the process of counting the quantities that are kept and scored by MCNP, such as collision events.

MCNP is instructed to keep track of particle current, particle flux, and energy deposition in several ways. Except in a few specific circumstances involving criticality sources, MCNP tallies are normalized to be per starting particle.

3.5.2.2 Neutron fluxes

Tallying events may also be used to generate neutron fluxes and currents. The product of the cross-section (Σ_t), with the flux (ϕ) and the volume (V) is equal to the collision rate (CR) in a region (Stacey, 2007). Thus, by tallying the collision rate, the flux can be calculated to be (Stacey, 2007):

$$\phi = \frac{CR}{\Sigma_t V} \tag{3-31}$$

The scalar flux may also be defined as the path length covered by all particles traveling through a volume per unit of time. By considering the weights of neutrons at various stages of their histories, the flux thus becomes Eq. (3-32) (Stacey, 2007):

$$\bar{\phi} = \frac{\bar{l}}{V} = \frac{1}{V}\frac{1}{N}\sum_{n=1}^{N} w_n l_n \tag{3-32}$$

Where:

N is the number of histories;

$\bar{l}$ is the track length per unit time in the volume in question of the *n*th history; and

w_n is the weight of the neutron on the n^{th} history had when it traversed the volume.

The variance (v_{ar}) in the flux estimate is given by (Stacey, 2007):

$$v_{ar} = \frac{N}{N-1}\left[\frac{1}{V^2 N}\sum_{n=1}^{N}(w_n l_n)^2 - \frac{1}{V^2 N^2}\left(\sum_{n=1}^{N} w_n l_n\right)^2\right] \tag{3-33}$$

3.5.2.3 Criticality problems

MCNP is used to calculate the multiplication constant (k_{eff}) and associated eigen solution for the flux distribution. The k_{eff} is defined as (X-5 Monte Carlo Team., 2003):

$$k_{eff} = \frac{fission\ neutrons\ in\ generation\ i+1}{fission\ neutrons\ in\ generation\ i} \quad (3\text{-}34)$$

In a criticality calculation, when the loss rate equals the production rate, with $k_{eff} = 1$- the system is critical, and the chain reaction of the fission neutrons is self-sustaining. One of the main concerns in criticality calculations is to prevent the total neutron population from increasing or decreasing in an uncontrollable manner (Stacey, 2007).

3.5.3 Source convergence

To assist users in analysing the convergence of the source distribution, MCNP calculates the Shannon entropy of the source distribution (H_{src}). The Shannon entropy is a parameter that MCNP6 uses to examine the convergence of the fission source spatial distribution. The Shannon entropy H_{src} can be calculated by the equation (Werner, 20217):

$$H_{src} = -\sum_{J=1}^{N_s} P_J \cdot ln_2(P_J) \quad (3\text{-}35)$$

where:

$N_s = Number\ of\ grid\ in\ a\ mesh$ (Or the number of tally bins for the source distribution);

$$P_J = \frac{Number\ of\ source\ sites\ in\ J^{th}\ mesh\ element}{Total\ number\ of\ sorce\ sites}$$

MCNP-6.2 calculates the Shannon entropy for each cycle. The convergence of the H_{src} in MCNP is controlled by the number of source points and the number of inactive cycles. If the H_{src} is not converged when the active cycles start, then MCNP will recommend a number of inactive cycles to be skipped. This is discussed in detail in section 4.6.5.1.1.

3.6 Reactivity

Reactivity (ρ) is defined as the measure of the relative departure of a reactor from criticality. The equation for reactivity is given below:

$$\rho = \frac{k_{eff} - 1}{k_{eff}} \quad (3\text{-}36)$$

Where:

ρ is the reactivity; and

k_{eff} is the multiplication factor.

Reactivity describes the deviation of an effective multiplication factor from unity (nuclear-power.net, 2021). When reactivity is multiplied by 10^5, the unit is then *pcm* (per cent mil).

3.6.1 Reactivity control system

The amount of reactivity in a reactor core determines how the neutron population, and the reactor power, are behaving at any given time. To control the reactivity in the reactor core, reactivity coefficients are used. A reactivity coefficient is defined as the amount that the reactivity changes for a given parameter change. For a reactor system, the total reactivity coefficient must be negative when the reactor is at a critical state for safety requirements.

Two reactivity control systems are used in a reactor, namely, control rods and soluble boron in the coolant\moderator. In addition, burnable poisons pellets are present at some locations in selected fuel assemblies to reduce the excess reactivity in the core at start-up.

The control rods are assembly tubes of neutron absorbing material (high absorption cross-section) whose movement in the reactor affects the critical state of the system. The removal or insertion into the reactor will either increase or decrease the reactivity and the neutron flux of the reactor. The absorber material used in the control rods is the Ag-Cd-In alloy.

Burnable Poison Rod Assembly (BPRA) are also used to create negative reactivity once they have been inserted in a reactor. BPRAs for the NA PWR consist of Al_2O_3-B_4C. (Refer to Figure 2-7).

An alternative method is to dissolve a soluble neutron absorber such as boric acid (H_3BO_3) in the primary coolant of PWRs. Boron is an ideal isotope to use to decrease the reactivity of the reactor due to its large thermal neutron absorption cross-section (Rui, et al., 2017). By increasing the boron concentration in the coolant, the neutron density is reduced, resulting in a decrease in reactivity (Freixa et al., 2009).

The boron coefficient, w_b is defined as the change in reactivity per the change in the boron concentration, as seen in the equation below. It is expressed in units of $pcm/g \cdot kg^{-1}$.

$$\alpha_B = \frac{d\rho}{dg/kg} \tag{3-37}$$

An alternate expression can be written in terms of Eq.(3-38), where a linear relation with k_{eff} is assumed in estimating the boron concentration (Rui, et al., 2017).

$$w_b = \frac{1}{k_{eff}} \cdot \frac{dk_{eff}}{dC_B} = \frac{1}{k_{eff}} \cdot \frac{\Delta k_{eff}}{\Delta C_B} = \frac{1}{k_{eff}} \cdot \frac{k_2 - k_1}{c_{b2} - c_{b1}} \tag{3-38}$$

Where:

$k_1$and k_2 are the two results of k_{eff} calculations, assumed to be close to unity; and

c_{b1}, c_{b2} are boron concentrations related to $k_1$and k_2, respectively (Rui, et al., 2017).

3.7 Boundary conditions

For the NA PWR model, the reflective and vacuum boundary conditions are applied. The reflective boundary conditions are used in NEWT to reflect (mirror) the neutrons back into the geometry for the FA, while the vacuum boundary conditions are used for the FC calculations in MCNP-6.2 and NESTLE. The vacuum boundary causes MCNP-6.2 to stop tracking the neutrons once they move out of (past) the boundary of the geometry. This is because a FC geometry is assumed to be a non-re-entrant, meaning that a neutron will be terminated after it has crossed the outer boundary (Leppanen, 2017).

3.8 Monte Carlo Method in SCALE

KENO-VI is a Monte Carlo criticality safety calculation code which was developed at Oak Ridge National Laboratory (Hollenbach, 2011). KENO-VI uses the SCALE Generalized Geometry Package, which provides a quadratic-based geometry system with much greater flexibility in problem modelling but with slower run-times. It performs the eigenvalue calculations for neutron transport primarily to calculate multiplication factors (k_{eff}) and flux distributions of fissile systems in both continuous energy and multigroup modes (Rearden & Jessee, 2018), using an ENDF/B-VII nuclear data file included in SCALE-6.2.3.

KENO-VI is not used in this study to produce results or perform tests. The NWURCS developer has included equivalent KENO-VI models as well, and these models can be plotted using the FULCRUM of the SCALE-6.2.3 visual package. This can, therefore, assist in verifying the geometry.

The MCNP-6.2 code package does not include the Visual Editor or VISED (Carter & Schwarz, 1995), which is designed to assist the user by displaying the geometry specified in the input file. VISED was distributed with MCNP-6.1. Due to the financial constraints of the study, VISED could not be acquired separately. Therefore, the NWURCS developer (who also had MCNP-6.1) also plotted the MCNP-6.2 input files for the geometric visualization using VISED. The two FC plots are shown in Figure 5-1 , to verify the MCNP-6.2 geometry plots against the KENO-VI geometry plots.

A study based on the verification of KENO-VI and MCNP-6.2 using NWURCS Version 3.1 was conducted by Mulasi (Mulasi, 2021).

3.9 Comparison equation for the multiplication factor

In order to get more insight into criticality studies, one can use the multiplication factor obtained in the solution for the one-group reactor equations to establish trends or to check whether models behave according to the physics governing them.

The multiplication factor can be expressed mathematically as shown in Eq.(3-39) (Stacey, 2007):

$$k = \frac{\nu \Sigma_f \phi}{D B_g^2 \phi - \Sigma_a \phi} = \frac{\nu \Sigma_f}{D B_g^2 - \Sigma_a} \tag{3-39}$$

Where:

B_g is known as the geometric buckling constant, and it is expressed as

$B_g^2 = \frac{\nu \Sigma_f - \Sigma_a}{D} = \frac{\nu \Sigma_f / \Sigma_a - 1}{L^2}$;

D is the diffusion coefficient expressed as $D = \frac{1}{3(\Sigma_t - \overline{\mu_0}\Sigma_s)} = \frac{1}{3\Sigma_{tr}}$ where $\overline{\mu_0} \approx \frac{2}{3}A$; and

$L^2\ is\ the$ neutron diffusion length $L^2 = \frac{D}{\Sigma_a}$.

3.10 NWURCS Version 3.1

The process of establishing and confirming accuracy and reliability in computer simulations is known as verification. Verification is performed by code developers to determine if the code accurately solves the equations as well as the models it is designed to solve (Brown, et al., 2003). In this study, verification is conducted on the NWURCS suite of codes.

NWURCS is used to create input for a few reactor systems such as HTRs, PWRs and MTRs as seen from studies by (Naicker, 2022; Naicker, et al., 2021; Nyalunga, et al., 2016; Nyalunga, et al., 2019; du Toit & Naicker, 2018a; du Toit & Naicker, 2018b; Sihlangu, et al., 2019). The NWURCS code is used in this study to generate the input files for T-NEWT, NESTLE, and MCNP-6.2 for the NA PWR model. NWURCS is used to extract the data (homogenized macroscopic cross-sections and other group constants) from the T-NEWT outputs and use them to generate NESTLE input files.

One of the methods used for the verification of the NWURCS code is by checking if the code can accurately produce input files, with output results that agree with those of input files that are built manually. Also, verifying the NWURCS code can be carried out by checking the input file that is generated by the code, to ensure that it represents the actual material and geometry definition of what it should look like, that is initially given by the user (Nyalunga, 2016). This can be done by line-by-line visual inspection using a text editor such as Notepad++.

NWURCS is currently in Version 3.1. From version 1 to version 2, important changes have been made that have enabled the modelling of axial layers independently; changed the definition of the volumes; included various switches that allowed changing from continuous energy to multi-group, changing from a fuel assembly to a full core model, and so on (Sihlangu, 2019). In version 3, the nested level nature of the reactor core has been exploited, in which the core is in the first level, the fuel assemblies are in the second nested level and the fuel pins are in the third nested level. With this structure, the definitions of the volumes and the lattices are standard input, and the dependence on whether they are in the core, the fuel assembly or the fuel pin does not require differing structures for the input files, as was the case in the earlier versions (Naicker, 2022). This leads to simpler model development. Version 3.1 of NWURCS is used to test the modelling capability using this nested level approach for the nodal reflector-full core model of the North-Anna Reactor.

The accuracy of the code's output results can be proven through validation against measured data, plant data and other similar real physical systems (Nyalunga, 2019). Validation is the process in which a code's outputs are compared to experimental results, to assess and

declare the code's accuracy. Validation ensures that the computational model is physically accurate and that the mathematical simplifications and correlations are valid (Perko, 2015). In this work, validation is not carried out since it is considered to be outside the scope of the work. Furthermore, it is noted that in terms of Option B of the master's programme in the Faculty of Engineering at the NWU, validation of models is not required.

It should also be noted that NWURCS is developed outside this work, and the actual FORTRAN code description is not given. However, a continual verification process of NWURCS is conducted, to verify that the outputs produced by NWURCS (i.e., the input for T-NEWT, NESTLE and MCNP6), regarding the material inputs volumes and the nodal development are correct.

3.11 Literature review

3.11.1 Literature review A

"Benchmark evaluation of zero-power critical parameters for the Temelin VVER nuclear reactor using SERPENT & NESTLE and MCNP" by (Novak, et al., 2019)

This study presents a benchmark study of a VVER 1000 core simulation of a hot zero power (HZP) test, using MCNP and a combination of Serpent and NESTLE which provided a lattice-to-diffusion nodal simulation. Parameters that were studied were the multiplication factor and moderator temperature coefficients (MTC).

According to (Novak, et al., 2019) several tests were conducted to benchmark and verify the reactor full core performance of a VVER-1000 reactor, using a Serpent and NESTLE combination (data from the Serpent's output files were transferred to the NESTLE full core calculation). The results generated by MCNP were used and compared against the results obtained from the SERPENT-NESTLE combination calculation.

The study conducted by (Novak, et al., 2019) is different from this study in the sense of modelling a different reactor type, and that they have also used a different lattice physics code to create the FA calculations. However, both studies use the same sequences of multigroup lattice and nodal analysis. Also, once the results were completed, the MCNP results were compared against the results obtained from the NESTLE calculation. The difference is that the actual SERPENT lattice calculations are continuous energy calculations as opposed to the multigroup XSProc/NEWT combination used in the current study.

Spacer grids were not considered in the inputs. Infinite lattice reflective boundary conditions were used for the lattice calculations (Novak, et al., 2019). All the SERPENT calculations had 10 000 neutron source points, 400 active cycles, and 50 inactive cycles (Novak, et al., 2019). The heat transfer and thermal-hydraulic feedback calculations, which are implemented in NESTLE, were utilized to modify the cross-section used in the NESTLE calculation. Three cases were studied, whereby the fuel temperature was set at 300K, 1005 K and 1800k, while the coolant temperature was set to 300K, 578 K and 615 K, for the SERPENT calculations, as seen in Table 3-1.

Table 3-1: Branch calculation parameter in SERPENT (Novak, et al., 2019)

Fuel temperature	300 K	1005 K	1800 K
Soluble boron concentration	0 ppm	525 ppm (3 g/kg)	1575 ppm
Coolant density	−15%	0 % (0.7169 g/cm^3)	+15 %
Coolant temperature	300 K	578 K	615 K
Control rod	No	Upper part	Lower part

The MCNP model was similar to the NESTLE model, as no reactor vessel was modelled. Both models used ENDF/B-VII.1 libraries. The fuel assemblies are modelled without the top and bottom nozzles and spacing grids (Novak, et al., 2019). For the MCNP calculations, the coolant, fuel, cladding, and structural components were all set to 600 K. The MCNP calculations used 60,000 neutrons per cycle, 50 inactive and 1,050 active cycles.

The study by (Novak, et al., 2019) obtained results which were in very good agreement with the actual critical state of the core as seen in Table 3-2.

Table 3-2: Branch calculation parameter in SERPENT (Novak, et al., 2019)

critical state	NESTLE k_{eff} [–]	difference [*pcm*]	MCNP k_{eff} [–]	difference [pcm]
First	0.99884	−116	–	–
Final	0.99955	−45	0.99953 ± 0.00008	−47

However, since the MCNP model used a different coolant and fuel temperatures which were around 326°C (600 K) to obtain the results present in Table 3-2, the k_{eff} of the MCNP calculation should have probably been around 300 pcm above criticality if the actual temperatures of plant operational values of 280°C (553 K) was used.

3.11.2 Literature review B

“Coupled Simulation of Gas Cooled Fast Reactor Fuel Assembly with NESTLE Code System” by (Osusky, et al., 2018)

“The paper focused on coupled calculations of the Gas Cooled Fast Reactor” (Osusky, et al., 2018), by validating the NESTLE code version 5.2.1. The calculation methodology and the codes used in this paper were similar to those used in this study. TRITON of the SCALE code package system was used to process the FA homogenised parametric multigroup macroscopic cross-section library for the NESTLE code core simulation.

TRITON calls the XSPRoc/NEWT sequence within the SCALE code package. It was used to estimate the neutron flux and it processes the homogenized collapsed and weighted macroscopic cross-sections, and also calculated the eigenvalue. The reference case had the following conditions: fuel temperature at 973.15 °C; coolant temperature at 673.15 °C and the coolant density of 4.9439 $kg \cdot m^{-3}$. The multiplication factor of the reference case simulation obtained by NEWT was 1.21519 (Osusky, et al., 2018).

For the NESTLE calculations, the GFR2400 model was set to have a reflective boundary condition in radial direction and zero flux boundary condition in axial direction (Osusky, et al., 2018). The data used in NESTLE, was populated from the TRITON and NEWT sequence simulations. The top and bottom axial core reflectors were not considered.

For the core to achieve an “uniformly distributed neutron flux in radial direction”, the core was mixed with two fuel zones with different enrichment. Then NESTLE calculated the neutron flux distribution, the temperature distribution, and the density of the coolant in the system.

Another simulation was performed for NEWT, where the temperature and density where averaged resulting in the multiplication factor to be 1.21401. The multiplication factor obtained by the NESTLE code was 1.19661 (Osusky, et al., 2018) .

As mentioned in the literature review A, this paper reports a study that was conducted on the simulation of a GFR while the study is based on a PWR, therefore the results presented in the paper were not used for comparison in this study, rather as a guided text of reference since the code sequence used was the same.

3.11.3 Literature review C

"SBLOCA with Boron Dilution in Pressurized Water Reactors, Impact to the Operation and Safety" by (Terradas, 2009)**.**

The Ph.D. Thesis by (Terradas, 2009) was based on the Small-break loss-of-coolant accidents (SB-LOCA) on a 3-loop Westinghouse PWR system to test the low-borated water effects on reactivity, using RELAP5. The focus was on the thermohydraulic behaviour of the PWR.

(Terradas, 2009) stated that 'during the first cycle, the reactor has an excess of reactivity compared to the other cycles' and therefore the boron is introduced to system to maintain the reactivity. However, 'if the core's reactivity was exclusively regulated with dissolved boron, the reactor would be supercritical even with a boron concentration higher than 2000 ppm' was added to the system (Terradas, 2009). Therefore, to lower the boron concentration, rods made of burnable poisons (with high neutron absorption) must be inserted into core during the first cycle.

(Terradas, 2009) also stated that, "the boron concentration for three loop Westinghouse design at the BOC is roughly 1700ppm, while the boron concentration varies among the different PWR designs, with some designs having a boron concentration of 2000ppm, 2200ppm, or even 2500ppm", (Terradas, 2009)**.**

Whilst the current study is a neutronic study and not a thermos-hydraulic study, the value of the boron concentration used can be used as a comparison to give confidence in the neutronic boron studies carried out in the current study. There is no claim to validate the current study with the studies of (Terradas, 2009) but rather to give confidence in the methodology that is being developed.

CHAPTER 4: METHODOLOGY

In this chapter, methods and procedures that are used to build the NA PWR FC models, with and without water nodes, are presented. The first section presents the NWURCs description and command sequence. The second part presents the input file descriptions for T-NEWT, NESTLE and MCNP-6.2. The last section presents all the methodology developments and steps that are used to build the FC model, using all the codes mentioned in this study.

4.1 Specifications

A Lenovo IdeaPad Laptop computer was used to run the codes in this study. It had the following properties: Windows 10 Home Single Language, 64-bit Operating System x64-based processor, 20 GB RAM, Intel(R) Core (TM) i7-8750H CPU @ 2.20 GHz 2.21 GHz processor (6 cores and 12 logical processors).

The text and source code editor, Notepad++, was used for the input editing for the codes.

4.1.1 Calculation sequences

The main goal of this study is to obtain a multigroup neutronic calculation chain to model the full core of the NA PWR. This consists of two parts, the lattice calculation, and the core calculation.

1. Lattice Calculation

   This calculation entails the following:

   - Calculate number densities and atomic fraction for model inputs and verify the calculated results.
   - Build a FA model in T-NEWT with and without water nodes, to obtain the homogenized few-group cross-sections flux data, and the multiplication factor, which is verified with those generated by NWURCS.
   - Extract nuclear data from T-NEWT, using NWURCS to create an input file for NESTLE.

2. A Full Core Model

   This calculation entails the following:

   - Develop FC MCNP model, with and without water nodes.

- Develop an FC NESTLE model and compare results with the MCNP-6.2 full core model.

4.2 NWURCS description

Studies by various authors (Nyalunga, 2016; Nyalunga, 2019; Sihlangu, 2016; Sihlangu, 2019), and (du Toit, 2017) have used NWURCS to generate input files for their reactor systems. NWURCS has not yet been used at the NWU to generate FC input files for use in NESTLE. The main focus of this study is to generate an FC model using both a deterministic nodal method and a stochastic method.

As mentioned in section 3.10, the NWURCS code was used in this study to generate the INP files for T-NEWT, MCNP-6.2 and NESTLE. NWURCS requires the following input to create these input files (Naicker, 2022)**:**

1. FA layout;
2. Core layout (fuel assembly, reflector, reactor pressure vessel, etc);
3. Temperature profiles;
4. Material specifications;
5. Cross-section library; and
6. Running parameters (number of sources points, number of active cycles, etc).

The parameters and material specifications used by NWURCS to generate the particular input files are obtained from Table 2-2, Table 2-3, and Table 5-2.

The material specifications, material temperatures, abundances, water densities and ENDF/B-VII.1 cross-sections are defined in the NWURCS input folder: '.\ixxxxx\...'.The inputs from the folder'.\ixxxxx\...' need to represent the structural reactor geometry and dimensions. The geometry specifications defined as specific levels with NWURCs are discussed next.

4.2.1 The NWURCS nested structure levels

NWURCS works by defining volumes, surfaces, lattices, and materials. It is structured to make the process of creating an input file for a calculation (such as that of a FC) easier and more time-efficient, for codes such as SERPENT, KENO-VI, MCNP-6.2, and T-NEWT.

It is designed to have a nested structure system, that consists of three levels, to form the input of the type of reactor studied. The NWURCs nested structure is illustrated in Figure 4-1. The

first level consists of the data and parameters needed for the core layout. The second level is assigned to data regarding the FA layout and the last level is assigned to the FP.

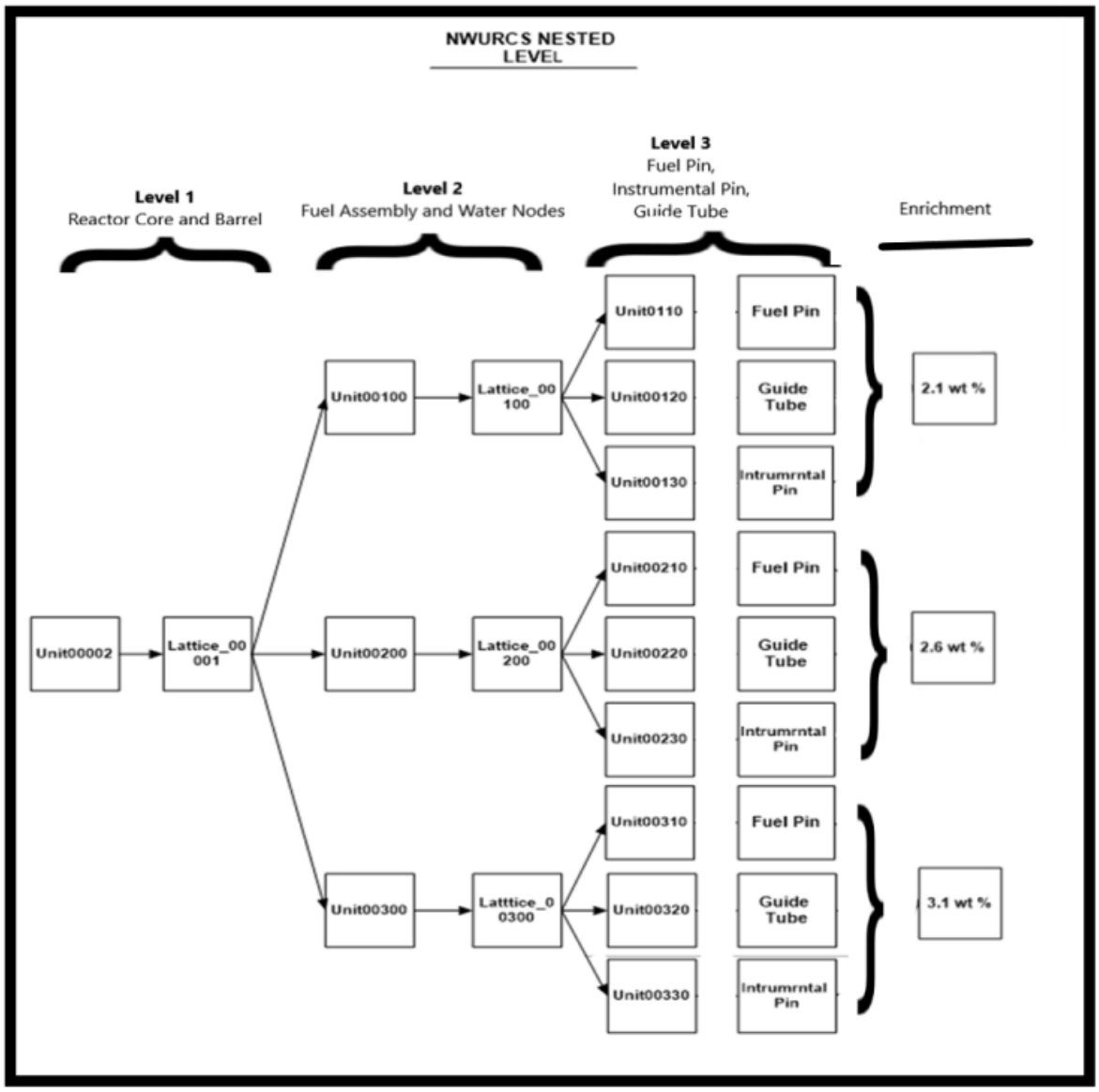

Figure 4-1: NWURCS nested structure

- **Level 1**

In the **input** package that is supplied by the NWURCS developer, the starting file is '.\ixxxxx\f007_01. i'. The NWURCS starting unit file is '.\units_da1\unit00002.da1'. In this file, the number of volumes, the type of each volume, its associated geometry and its temperature index are defined. This file leads to a lattice file '. \lattices_da1\lattice00001.i', which consists of the full core lattice structure. The lattice file '. \lattices_da1\lattice00001.i' consists of fuel assembly unit file numbers. There are three numbers representing the three enrichments.

In the file '.\lattices_da1\lattice00001.i', the 3.1wt% enrichment is expressed by unit 300 which is the unit file '.\units_da1\unit00300.da1'. The 2.6wt% enrichment is expressed by unit 200 which is the unit file '.\units_da1\unit00200.da1' and the 2.1wt% enrichment is expressed by unit 100 which is the unit file '.\units_da1\unit00100.da1'.

- **Level 2**

Units '.\units_da1\unit00100.da1.', '.\units_da1\unit00200.da1.', and '.\units_da1\unit00300.da1.' are the foundation for the second level in NWURCS. Consider unit 300: '.\units_da1\unit00300.da1'. Unit file ['.\units_da1\unit00300.da1'], leads to a lattice file '.\lattices_da1\lattice00300.i', which consists of a Fuel Assembly lattice structure.

In the file '. \lattices_da1\lattice00300.i', the fuel unit cells of the FA are expressed by unit 310 which is the unit file '.\units_da1\unit00310.da1'. The guide tube unit cells are expressed by unit 320 which is the unit file '.\units_da1\unit00320.da1' and the instrumentation pin unit cell is expressed by unit 330 which is the unit file '.\units_da1\unit00330.da1'].

- **Level 3**

Units '.\units_da1\unit00310.da1', '.\units_da1\unit00320.da1', and '.\units_da1\unit00330.da1', are the foundation for the third level in NWURCs. In the units, no further lattices need to be defined since this is the deepest level.

By focusing on unit 310: '.\units_da1\unit00310.da1', four volumes within the unit are defined which constitute the fuel pin unit cell structural arrangement. The FP consists of the fuel pellet, the helium gap, the zircaloy clad, and the moderator.

Unit 320 and 330 define the guide tubes and instrumentation pins, respectively. They both have the same geometry for empty instrumentation pins consisting of three volumes: inner moderator, guide tube and outer moderator.

Once the material input is defined in the '.\ixxxxx\inputmat' file, the structural geometry and dimensions are defined in the unit files in the folder: '.\units_da1\.', and the lattice structures are defined in the lattice files in the folder '.\lattices_da1, then a sequence of commands is performed in the command window to generate the input files, calling the specific codes in NWURCS. The NWURCS command prompt for the different codes is shown in Table 4-1.

Table 4-1: NWURCS command input (Naicker, 2022)

	Command-prompt input	Command Description
A	**cd**	Change to root directory
B	**cd 0_tr**	Change to c:\0_tr folder
C	**cd m001**	Change to c:\0\m001_tr folder In this folder m001 (folder location name), input changes are made to the following files: - .\unit****.da1 - .\lattice***.da1 - .\ixxxxx\f004.i - .\ixxxxx\f005.i - .\ixxxxx\f006.i
D	**Generateinput.bat** (Current version of NWURCS used by the user was provided in 2021_10_20)	This batch file creates a set of input files and codes used in NWURCS. The generated codes called in this batch file include: • la_sep2021: Writes input description in [.\oxxxxx] • le_sep2021: Prepare the material library • li_sep2021: Obtain the list of da1 files • lb_sep2021; Converts [.da1] files to [.da2], write out in terms of x0, y0 and z0 • lf_sep2021: Calculation of axial discretization, writes file [.\ioxxxx\f052.io] • ag_sep2021: Axial discretization: da2 > da3 • lm_sep2021: Discretize nodes in xy plane and assign ijk: da3 > da4 • mb_sep2021: Set tally switches in lattice and da4 files • mi_sep2021: Updates runparameters.io • ml_sep2021: Sets boundary condition • mk_sep2021: Moves controls rods as required • mm_sep2021: copies file f083.i and f007*da4 files as base files • mq_sep2021: converts ADF switches as required.
E	**Ls_sep2021**	Creates runn2.bat input for T-NEWT
F	**Runn2.bat**	Creates the T-NEWT input files, and runs T-NEWT, while it copies the input and output files to.\newtio. Output files in .\iter01\nontax are also generated.
G	**Lr_sep2021**	Prepares the RELAP5-3D input for NESTLE calculations only. This command initiates: • Lp_sep2021: It extracts collapsed data from NEWT • Lt_sep2021: It creates maps for NESTLE
H	**Runr.bat**	Run batch file for RELAP5-3D
I	**Lc_sep2021**	Create M/K/N/S input. (M = MCNP-6.2; K= KENO-VI; N = NEWT; S = SERPENT) The Lc_sep2021 command is used immediately after generatinput.bat for MCNP calculations.
J	**Runm.bat**	Run batch for MCNP-6.2 calculations. This will create output files in the c:\0_tr\m001\iter01\mcnpxxx folder.

K	**mh_Sep2021**	Creates runm2a.bat to run many calculations for the tally field in MCNP-6.2. In the case of running tally calculations, the mh_sep2021 command is used immediately after Lc_sep2021, to create runm2a.bat.
L	**runm2a.bat**	Run batch for MCNP-6.2 tally calculations to run. In the runm2a batch file, mj_sep2021 and la_sep2021 are called, and runm2b.bat is created.
M	**md_sep2021**	Extract fluxes from MCNP output
N	**Me_sep2021**	Converts MCNP Tally Data

It should be noted that, for each model advancement, development, addition, and change made in the input models, NWURCS is modified and re-programmed by the developer.

If any errors are found in one of the command sequences, an error is displayed on the command line explaining where the problem is, before proceeding to the next executable command (Nyalunga, 2016). Therefore, the errors detected within the code by users are reported, so that NWURCS can be re-programmed where applicable. It is possible however, that there can still be errors made by users in building the input which the programmer did not foresee.

In this study, starting with the first version of NWURCS - Version 3 that was given to the user, eight updated versions of NWURCS-Version 3 have been used by the user. The latest version used to model the results presented in this study was provided in 2021_10_20 - NWURCs Version 3.1, Beta (Naicker, 2021, December). Since this is a 'Beta Version', constant communication between the user and the developer is sustained to enable NWURCS user efficiency.

4.3 T- NEWT input – SCALE-6.2.3

T-NEWT provides significant functionality to support lattice-physics calculations, including cross-section homogenization and collapsing, and calculation of assembly discontinuity factors. To perform a SCALE calculation, an analytical sequence is selected which is characterised by the type of analysis to be performed, such as criticality or shielding.

4.3.1 T-Newt structural input

The T-NEWT input file contains a nuclear data library name within the title block, a material composition block, a cell data block, a parameter block, a geometry definitions block, a broad-group collapse block, a homogenization instructions block, an assembly discontinuity factors

block, a boundary condition block, and an array specifications block. T-NEWT runs two modules, XSProc and NEWT.

Section 4.3.1.1 discusses the nuclear data library and the material composition required for the model. Section 4.3.1.2 discusses the XSProc required input, and 4.3.1.3 discusses the NEWT required input. The complete T-NEWT input file layout is presented in section 7.1 of the Appendix.

4.3.1.1 Nuclear data library and material composition definition

(a) **Nuclear data library definition**

The ENDF/B-VII.1 nuclear data file is included in the SCALE-6.2.3 package. The multi-group neutron libraries are available in both 252 and 56-group configurations, with the 252-group library being designed for general-purpose reactor physics and criticality safety applications and the 56-group library being designed for light water reactor analysis (Rearden & Jessee, 2018). These libraries have been generated using a new weighting spectrum with improved resonance self-shielding procedures. The type of nuclear library that is used is defined in the title card as ‘V7-252’.

(b) **Material composition definition**

In the T-NEWT input file, the material data was specified for each mixture (or compound) in the composition block. In the composition block, the material name, number, and temperature are defined. The input manual of SCALE-6.2.3 gives a detailed description of the input parameters, which is essential to the user when preparing input. However, since the exact text must be followed, the description is not repeated here and the interested reader is referred to section 7.1.3.3 of the input manual (Williams, et al., 2018).

An example of the T-NEWT Base-Model input file is presented in section 7.1 of the Appendix. The apostrophe ['] in the T-NEWT input file is used to address a comment and it is ignored during the calculations.

4.3.1.2 XSProc definitions

For all sequences that employ XSProc, the title, cross-section library name (multi-group cross-sections), and the READ COMP input block are needed. The XSProc parameters are defined in the Celldata block, which provides the unit cell descriptions that are only used for multi-group self-shielding calculations. The Celldata block contains the LATTICECELL description

which is assigned for the self-shielding calculations of arrays of repeating cells, such as the fuel assembly lattice. This provides accurate problem-dependent cross-sections. The NA PWR has a square grid geometry, and so, a regular fuel cell input geometry setup is used, where the central region is fuel, surrounded by a gap, a clad, and an external moderator. The NA PWR core consists of three types of fuel assemblies which differ only by fuel enrichments, as described in section 2.2.2. For a given fuel assembly, the fuel enrichment is the same. Therefore, three T-NEWT input file calculations were performed, corresponding to these three fuel assemblies, each with a different fuel enrichment. In each input, one LATTICECELL data information was defined according to the enrichment.

As mentioned in section 4.3.1.1, the input manual of SCALE-6.2.3 gives a detailed description of the input parameters and the interested reader is referred to section 7.1.3.5 of the input manual (Williams, et al., 2018).

During the calculation execution process, the TRITON sequence calls XSProc, and the deterministic multi-group code NEWT (the 2D deterministic transport code). XSProc reads the cross-section data from the ENDF/B-VII.1 data files and calculates the flux distribution in the geometry of the pin cells. Using these fluxes, it then compresses the cross-sections into 252 groups.

4.3.1.3 NEWT input

The Newt input consists of the following blocks: material, parameter, collapse, homogenization, assembly discontinuity factors, geometry, arrays, and boundary conditions.

4.3.1.3.1 The material block

The composition block must be accompanied by the Material block when running NEWT. The data under READ MATERIAL is defined in the following format: the mixture number (M), the scattering order *PN*, an embedded comment (com=) and the terminator (END). For the value of *PN*, 1 is assigned to any material in the composition and 2 is only assigned for water.

4.3.1.3.2 The parameter block

The Parameter block contains the problem control parameters which commands NEWT on what to calculate and print out in the output file (Jessee & DeHart, 2018). The type of parameters used in this study are mentioned in the input file layout in section 7.1 of the appendix.

4.3.1.3.3 The collapse block

In the collapse block, a broad group is assigned to each fine energy group. The calculations for this part of calculation chain are performed using the 252-energy-group library produced in XSProc. The 252-energy-group library is collapsed into two groups, where the first group is collapsed from the first 213-groups and the second group is collapsed for the remaining 39-groups.

4.3.1.3.4 The homogenization block

In the homogenization block, NEWT is used to calculate the broad-group cross-sections in terms of the FA as a single node. These are written as microscopic cross-sections for each nuclide present in the input mixture.

4.3.1.3.5 Assembly discontinuity factors (ADFs)

The specification of the ADFs in terms of lattice boundary at which they must be calculated are specified in the *read adf* data block.

4.3.1.3.6 Geometry definition

The geometry block contains all the geometric descriptions for all bodies included in the model. Since the reactor that is being studied is that of a PWR design, the structural bodies being investigated are cuboids and cylinders. The geometric arrangements in NEWT are based on a fundamental building block called a unit (A *unit* is defined as a collection of shapes, one of which must be defined as the unit boundary) (Jessee & DeHart, 2018).

The units of the geometry are combined in rectangular arrays (an array is used as a method for arranging one or more units within another unit), or they can be inserted in other units and can be completely enclosed by the next single larger unit. For a fuel assembly model, the largest unit is a global unit, which forms the outer boundary for the entire problem.

The final section of a unit description is the *boundary* specification. This input record serves two purposes: to specify the shape that defines the outer bounds of the unit, and hence the shape of the unit, and to specify the underlying grid associated with the unit.

4.3.1.3.7 Boundary conditions

The *geometry data* block is followed by the *bounds* data block, in which boundary conditions for the sides of the bounding shape in the global array are specified.

The boundary conditions are used to reduce the problem to a tractable size while modelling the action of the outside domain on the particles that leave the domain (Sanchez, et al., 2002). The boundary condition used in this study is the reflective boundary specified for the ±x and ±y faces of a boundary cuboid. For the reflected boundary condition, the reflection angle of the reflected angular flux is set equal to the incident angle of the angular flux incident on the boundary from within the cell (Jessee & DeHart, 2018).

$$\psi_{in}(\mu) = \psi_{out}(-\mu). \quad (4\text{-}1)$$

Array placement definition

Arrays specifications are typically used when units are placed in a repeating pattern. The array placement operator is used to locate an array within a unit (Jessee & DeHart, 2018).

Detailed description of input

Similar to that as mentioned in section 4.3.1.1, the input manual of SCALE-6.2.3 gives a detailed description of the input parameters associated with all the NEWT input blocks listed above and the interested reader is referred to section 9.2.3 of the input manual (Jessee & DeHart, 2018). Examples of the NEWT input blocks are presented in section 7.1 of the appendix.

4.3.2 T-Newt commands in NWURCS

From Table 4-1, the commands shown below are entered in the command window to produce the T-NEWT input. files

[A] cd\	B] cd 0_tr	[C] cd m001
[D] Generateinput.bat	[E] Ls_sep2021	[F] Runn2.bat

Between items [C] and [D], relevant changes are made in the NWURCS input files. Thereafter the generateinput.bat command from item [D] is entered in the command window. Item [E] is entered next to create the T-NEWT input file in the folder '…\newtio\.'. When item [F] is entered, T-Newt runs, and it produces the T-NEWT output files in the folder '. \iter01\newtxxxx'. The results of the output file in the folder '. \iter01\newtxxxx' are analysed and relevant data is extracted to be used for the NESTLE input file.

4.4 Method of preparation of the NESTLE tt1.i input file

The NESTLE tt1.i input file is generated by NWURCS. NWURCS runs the NESTLE calculations directly after the T-NEWT output files have been generated and stored within the NWURCS library folders. The following commands are used to generate the NESTLE input according to Table 4-1.

[G] Lr_jul2021 [H] Runr.bat

These Nestle commands are entered after the T-NEWT commands, discussed in section 4.3.2. When item [G] is entered, the homogenised few-group cross-section (XS) generated by the T-NEWT output files are extracted and are printed out in folder '. \xscoll\.'. Then the NESTLE input file 'TT1.i' in file '. \iter01\relapxxx\tt1.i' is generated which uses the homogenized data from '.\xscoll\.' folder. Then item [H] is entered to run file 'ttl.i'.

4.4.1 NESTLE input

The NESTLE input ttl.i is described in terms of cards. The input consists of a title card, an optional comment card, the job control and time step control cards, the data cards, and a terminator card.

The input file TT1.i is presented in section 7.3 of the Appendix, where the data cards, such as the problem type; time step control; hydrodynamic components; core heat structure; general table data; heat structure thermal property data, neutronic core layout, cross section definitions, mapping of temperatures from the thermodynamic calculation to the neutronic calculation, and the reactor kinetics input cards, are found.

As with the input for SCALE-6.2.3, a detailed description of the input parameters for NESTLE is also given in the Relap5-3D input manual (RELAP5-3D Team, 2014) and the interested reader is referred to sections 1.3 to 1.7 of the input manual. It is not meaningful to summarize the instructions here, since exact adherence to the input instructions is required in order for the code to run without errors.

It should be noted that in the input file tt1.i, the cards identification are specified by numbers. Using these numbers, the information about a specific card may be obtained from the manual, as it helps interpret the code from the data entered on the card. The cards are arranged by increasing card numbers in input ttl.i.

4.5 The MCNP-6.2 INP01 input file

The sequence that is followed when generating the MCNP-6.2 input file INP01 is given in Table 4-1.

To run MCNP using NWURCS, items [A] to [B] are entered in the command window.

[A] cd\	B] cd 0_tr	[C] cd m001
[D] Generateinput.bat	[I] Lc_jul2021	[J] Runm.bat

Changes to the MCNP INP01 file are made after item [C] is carried out, before entering item [D], the generate.bat command. Item [D] generates the inputs according to the defined specifications and changes made after item [C]. Then command from item [I] creates the MCNP INP01 input file. Item [J] is thus used to run the INP01 input file.

The generated outputs files are printed in the folder '.\iter01\runmcnp6.'. The results of these outputs are discussed and compared with those generated by the T-NEWT/NESTLE FC model in Chapter 5.

4.5.1 MNCP-6.2 input file layout description

The NWURCS code is used to generate the MCNP6.2 INP01 file. The MCNP6.2 INP01 file begins with a message block which is used to give MCNP an execution command (message). Three sections proceed after the execution command.

The first section consists of the cell definitions, in which the volumes and materials of each cell is defined. The lattices for nested levels are also defined in this section.

The second section defines all the surfaces used for the geometry. These consists of planes, cylinders, and cuboids.

The third section defines the material definitions and other input such are the number of source points, the number of inactive and active cycles and the tally definitions.

As with the input for SCALE-6.2.3, a detailed description of the input parameters for MCNP6.2 is also given in the (Werner, 20217) manual and in the (Shultis & Faw, 2011) primer. The interested reader is referred to Chapter 2 and 3 of the input manual.

4.6 Model development of the North-Anna FA and FC calculations

4.6.1 Model assumptions

The FA and FC calculations of the NA PWR, which include the water node models were performed, based on the assumption that the control rods are fully withdrawn from the PWR system. This is done so that simpler critical calculations may be performed to analyse the neutron interactions, multiplication factor, the cross-sections and the flux within the core and the surrounding reflector region. This is in line with the scope of the project that methodology is to be developed, and therefore, the simpler system must be modelled and tested before proceeding to more complicated systems.

The assumptions are as follows:

- The study is based on a fresh fuel model at beginning of cycle BOC; therefore burn-up calculations are not included in the study.
- The gap between the cladding and UO_2 fuel is filled with helium.
- For the T-NEWT calculations, a homogeneous material is assumed for the reflectors.
- No change in boron in the water is assumed during the neutronics analysis.
- The top and bottom nozzles (of the FAs), as well as the spacer grids, are not modelled.
- The outer boundary of the model is at the outer surface of the core barrel (for the MCNP-6.2 FC calculations.

4.6.2 North-Anna fuel pin and fuel assembly model using T-NEWT

Though NWURCS can generate input files for the SCALE-6.2.3, MCNP-6.2 and RELAP codes, it still needs to be verified. Hence, T-NEWT inputs were manually generated by the users for verification purposes.

T-NEWT model development:

- **Step 1:** Firstly, the NEWT4.inp sample file which had a one-quarter assembly structure was used. Using NEWT4's input layout, a fuel pin input model was developed, as this was the simplest input model to construct.

It should be noted that the SCALE_6.2.3 package is a verified and validated licenced package, thus the samples provided by the SCALE developer have been validated before distribution. Therefore, the NEWT4.inp and NEWT5.inp sample examples provided from the package were used as a template for the input syntax, providing a calculation overview and starting point for the FA base-model input.

The NA PWR geometrical dimensions and material composition specifications provided in Table 2-3, were modified into the composition, material, celldata, and geometry blocks of the input file model. Fuel pin calculations for all three individual enrichments which had a pellet, clad, gap and moderator were performed.

- **Step 2:** To reduce model complexity, a fuel assembly which consisted of only fuel pins was developed. The 17×17 lattice array and boundary conditions were defined in the input. The fuel assembly pitch dimensions were also specified in the geometry, array, and boundary blocks. Therefore, the input consisted of 289 fuel pins unit cells in the lattice array.

- **Step 3**: A model with an instrumentation pin in the centre of the lattice array was developed according to NA specifications from Table 2-3. The data for the instrumentation pin was defined in the composition, material, geometry and in the array blocks. Once the model ran to completion, then 24 guide tubes were added to the input, and thus the lattice array consisted of a single instrumentation pin, 24 guide tubes, and 264 fuel pins.

- **Step 4:** A gap around the assembly was added to the input file, as stated in NA FSAR. Once the model ran to completion, the homogenization, collapse and ADF blocks were added to the input, along with the modelling parameters from section 4.3.1.2, to create the desired base-model (BM) input file. Three BM calculations of the NA PWR fuel assembly were conducted, for the three different enrichments as seen in Figure 4-2.

- **Step 5**: Using the 3.1 wt% enrichment FA base-model input file as well as the NEWT5 input sample, a calculation with a reflector (water node) was conducted, as seen in Figure 4-3. The actual implementation of the T-NEWT NA fuel assembly base-model development is presented in Appendix B in section 7.1.

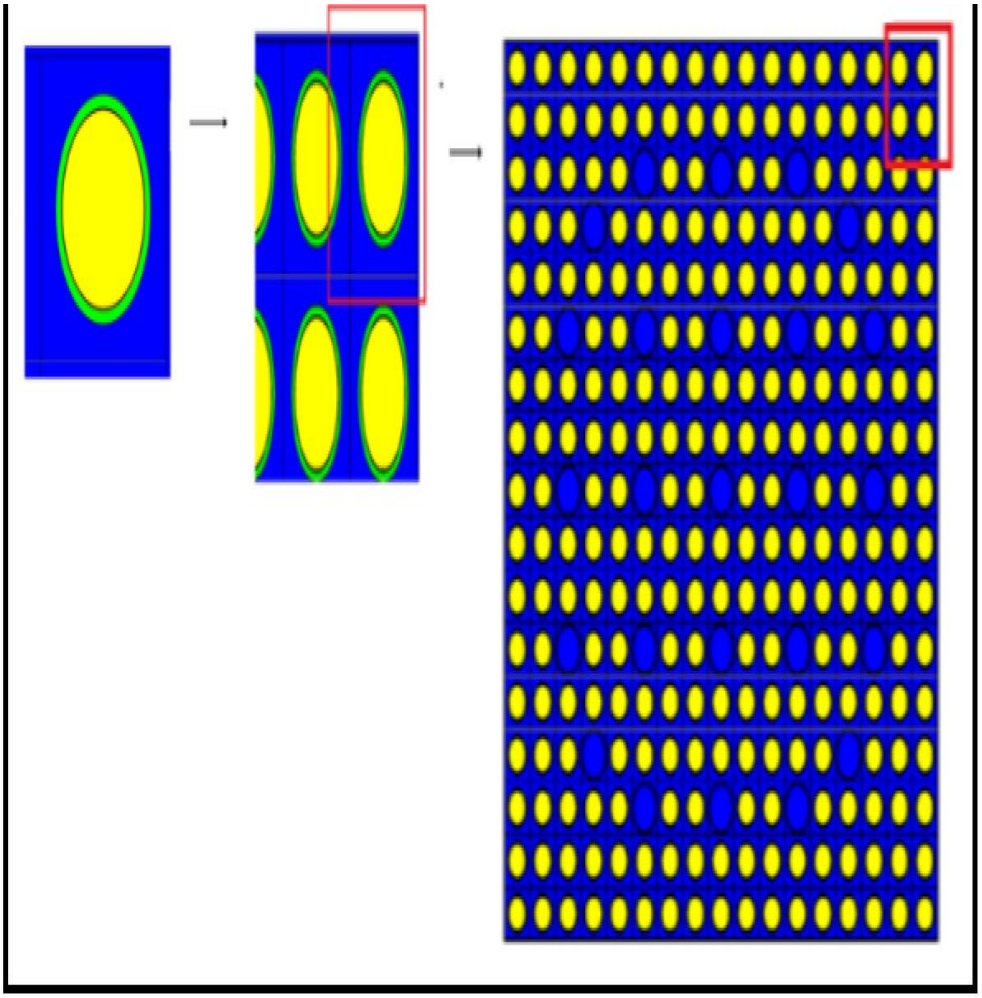

Figure 4-2: Fuel assembly with gap model

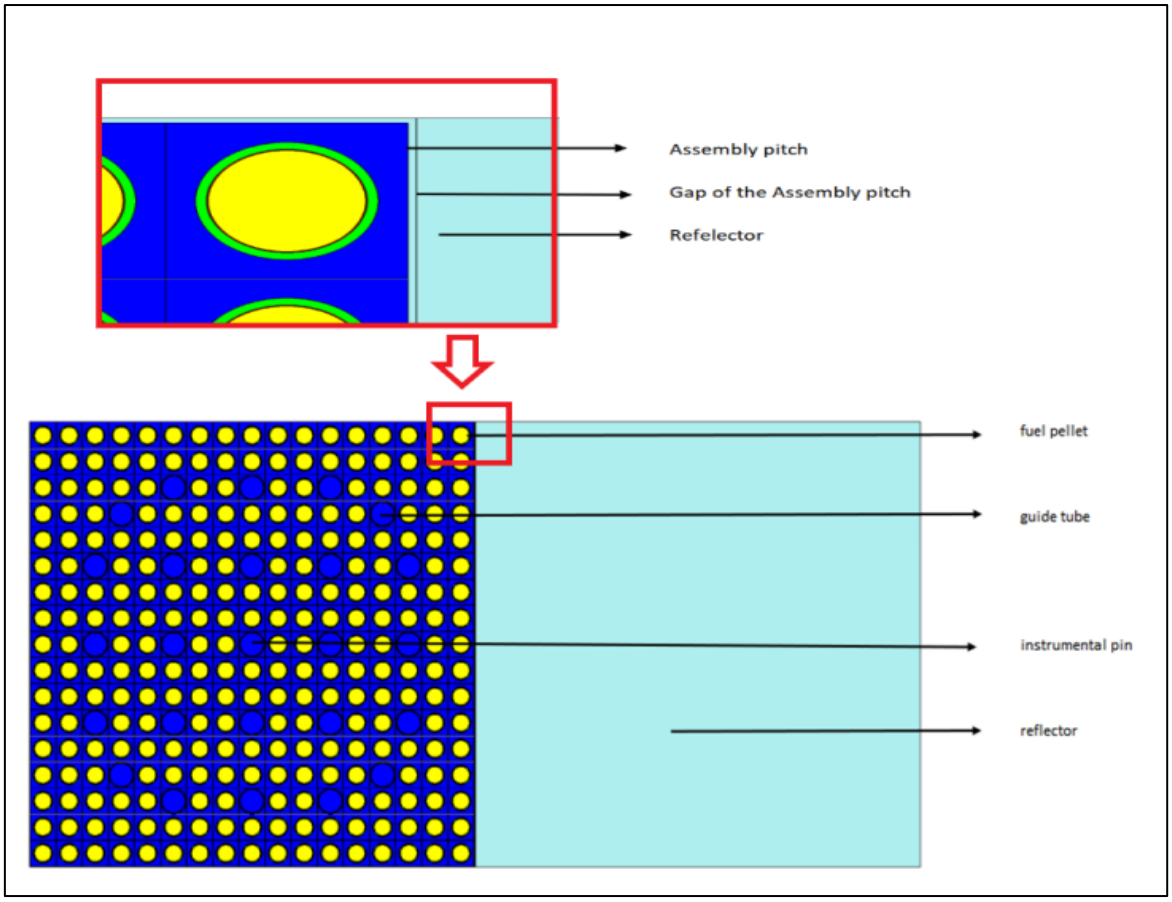

Figure 4-3: Base-model development

4.6.3 Verification method of NWURCS and T-NEWT

Firstly, the verification of the NWURCS code was performed by comparing the manual calculations that were computed by the user, to obtain the number densities and atomic fractions of the materials that are used in the FA and FC models, to those computed by NWURCS. The material specifications were obtained from the FSAR (VEPCO, 2016). An Excel spreadsheet was created to confirm that the calculations were in agreement.

The equation used for calculating the number (atomic) densities in the Excel spreadsheet is given by the formula below (Nyalunga, 2016):

$$N_i = \frac{\rho \cdot N_A \cdot W_i}{A} \qquad (4\text{-}2)$$

Where:

ρ is the molecular density of the compound in $\left(\frac{g}{cm^3}\right)$;

N_A is Avogadro's number (0.6022 $\frac{atoms \cdot cm^2}{mol \cdot barn}$);

W_i is the weight fraction of each element in the compound; and

A is the atomic weight of the compound.

To obtain the atomic fraction f for each element, the number density of each element is divided by the total number density N_T (Nyalunga, 2016) (to obtain the atom density of the compound, all the values of the atom densities of each element are summed);

$$f = \frac{N_i}{N_T} = \frac{N_i}{\sum_{i=1} N_i} \tag{4-3}$$

Once the atomic fractions were computed, the percentage difference, % $diff$, between the manual calculations conducted by the user with the data (fractions) generated by NWURCs was obtained by using Eq.(4-4). The results are discussed in sections 5.2.1. The % $diff$ was calculated using:

$$\%diff = 100 \, \frac{(A - B)}{\langle A, B \rangle} \tag{4-4}$$

Where:

A is the result obtained from a manually generated calculation;

B is the result obtained from NWURCS; and

$\langle A, B \rangle$ is the average of *A* and *B*.

Secondly, the input files generated manually by the user from T-NEWT, as well as the output files, were compared to the input and output files generated by NWURCS, which were obtained from ['…\newtio\...']. This was done to assess the accuracy of the NWURCs model, by proving that the models were equivalent to each other.

The NWURCS code allows the user to describe each section of the T-NEWT INP file separately, making it easier for the user to navigate through each section to confirm whether any errors have been made before even running the calculations (Nyalunga, 2016). The T-NEWT capability is limited to only FA calculations, and in this system, the FA is modelled as a repeating lattice, extending to infinity, using reflective boundary conditions. It was assumed

that there was no neutron leakage, therefore, the infinite multiplication factor k_{inf} was used and it was defined as the ratio of the neutrons produced by fission to the number of neutrons lost through absorption in a generation.

4.6.4 North-Anna full core models for MCNP-6.2 and T-NEWT/NESTLE

MCNP-6.2 and T-NEWT/NESTLE were used to develop the FC model of the NA PWR. The MCNP-6.2 INP01 and the NESTLE TT1.i files were generated by NWURCS, and therefore NWURCS input files were checked to verify if the code produced accurate results, as both codes use the same geometry and reactor information. In both models, an isothermal temperature of 300 K was used for all structural components. Control rods were not modelled, and there was no boron in the coolant. It should be noted that the user-generated manual input models for MCNP-6.2 and NESTLE were not created (as it was carried out for the T-NEWT models, therefore the FC models generated by MCNP-6.2 INP01 and NESTLE tt1.i had to be verified using other methods. Amongst these was specifically comparing the multiplication factor of both codes.

To carry out the comparison, the differences were calculated in terms of the unit for reactivity *pcm* as defined by Eq. (3-36). However, with k_{eff} close to one, an approximation can be used, given in Eq.(4-5) and Eq.(4-6).

$$\left(k_{Mcnp} - k_{critical}\right) \times 100000\, pcm \tag{4-5}$$

And

$$\left(k_{NESTLE} - k_{critical}\right) \times 100000\, pcm \tag{4-6}$$

4.6.4.1 FC model verification: Error in NESTLE

The geometry and reactor specifications entered in the initial MCNP-6.2 and NESTLE models generated by NWURCS, had a difference in k_{eff} of 4832 *pcm*, as seen in Table 4-2. This difference between the codes was high.

Table 4-2: Initial MCNP-6.2 and NESTLE comparison of 1st Version of NWURCs 3.1

	MCNP k_{eff} & σ (STD)	**NESTLE k_{eff}**	**Difference**	**pcm**
k_{eff}	1.32786 ±0.00019	1.27954	0.0482	4832

By going through the INP01 and tt1.i files, the cause of the large difference between the input files was found. An error was detected in the original initial NESTLE tt1.i file. NWURCS extracts the homogenized cross-sections from the T-NEWT output file as seen in Figure 4-4. Although the extraction process was successful, the cross-sections were arranged incorrectly in file '…\scold\xs_collapsed_00001 to …\xscoll\xs_collapsed_00004' and in the tt1.ifile.

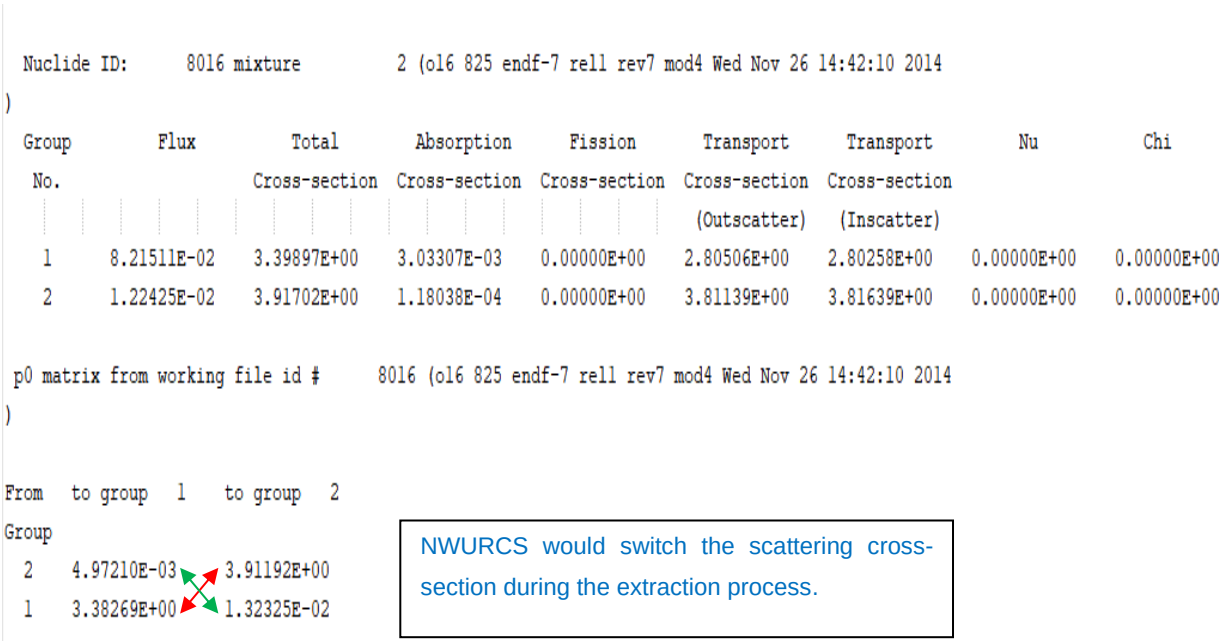

Nuclide ID: 8016 mixture 2 (o16 825 endf-7 rell rev7 mod4 Wed Nov 26 14:42:10 2014
)

Group No.	Flux	Total Cross-section	Absorption Cross-section	Fission Cross-section	Transport Cross-section (Outscatter)	Transport Cross-section (Inscatter)	Nu	Chi
1	8.21511E-02	3.39897E+00	3.03307E-03	0.00000E+00	2.80506E+00	2.80258E+00	0.00000E+00	0.00000E+00
2	1.22425E-02	3.91702E+00	1.18038E-04	0.00000E+00	3.81139E+00	3.81639E+00	0.00000E+00	0.00000E+00

p0 matrix from working file id # 8016 (o16 825 endf-7 rell rev7 mod4 Wed Nov 26 14:42:10 2014
)

From to group 1 to group 2
Group
2 4.97210E-03 3.91192E+00
1 3.38269E+00 1.32325E-02

NWURCS would switch the scattering cross-section during the extraction process.

Figure 4-4: T-NEWT Cross-Sections

Figure 4-4 presents the cross-section arrangement of the T-NEWT output. NWURCS extracts both group1 and group 2's total cross-sections, the absorption cross-sections, and the macroscopic scattering cross-sections. During the extraction process, NWURCS swapped the macroscopic scattering cross-sections data and arranged them incorrectly in the NESTLE TT1.i file. More details are given in section 5.2.2, while the proper arrangement that had to be followed, is given in section 7.3 of the appendix, specifically the section on the Neutron Base Cross-Section Data - Card 32CCCC0GN.

4.6.4.2 FC model verification: Incorrect axial dimensions and CB material used in MCNP

The input initially generated by NWURCS specified incorrect core height and core barrel dimensions. Using Table 2-2 and Table 2-3, the correct dimensions of the core barrel with an outer radius of 175.1825 cm, inner radius of 170.0213 cm and the core height of 364.998 cm were entered in the NWURCS file .\units_da1\unit00002.da1.

The initial input was also using the incorrect core barrel (CB) material. The CB material used in the initial model was that of Ag-Cd-In, which is a designated CR absorber material. From the FSAR (VEPCO, 2016) the CB material should be Stainless Steel – 304 (SS-304). The change in CB material caused k_{eff} to increase. The Ag-Cd-In material has a higher neutron absorption cross-section, while the SS-304 has a lower absorption cross-section. According to Eq.(3-39), the larger the absorption cross-sections, the lower the value of k_{eff}. So, replacing the CB material with material that has a lower absorption cross-section, would increase k_{eff}.

To further substantiate the effects of the CB on k_{eff}, more tests were done to test whether there were significant changes in k_{eff}.

The core barrel (CB) tests were divided into the following subsections:

A. No CB present;

B. CB changed to that of helium;

C. Change in the thickness of the CB material; and

D. Water is used as the material for the barrel.

The actual implementation of the NESTLE and MCNP-6.2 NA fuel core base-model development is presented in section 7.5 of the appendix.

4.6.4.3 NWURCS Version 3.1

NWURCS is still under development and is currently always released as a 'beta' version. New modifications are always added to the system by the developer. The results presented in Table 4-2 were generated from the NWURCS code given in 2020_10_09, which operated with files created in July 2020. Work was done to verify that the correct material compositions, material densities and that all structural components had the correct dimensions and material allocations. The 6th modification of NWURCS 3.1 after the 2020_10_09 release, given in 2021_04_15, was run with the modified files created in July 2020. Calculations from this version produced a 917 *pcm* difference between the MCNP and NESTLE calculations as seen in Table 4-3. In this version, the error obtained by the user in the NESTLE code presented in section 4.6.4.1 had been rectified by the developer (refer to section 5.2.2).

Table 4-3: MCNP and NESTLE comparison 5th Version of NWURCs 3.1

	MCNP $k_{eff} \pm \sigma$	**NESTLE k_{eff}**	**Difference**	**pcm**

k_{eff}	1.32786 ± 0.00020	1.31869	0.00917	917

It was later discovered that the calculations from the 2021_04_15 NWURCS 3.1 version were also incorrect, as the core layout coded in ['.\lattices_da1\lattice_00001.i'] was arranged incorrectly. The core layout had four more FA's with 3.1 wt % enrichment as seen in Figure 4-5. By having four extra FAs with a high enrichment, the value of k_{eff} will therefore be higher.

```
1     1     1     1     1     1    16    16    16    16    16     1     1     1     1     1     1
1     1     1     1    16    16    16   300   300   300    16    16    16     1     1     1     1
1     1     1    16    16   300   300   300   100   300   300   300    16    16     1     1     1
1     1    16    16   300   300   200   100   200   100   200   300   300    16    16     1     1
1    16    16   300   300   200   100   200   100   200   100   200   300   300    16    16     1
1    16   300   300   200   100   200   100   200   100   200   100   200   300   300    16     1
16   16   300   200   100   200   100   200   100   200   100   200   100   200   300    16    16
16  300   300   100   200   100   200   100   200   100   200   100   200   100   300   300    16
16  300   100   200   100   200   100   200   100   200   100   200   100   200   100   300    16
16  300   300   100   200   100   200   100   200   100   200   100   200   100   300   300    16
16   16   300   200   100   200   100   200   100   200   100   200   100   200   300    16    16
1    16   300   300   200   100   200   100   200   100   200   100   200   300   300    16     1
1    16    16   300   300   200   100   200   100   200   100   200   300   300    16    16     1
1     1    16    16   300   300   200   100   200   100   200   300   300    16    16     1     1
1     1     1    16    16   300   300   300   100   300   300   300    16    16     1     1     1
1     1     1     1    16    16    16   300   300   300    16    16    16     1     1     1     1
1     1     1     1     1     1    16    16    16    16    16     1     1     1     1     1     1

Unit name | material specification      | number of units  |
Unit   1   | water node                  |     182          |
Unit   16  | water node                  |     65           |
Unit   300 | FA with 3.1 wt% enrichment  |     56           |  incorrect --> 52
Unit   200 | FA with 2.6 wt% enrichment  |     52           |
Unit   100 | FA with 2.1 wt% enrichment  |     49           |  incorrect --> 53
```

Figure 4-5: NWURCS lattice - Core layout

The error in the core layout was rectified, but this latest release kept overriding the correct core layout changes. Thus, an updated version of NWURCS 3.1 correcting this, was provided.

4.6.5 FC model verification: Investigations

Another reason that could have resulted in a large difference between the MCNP and T-NEWT/NESTLE calculations, could be a result of factors such as the environmental conditions between the T-NEWT/NESTLE calculations being different, and due to the coding effects, e.g., deterministic nodal diffusion calculations versus those of the stochastic Monte Carlo calculations since the T-NEWT/NESTLE calculation combination and that of the MCNP-6.2 calculation use two different computational sequences and algorithms.

Further investigations had to be conducted to determine the cause of the large difference between the codes. The investigation included the following:

1. Convergence of MCNP, T-NEWT and NESTLE calculations (explained in section 4.6.5.1);

2. Water node studies at the square boundary of the problem (explained in section 4.6.5.2);

3. Variations in boric acid concentrations (explained in section 4.6.5.4);

4. Flux data analysis (explained in section 4.6.5.3); and

5. Temperature variations of the fuel and moderator.

4.6.5.1 Convergence

4.6.5.1.1 Convergence in MCNP

MCNP calculations are converged in two ways. The first way is by ensuring that the source is statistically distributed over all fission sites before tallies of k_{eff} can be counted. This is determined by the parameter called the Shannon Entropy (SE), discussed in Section 3.5.3. The second way is conducted by running enough cycles so that k_{eff} becomes fairly constant, with a small standard deviation (statistical error).

Convergence of Shannon Entropy

The first convergence, that of the source, needs to be calculated from cycle to cycle, and when it approaches a constant value, then the source can be considered converged. This means, that for a given number of source points (NSRC is the neutrons per cycle), the number of cycles to be skipped should be varied until the Shannon entropy is constant.

Initially, the user defines the number of cycles to be skipped (these are called inactive cycles) and the number of fission source points. These are written in the NWURCs file '.ixxxxx/F005.i', which will insert them into the MCNP INP.01 file under 'KCODE', as the fission source points and the number of inactive cycles.

MCNP calculates the Shannon Entropy (SE) using Eq.(3-35). If the SE is not converged within the number of inactive cycles after the calculation, then a message is printed in the output file stating that the SE is not converged, as well as a recommendation for the number of cycles that should be skipped (inactive cycles). The user should then redo the calculation, with either more inactive cycles or the number of source points, or even increase both.

Convergence of k_{eff}

Convergence of k_{eff} is obtained for the active cycles (AC). Convergence, in this case, means that the statistical deviation (error) reaches a certain value (reducing the statistical error of the calculation). This can be achieved by changing the number of source points, the number of active cycles, or even both. Given the statistical nature of the calculation, the total number of active histories should be monitored, which is the product of the number of source points with the number of active cycles.

4.6.5.1.2 Convergence in NESTLE

To assess the convergence of k_{eff} in NESTLE, the major edit time function needs to be increased or decreased, to evaluate if the flux will reach a constant value. As the time increased, the flux decreased and the value of k_{eff} to became smaller. But both these parameters did not change significantly, and thus the NESTLE calculations were considered converged with the given parameters.

4.6.5.1.3 Convergence in T-NEWT

In T-NEWT calculation, many parameters contribute to the convergence of k_{inf}. However, studies by (Nyalunga, 2019) and by (Sihlangu, 2019) showed that only certain parameters within the T-NEWT calculation are significant. Therefore, in this study, only a few of those parameters from T-NEWT were used to test the convergence of k_{inf}, as the system used in this study is different from that of (Nyalunga, 2019) who tested the convergence on a VVER system, and (Sihlangu, 2019) who tested the convergence on a prismatic HTR. A more detailed study is recommended, as further work, that uses all the parameters for this type of system.

In T-NEWT, the convergence of k_{eff} is studied in terms of the grid structure dimensions. The global grid (GG) is given in integers (>2), and it specifies the number of rectangular cells to be placed in a global unit. The local grids (LG) specifies the number of rectangular cells to be placed in the other units in the x- and y- directions placed within the global unit (Jessee & DeHart, 2018). The more the GG and LG are increased, the more the k_{inf} is converged, but the more computational time is required. Therefore, the GG and LG were tested, to obtain an accurate (converged) value of k_{inf} at the optimal time. There would however be a limit on these numbers due to numerical constraints.

First, the T-NEWT base-model calculations were performed using the default value of the global grid dimension at $GG = 8 \times 8$ and the default local grid (LG) value of $LG = 4 \times 4$. The

convergence of k_{inf} in terms of grid dimensions was then studied by setting the GG and the LG to the following parameters: $GG = 16 \times 16; 20 \times 20; 32 \times 32; 48 \times 48; 64 \times 64$ and $LG = 8 \times 8, 12 \times 12, 16 \times 16, 24 \times 24$.

Convergence in T-NEWT was also established through defining (increasing) parameters in XSProc. The default value of N for the discrete ordinate's method S_N is 6. To obtain the convergence of k_{inf} for the S_N method, the following parameters were assigned to the N of the S_N method: $N = 4;\ 6;\ 8;\ 12$.

These parameters cause changes in the k_{inf} but will also cause changes in the homogenized cross-sections (such as the transport cross-section, the absorption cross-section, and scattering cross-sections) that are produced in the output file. Therefore, once the desired N value in terms of the S_N method as well as the $GG\ and\ LG$ parameters were obtained, and a model with those parameters were calculated, to compare the percentage difference ($\%diff$) of the calculated homogenized cross-section results with the T-NEWT BM results.

The $\%diff$ was obtained using the following formula:

$$\%diff = 100\frac{XS1_{16} - XS1_4}{XS1_{16}} \tag{4-7}$$

The same equation may be applied for the GG and LG calculations.

4.6.5.1.4 Error detected in NWURCS

There was an error detected in NWURCS. Input changes to S_N, GG and LG are done in file '.\ixxxxx\f005' in NWURCS. Once the T-NEWT input files from '.\iter01\newtxxxx\calc1.input' and '.\newtio\calc1_input_00001 to calc1_input_00004' were generated, the changes made in file '.\ixxxxx\f005' were not accepted in the input files. The other parameters from both the input files were affected, due to this change. For instance, once the $S_N$value was changed (increased), it would increase the GG and LG values automatically in the input when it should not. The same error was applied when changes were made to the GG. The LG and S_N parameters were changed when they should have not been. Therefore, the calculation regenerated its own incorrect input parameters, due to the single parameter change. The aim was to change one parameter while the rest remain constant. This is mentioned in detail in section 5.3.1.2.

4.6.5.2 North-Anna Square model definition for MCNP-6.2

It should be noted that different core boundary conditions are used for the MCNP and NESTLE models. A cylindrical boundary condition is applied to the core in MCNP, while a rectangular boundary condition is applied in NESTLE. NESTLE, having a structured geometrical mesh, can model either cuboids or hexagonal prisms. Curved surfaces such as the cylinder cannot be modelled explicitly in NESTLE for the core. An exact comparison between a cylindrical model between MCNP and NESTLE cannot be carried out.

A 13×13 square lattice model was created by NWURCS for MCNP-6.2. This model was created to test whether the core boundary used in MCNP-6.2 contributed significantly to the difference between the two codes. This is because in the cylindrical system from the MCNP model, the boundary nodes are intersected by the cylindrical boundary, resulting in different volumes for these nodes (the volumes at the edges which are cut by the boundary will not be volumes of complete nodes).

NESTLE, which has a square lattice boundary condition, has the boundaries set at the lattice edges, hence it models the full nodes. Further to this, NESTLE only allows full nodes to be modelled. Therefore, nodes which are smaller in size because they are cut by the boundary are not presented with the exact geometry (volume) in the NESTLE input.

The 13×13 square boundary MCNP model has 169 FAs. To model the NA PWR, 157 FAs are needed, which means 12 assemblies from the 169 FAs were considered as water nodes as presented in Figure 4-6. The effect of the water nodes on k_{eff} was also analysed.

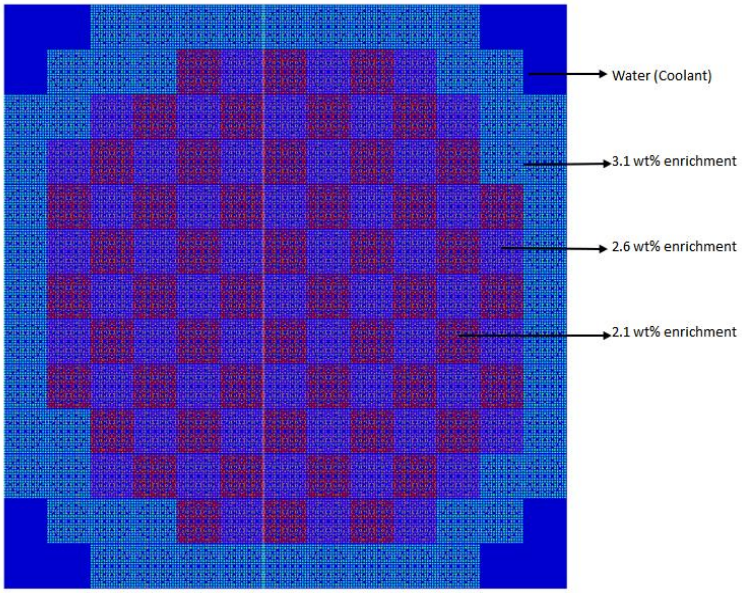

Figure 4-6: Full core square lattice model from Keno-VI

4.6.5.3 Flux data

The fast-flux and thermal-flux data in the radial direction for both MCNP and NESTLE were analysed and plotted in section 5.3.4. It should be noted that the magnitude of the fluxes were not the same. This is because NWURCS does not have the capability, as yet, to calculate the fluxes in terms of actual values. Therefore, the results are presented as least-square-fits, of the fast and thermal flux for MCNP and NESTLE respectively. The steps taken to calculate the least square fit of the fluxes are shown in Appendix 7.6.

4.6.5.4 Boric acid concentration

Boric acid (H_3BO_3) is used as a soluble neutron absorber in the primary coolant of pressurized water reactors, to control the reactivity in normal operations. The boric acid was added to the system, at various concentrations (ppm) with a constant increment of 300 ppm, in the MCNP and NESTLE models using NWURCs, and the effects of H_3BO_3 on k_{eff} analyzed.

The 2020_04_15 5th version of NWURCS 3.1 also calculates the H_3BO_3 concentrations using an alternative calculation method from the calculations conducted by the user. In this alternative calculation, one gram of boron (B) in one million grams of H2O was calculated instead of one gram of H_3BO_3 in one million grams of water.

It should be noted that the current version of NWURCS allows the user to use either definition, as both are equivalent, but they will have different scales on the x-axis of the boron or H_3BO_3 concentration vs k_{eff} plots.

4.6.5.4.1 Differential boron worth

By analysing the slope of the graph at two points, the differential boron worth (w_b), can be approximated using Eq.(4-8), provided that c_{b2} is close to c_{b1}.

$$w_b = \frac{d\rho}{dc_b} = \frac{k_2 - k_1}{c_{b2} - c_{b1}} \quad (4\text{-}8)$$

Where:

$k_1$and k_2 are the two results of the criticality calculations, assumed to be close to unity; and

c_{b1}, c_{b2} are boron concentrations related to $k_1$and k_2, respectively.

4.6.6 FC model verification: KENO-VI

In section 3.8, it was mentioned that the MCNP6-2 code used in this study does not have a built-in visual editor VISED, therefore the FC model generated by MCNP-6.2 could not be visually inspected. Since equivalent FC KENO-VI input files are generated within NWURCS when the MCNP-6.2 INP01 files are generated (Refer to item [I] in Table 4-1, the KENO-VI files are used to plot the geometry of the FC using FULCRUM of the SCALE-6.2.3 visual package and thus add to the verification of the model. The KENO-VI FC plot is presented in section 5.2.3.

A request to plot the MCNP-6.2 FC BM structural geometry was made to the NWURCS developer, as the NWURCs developer had earlier versions of MCNP with which the visual plotter, VISED was distributed. This is done to compare and verify the KENO-VI plot with that of the MCNP plot.

4.7 Sensitivity in calculations

Sensitivity calculations were conducted to:

1. Test if the amount of the fuel and moderator temperatures could reduce the difference in k_{eff} between the codes (MCNP-6.2 and NESTLE);
2. Test the effect of the burnable poisons such as borosilicate glass on the system.

Details on the sensitivity analysis are discussed in section 5.4.

CHAPTER 5: RESULTS AND DISCUSSION

This chapter is divided into five parts. The first part presents the base model calculations. The second part presents the verification of the results obtained from the manual calculations generated by the user (of the number-density and material specification) to those generated by NWURCS. The third part presents verification of the T-NEWT FA model with that of the NWURCS FA model. The fourth part demonstrates the verification of the MCNP-6.2 FC model with that of the FC NESTLE model. The last section presents sensitivity calculations. In each section provided, the effects of k_{eff} due to nuclear data is analysed.

5.1 State of calculation

One of the main objectives of this study was to generate a T-NEWT/NESTLE lattice-to-nodal diffusion FC model, parallel to that of an MCNP-6.2 FC model. To verify that the objectives are achieved, parameters, such as fluxes and the multiplication factor, generated by the different codes are compared against one another.

For a reactor to run and produce power safely, it must be critical. Given all the parameters for a critical state, a critical calculation should therefore yield k_{eff} = 1.0000. From the MCNP and NESTLE FC Base-Models (BM) that were generated in this study, the following results were obtained.

Table 5-1: MCNP and NESTLE BM comparison

	Model	k_{eff}	$K_{critical}$	k_{eff} - $k_{critical}$	pcm
1	**MCNP (k_{eff} ± σ)**	1.32589 ± 0.00018	1.0000	0.3259	32589
2	**NESTLE**	1.317149	1.0000	0.3171	31715
3	**KENO (k_{eff} ± σ)**	1.32574 ± 0.0002	1.0000	0.3257	32574
4	**MCNP - NESTLE**				874
5	**MCNP - KENO**				15

Table 5-1 presents the BM results obtained from the MCNP-6.2 and NESTLE FC calculations. The FC models for MCNP-6.2 and NESTLE are not in good agreement with regards to having the system in ‘a critical state’, as both models are supercritical.

As calculated using Eq. (4-5) & (4-6) from section 4.6.4, the difference between the MCNP and NESTLE systems was 874 pcm. The BM systems are supercritical as they are calculated at beginning of cycle, therefore the systems contain fresh fuel, and xenon and samarium and

other fission products are not present that would be produced after the first few hours following start-up.

Furthermore, there are no neutron poisons added to both the BM systems (no burnable poisons, and no boron in the coolant). It should also be noted that isothermal calculations were conducted for both codes, whereby the temperatures of all the reactor components were set at 300 K. A hot reactor will have a lower multiplication factor. Finally, the control rods were not modelled, since at start-up, these control rods can also reduce the multiplication factor. Given all of this, the large value for k_{eff} is therefore accepted for this particular model.

The KENO-VI calculations are not of further importance as KENO-VI is not used to produce further results in this study. It is used to verify the first MCNP-6.2 BM calculation, and it can be seen that the difference between the KENO and MCNP model is 15 pcm. A value greater than 50 pcm can be of concern based on studies by (Sihlangu, 2019) and (Nyalunga, 2019). Therefore, a value of 15 pcm is in good agreement, and it contributes to the verification that the MCNP model is working correctly.

The difference in the k_{eff} between the MCNP-6.2 and NESTLE BMs is relatively high and can be influenced by many factors. Hence, investigations were conducted to understand the cause of the differences. The investigation included the following:

- Model verification of T-NEWT;
- Verification of MCNP and T-NEWT/NESTLE model;
- ADF insertion in NESTLE input;
- Boron (H_3BO_3) concentration tests; and
- Sensitivity Analysis.

5.2 Investigation test 1: Model verification

5.2.1 Material verification of NWURCS and T-NEWT

Using the material information in Table 2-2 and Table 2-3, the material definitions, such as number densities of the NA PWR were manually calculated in an excel spreadsheet for the FA and FC materials (fuel pellet, water, stainless steel, etc) using Eq. (4-2) & (4-3) from sections 4.6.3. The calculations were compared to those calculated and generated by NWURCS. Table 5-2 provides the data of the material densities for the fuel pin, specifically presenting the data for UO_2 -3.1 wt %, helium in the gap, water and the zircaloy cladding.

Table 5-2: Calculated Number density for NA PWR

$U0_2$ 3.1wt%	NWURCS - atoms/barns	Manual- atoms/barns	Difference	Average	Ratio	Percentage
O_16	4.64E-02	4.64E-02	8.24E-06	4.64E-02	1.77E-04	0.02
O_17	1.77E-05	1.77E-05	3.13E-09	1.77E-05	1.77E-04	0.02
U_235	7.29E-04	7.29E-04	1.26E-07	7.29E-04	1.73E-04	0.02
U_238	2.25E-02	2.25E-02	3.89E-06	2.25E-02	1.73E-04	0.02
Zircaloy Comparison	**NWURCS** - atoms/barns	**Manual-** atoms/barns	**Difference**	**Average**	**Ratio**	**Percentage**
cr-50	3.30E-06	3.30E-06	6.14E-09	3.30E-06	1.86E-03	0.19
cr-52	6.37E-05	6.36E-05	1.18E-07	6.36E-05	1.86E-03	0.19
cr-53	7.22E-06	7.21E-06	1.34E-08	7.21E-06	1.86E-03	0.19
cr-54	1.80E-06	1.79E-06	3.34E-09	1.80E-06	1.86E-03	0.19
fe-54	8.25E-06	8.26E-06	-3.29E-09	8.26E-06	-3.99E-04	-0.04
fe-56	1.30E-04	1.30E-04	-5.17E-08	1.30E-04	-3.99E-04	-0.04
fe-57	2.99E-06	2.99E-06	-1.19E-09	2.99E-06	-3.99E-04	-0.04
fe-58	3.98E-07	3.98E-07	-1.59E-10	3.98E-07	-3.99E-04	-0.04
zr-90	2.19E-02	2.18E-02	3.30E-06	2.18E-02	1.51E-04	0.02
zr-91	4.76E-03	4.76E-03	7.19E-07	4.76E-03	1.51E-04	0.02
zr-92	7.28E-03	7.28E-03	1.10E-06	7.28E-03	1.51E-04	0.02
zr-94	7.38E-03	7.38E-03	1.12E-06	7.38E-03	1.51E-04	0.02
zr-96	1.19E-03	1.19E-03	1.80E-07	1.19E-03	1.51E-04	0.02
sn-112	4.83E-06	4.83E-06	-8.18E-10	4.83E-06	-1.69E-04	-0.02
sn-114	3.29E-06	3.29E-06	-5.57E-10	3.29E-06	-1.69E-04	-0.02
sn-115	1.69E-06	1.69E-06	-2.87E-10	1.69E-06	-1.69E-04	-0.02
sn-116	7.25E-05	7.25E-05	-1.23E-08	7.25E-05	-1.69E-04	-0.02
sn-117	3.83E-05	3.83E-05	-6.48E-09	3.83E-05	-1.69E-04	-0.02
sn-118	1.21E-04	1.21E-04	-2.04E-08	1.21E-04	-1.69E-04	-0.02
sn-119	4.28E-05	4.28E-05	-7.25E-09	4.28E-05	-1.69E-04	-0.02
sn-120	1.62E-04	1.62E-04	-2.75E-08	1.62E-04	-1.69E-04	-0.02
sn-122	2.31E-05	2.31E-05	-3.91E-09	2.31E-05	-1.69E-04	-0.02
sn-124	2.89E-05	2.89E-05	-4.89E-09	2.89E-05	-1.69E-04	-0.02
Helium Comparison	**NWURCS-** atoms/barns	**Manual-** atoms/barns	**Difference**	**Average**	**Ratio**	**Percentage**
he-3	2.41E-10	2.40E-10	5.67E-14	2.40E-10	2.36E-04	0.02
he-4	2.41E-04	2.40E-04	5.69E-08	2.40E-04	2.37E-04	0.02
Water comparison	**NWURCS-** atoms/barns	**Manual -** atoms/barns	**Difference**	**Average**	**Ratio**	**Percentage**
h-1	6.69E-02	6.69E-02	-5.06E-06	0.033437	-1.51E-04	-0.02
h-2	7.69E-06	7.69E-06	-5.81E-10	3.85E-06	-1.51E-04	-0.02
o-16	3.34E-02	3.34E-02	-2.52E-06	0.016714	-1.51E-04	-0.02
o-17	1.27E-05	1.27E-05	-9.57E-10	6.35E-06	-1.51E-04	-0.02

Using Eq.(4-4), the percentage difference (% $diff$) as seen in the fifth column of Table 5-2, was obtained between the manually calculated values and those calculated by NWURCS. An agreement between both sets of data for all the materials was achieved, as the % $diff$ is less than 0.5 %.

The reason for the difference obtained for the zircaloy and water, “may be due to slight differences in either the molar masses or weight fractions used” (Nyalunga, 2019).

From Table 5-2, it can be deduced that the material definition for the NA PWR that were manually calculated, and the material definition generated by NWURCS are in good agreement with each other. Therefore, NWURCS can easily generate the MCNP-6.2, and NESTLE input file, as the material specifications are proven to be in good agreement.

5.2.1.1 Verifying T-NEWT input file calculations

To verify NWURCS capability, the T-NEWT input file calculation generated by the user using SCALE-6.2.3 and FULCRUM, and those generated by NWURCS were compared against one another.

Calculations for FAs with the 3.1 wt%, 2.6 wt%, 2.1 wt% enrichments and a FA with a reflector at 3.1 wt%, were conducted and the k_{inf} was obtained and analysed from the output files. Table 5-3, presents the k_{inf} results obtained from the different enrichment calculations.

Table 5-3: NA enrichment vs k_{inf}

Enrichment wt %	Manual k_{inf}	NWURCS k_{inf}	NWURCS - Manual	Average	Ratio	%
Reflector3.1 wt%	1.2631	1.2637	0.0006	1.2634	0.0005	0.048
3.1	1.4100	1.4102	0.0002	1.4101	0.0002	0.015
2.6	1.3649	1.3651	0.0002	1.3650	0.0001	0.011
2.1	1.3036	1.3037	0.0001	1.3036	0.0001	0.006

The % $diff$ of less than 0.5% was obtained between the two calculations (NWURCS and the manually generated T-NEWT calculations). This implies that NWURCS and the manually generated T-NEWT calculation are in good agreement with each other as they are equivalent to each other.

The verification process conducted in section 5.2.1 and Table 5-3, verifies that the NWURCS input file generation capability functions correctly in terms of the T-NEWT calculations.

5.2.2 Verification of NESTLE model

The Nestle model was verified by checking if the nuclear data extracted from T-NEWT was inserted correctly into the NESTLE input file. In section 4.6.4.1, it was stated that an error was detected in NWURCS. T-NEWT produces all the required cross-sections which are extracted by NWURCS. The extracted data was populated incorrectly in file '…\xscoll\...' and the ttl.i file.

Therefore, the tt1.i was analysed. Examining 'composition 2' from the tt1.i file, it was found that the scattering cross-sections were inserted in wrong positions, verifying that the extraction process was conducted incorrectly by NWURCS. According to section A15-38 of the NESTLE manual by (Team, 1997), the group macroscopic scattering cross-sections from group j must go into group g; where j = 1, ng; j ≠ g. (n is the cross-section type and g is the group). This implies that the data was swapped and should have been extracted from a (1 to 2) and (2 to 1) process, as presented in Figure 4-4. The NWURCS developer was notified about the coding error and the error was subsequently fixed.

5.2.3 Verification of MCNP-6.2 model

The MCNP model was verified through visual inspection of MCNP-6.2 and KENO-VI FC plots. In sections 3.8 and 4.6.6, it was stated that MCNP-6.2 would be verified by using plots generated by KENO-VI, as the NWURCS generates equivalent FC KENO-VI input files when it generates the MCNP-6.2 INP01 files. The FC plot of the KENO-VI input file which was opened in the FULCRUM window of the SCALE-6.2.3 package is shown in Figure 5-1. An equivalent MCNP-6.2 plot provided by the NWURCs developer is presented adjacent to the KENO-VI plot in Figure 5-1.

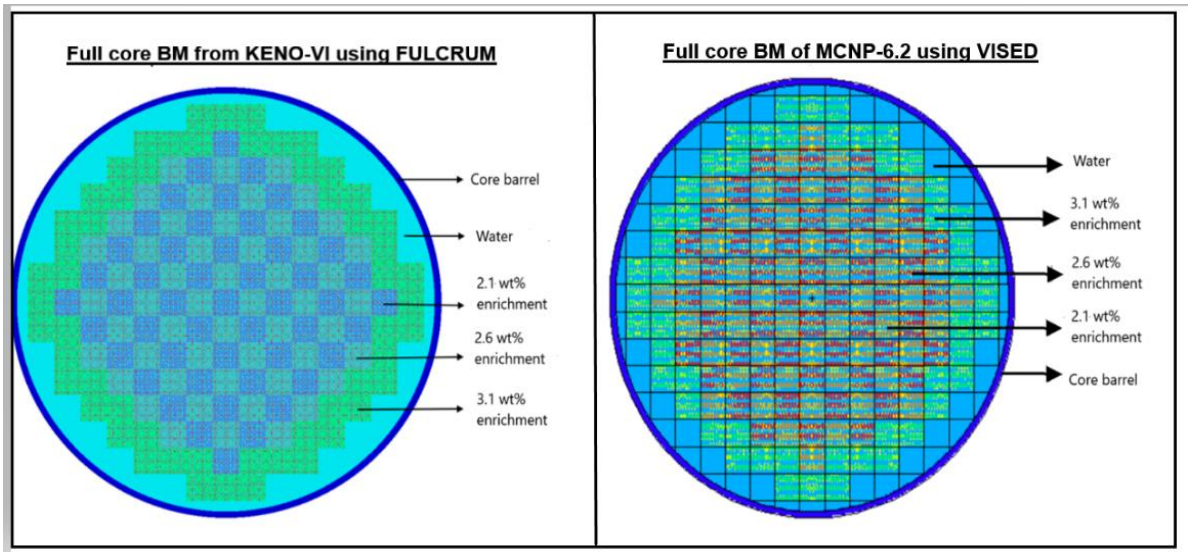

Figure 5-1: KENO-VI and MCNP-6.2 full core plots

5.3 Investigation test 2 – Verification of MCNP and T-NEWT/NESTLE

A series of tests were conducted to establish the reason behind the difference that lies between the MCNP BM (BM) and the NESTLE BM, given in Table 5-1. Therefore, a convergence study was conducted, as it was assumed that the MCNP and NESTLE BMs may not be fully converged.

5.3.1 Convergence

The MCNP BM needs to be converged by both calculating the Shannon entropy and through the convergence of k_{eff} as stated in sections 4.6.5.1.1.

In section 4.6.5.1.3, it was stated that only a few parameters from T-NEWT are used to test the convergence of k_{inf}, as most of the parameters have already been tested by (Nyalunga, 2019) and by (Sihlangu, 2019). In this study, the T-NEWT model is converged in terms of XSProc which uses parameters, such as S_N (by varying the value of N); while in the NEWT section, the k_{inf} convergence is conducted by redefining the global grid (GG) and the local gid (LG).

5.3.1.1 Convergence of MCNP

Convergence of the Shannon Entropy in MCNP is achieved by either increasing the number of source points or the number of inactive cycles or both.

According to Table 5-4, the MCNP BM calculation was set to have 100 000 source points (NSRC), 155 inactive cycles (IC) and 250 active cycles (AC) in the KCODE command line. This calculation had a standard deviation (statistical error) of 0.00018. With the KCODE set to these values, the source-convergence check did pass, but the statistical error was high. The objective is to get the source converged and to reduce the statistical error.

First, the number of source points was kept constant, as well as the number of active cycles, but the number of inactive cycles was increased, as seen in Table 5-4.

Table 5-4: Source convergence

	Source Point	In Active Cycle	Total AC	AC	k_{eff}	Std	MCNP recommendation

BM	100000	155	250	95	1.32589	0.00018	151
1.	100000	165	250	85	1.32593	0.00019	151
2.	100000	185	250	65	1.32573	0.00022	151
3.	100000	195	250	55	1.32569	0.00026	151
4.	100000	230	380	150	1.32606	0.00014	215
5.	100000	250	380	130	1.32603	0.00015	215
6.	100000	250	400	150	1.32610	0.00014	217
7.	100000	230	400	170	1.32612	0.00013	217
8.	100000	300	1100	800	1.32596	0.00006	239
9.	100000	245	1100	859	1.32597	0.00006	239
10.	900000	155	250	95	1.32599	0.00006	151
11.	900 000	165	250	85	1.32600	0.00006	151
12.	900 000	175	250	75	1.32596	0.00007	151
13.	900 000	315	550	235	1.32595	0.00003	300
14.	900 000	750	1100	350	1.32586	0.00003	380
15.	900 000	400	1100	700	1.32589	0.00002	380

It should be noted that for all the calculations presented in Table 5-4, the source-convergence test passed. For a given number of source points (at 100000), and with the number of active cycles kept constant, one expects that the number of recommended inactive cycles should be constant. This is seen in items 1 to 3 from Table 5-4. Although the number of inactive cycles was increased, the recommended number of inactive cycles remains constant, but the accuracy in the statistics of the calculation increases.

Once the number of active cycles was increased, then the recommended number of inactive cycles increases, as seen in items 4 and 5, items 6 and 7, as well as in items 8 and 9. This was done to reduce the statistical error of the calculations since the source convergence was achieved. It is recalled that Shannon entropy is calculated in terms of the percentage of fission sites that are occupied by source points, as given by Eq. (3-35). However, MCNP calculates the average Shannon entropy for the last half of the cycles and then reports the first cycle found where the number of source points falls within one std deviation of the average calculated (Werner, 20217). Therefore, as the active cycles increase, the statistics of the calculations also change, and therefore the average number of inactive cycles are not necessarily constant.

Once the number of source points was increased to 900 000, a similar trend is seen in items 10 to 12, and 13 to 15 in Table 5-4. The statistics of the calculations change (decrease). But the change is mostly influenced by the effects of the active cycles.

Now considering 'the convergence of k_{eff}, the average of all the k_{eff} from Table 5-4 is 1.325976, and the difference of the individual values from the average is equal to or less than the standard deviation. Therefore, even though the MCNP recommendations are differing (regarding the IC), there is no effect on k_{eff}.

It should be noted that the number of active cycles (which equates to. The Total cycles – Inactive cycles) determines the standard deviation of the result. Therefore, the larger the active cycles, the smaller the standard deviation (sigma). As the active cycles are changed or increased, the number of inactive cycles needs to be adjusted accordingly based on the recommendation message printed from the MCNP output file. Given the statistical nature of the calculation, the total number of active histories should be monitored, which is the product of the number of source points (NRCS) with active cycles.

Table 5-5 (the rearranged form of Table 5-4), presents an analysis based on the descending arrangement of the statistical error as well as the total number of active histories in ascending arrangement.

Table 5-5: Total cycles and standard deviation analysis

	Source Point	In Active Cycle	Total Cycle	AC	NRCS*AC	k_{eff}	std
1.	100000	195	250	55		1.32569	0.00026
2.	100000	185	250	65	6500000	1.32573	0.00022
3.	100000	165	250	85	8500000	1.32593	0.00019
BM	100000	155	250	95	9500000	1.32589	0.00018
4.	100000	250	380	130	13000000	1.32603	0.00015
5.	100000	230	380	150	15000000	1.32606	0.00014
6.	100000	250	400	150	15000000	1.32610	0.00014
7.	100000	230	400	170	17000000	1.32612	0.00013
8.	900 000	175	250	75	67500000	1.32596	0.00007
9.	900 000	165	250	85	76500000	1.32600	0.00006
10.	100000	300	1100	800	80000000	1.32596	0.00006
11.	900000	155	250	95	85500000	1.32599	0.00006
12.	100000	245	1100	859	85900000	1.32597	0.00006

13.	900 000	315	550	235	211500000	1.32595	0.00003
14.	900 000	750	1100	350	315000000	1.32586	0.00003
15.	900 000	400	1100	700	630000000	1.32589	0.00002

The objective is to decrease the statistical error since, in Table 5-4, the source was converged for all the calculations listed. As seen in Table 5-5, as the number of active histories increased, the more the statistical error of the system reduced (provided that the number of inactive cycles was kept to a minimum, as recommended in the MCNP output file), thus the STD is greatly influenced by the number of active cycles and the number of source points. Therefore, Figure 5-2, was plotted to graphically represent the trend.

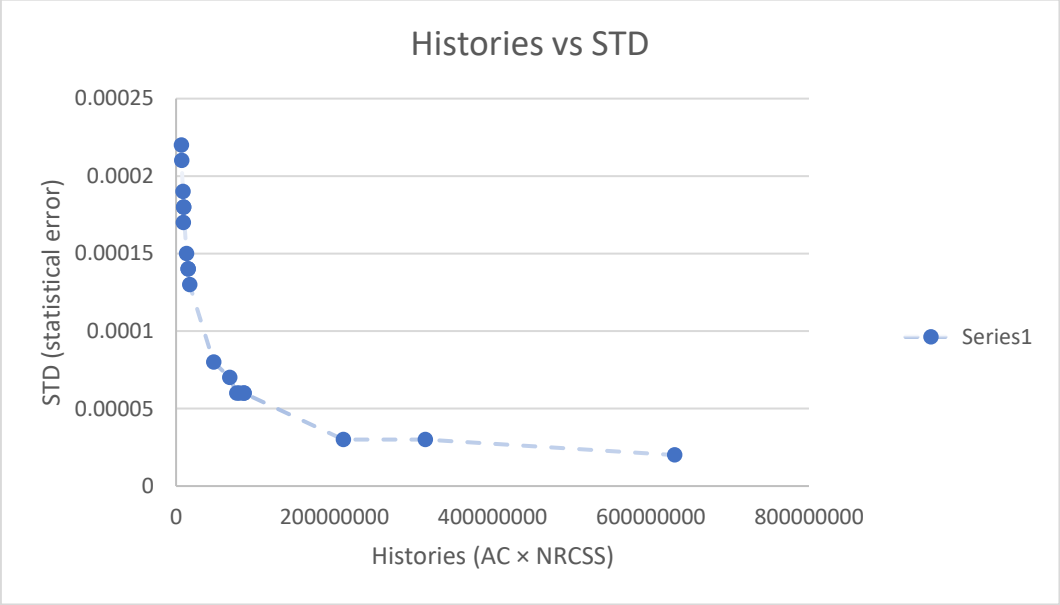

Figure 5-2: Total number of histories against the statistical error plot

It is ideal to calculate the MCNP models with 900 000 source points, 400 inactive cycles and 1100 active cycles, as this makes the models more accurate as the source would have converged and the error is greatly reduced.

However, although the calculations with 900 000 source points produce a more accurate value of k_{eff} due to the lower statistical error they produce, the calculations with 100 000 source points require less computational time compared to those with 900 000 source points.

5.3.1.2 Convergence of T-NEWT/ NESTLE

In terms of the S_N convergence study, for $N = 4;\ 6;\ 8; 10;\ 12;\ 14; 16$ the following parameters were kept constant [$GG = 8 \times 8, and\ \ LG = 4 \times 4$].

In Figure 5-3, it is seen that as the N value of S_N value increases, k_{inf} increases as well. k_{inf} converges at around $N = 12$, as this is where the levelling of the curve is observed (as k_{inf} becomes constant). Also, from this point onward, the maximum difference between the points was 0.65 pcm (between $N = 12 \text{ and } 14$).

By increasing the value of the N, the time increases, as seen in Figure 5-4. The computational time at $N = 12$ was $CPU = 2789\ s$ and at $N = 14$ it was $CPU = 3545\ s$. The ratio of the two points is 1.4, therefore at $N = 14$, the calculation took about 1.4 times longer to run compared to that of $S_N = 12$. This can be quite a significant difference, especially for studies where many calculations are required Therefore, a value of $N = 12$ (where $S_{N=12}$) is selected.

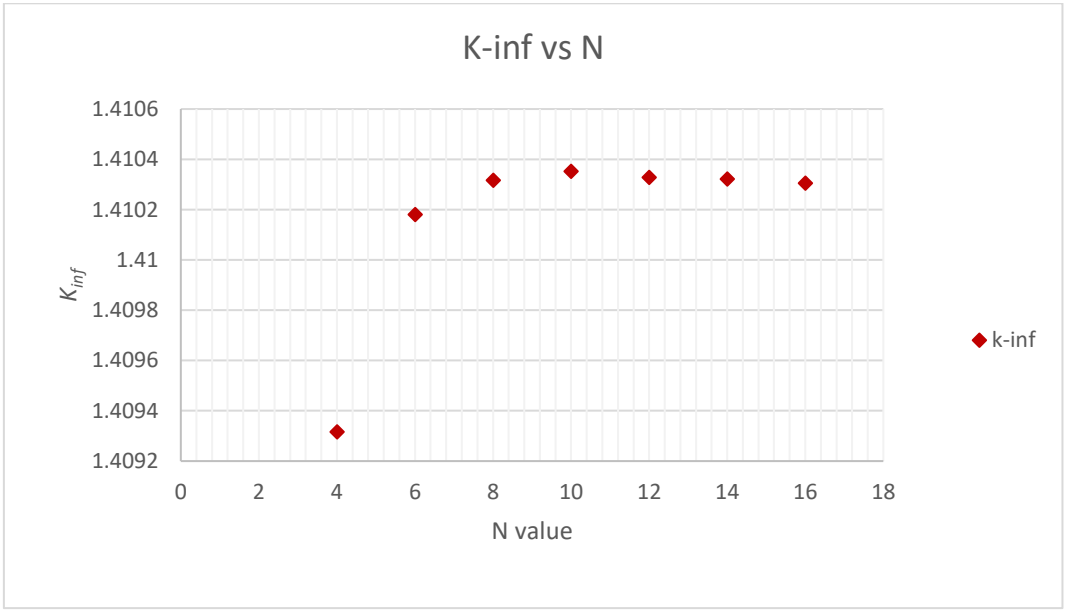

Figure 5-3: Effects of k_{eff} on the N (of the S_N)

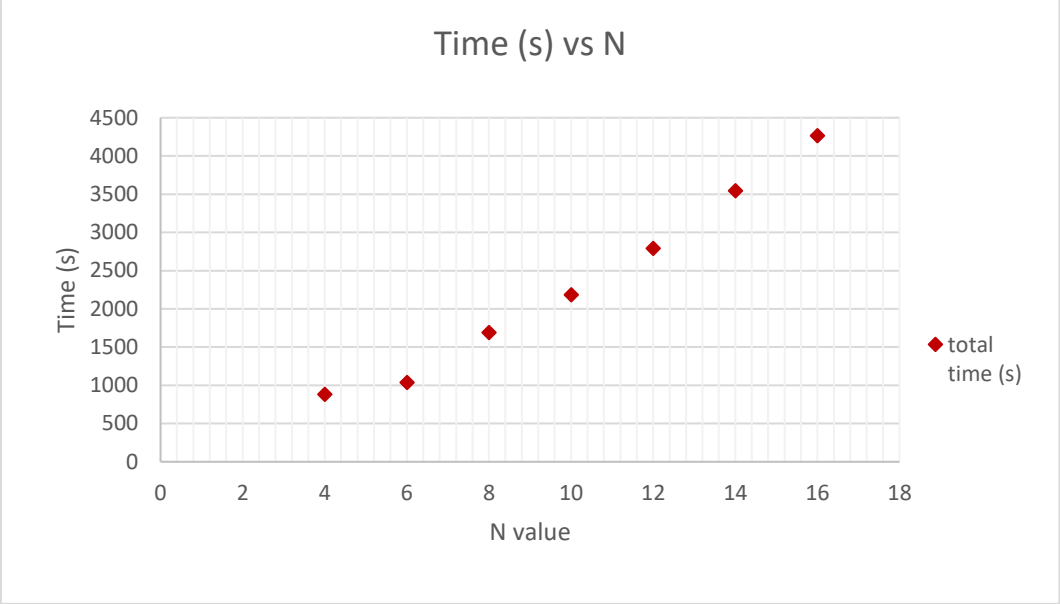

Figure 5-4: Computational time for N

In terms of the global grid dimensions, at $GG = 16 \times 16;\ 24 \times 24;\ 32 \times 32;\ 48 \times 48;\ 64 \times 64$, the following parameters were kept constant $[\ S_{N=6},\ LG = 4 \times 4]$. In Figure 5-5, it can be seen that the k_{inf} decreases as the grid increases.

However, it also seems that $GG = 32$ could be an inflection point. This is not expected, since convergence would normally mean that the curve 'flattens' out. The effect can possibly be explained as a numerical effect. In this regard it is noted that the gap between fuel assemblies is in the model, and this gap is relatively small compared to the fuel assembly width. This small size could be leading to the numerical effect. The gap does not get modelled by the local grids, since it lies outside the region of the local grids in the model.

Therefore, if the data after $GG = 48$ is neglected, the data converges towards a constant value as the global grids increase from $GG = 16$ to $GG = 48$, which then gives the expected trend for a convergence study.

However, when more grids are defined, more computational time is required, as seen in Figure 5-6. The difference between $GG = 16\ \&\ 24$ is calculated to be 1.35 pcm. Therefore, $GG = 16$ is selected, as this can be taken as the point where the k_{inf} begins to converge, in terms of a small difference with the asymptotic value being the metric, and it requires less computational time compared to $GG = 24$.

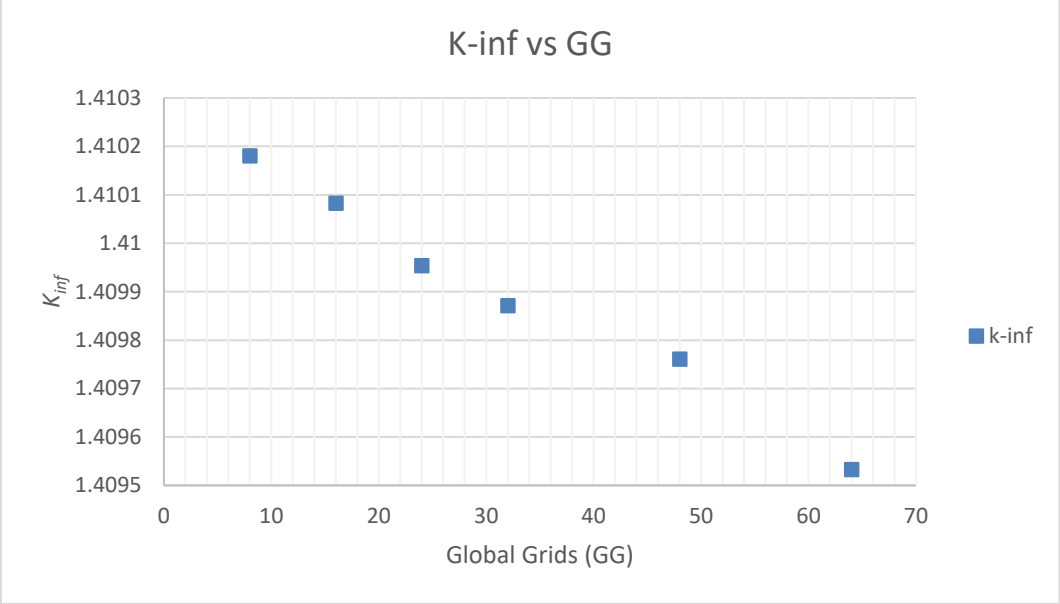

Figure 5-5: Effects of the K_{inf} due to the GG

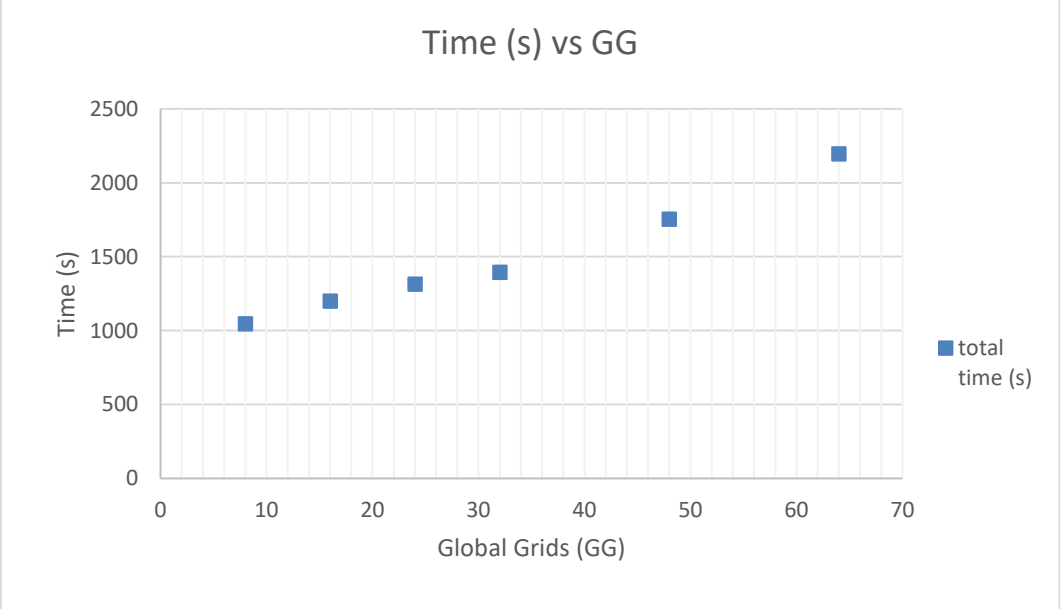

Figure 5-6: Computational time for GG

In terms of local grids, the grids were tested for $4 \times 4, 8 \times 8, 12 \times 12, 16 \times 16, 24 \times 24, 32 \times 32$ grids, with the following parameters kept constant $[S_{N=6},\ GG = 64 \times 64]$. A GG of 64 x 64 is selected in this case to allow more LG calculations to be tested with this large GG.

In Figure 5-7, the higher the local grid, the smaller the value of k_{inf} becomes. At $LG = 12\ \&\ 24$, the calculation could not be processed as these values caused the code to stop working. It is possible that the change and relationship between the grids produced the numerical instability. Therefore, only $LG = 4, 8, 16, \&\ 32$ were calculated. The difference between $LG = 8\ \&\ 32$ and

$LG = 8 \,\&\, 16$ is around 36 and 32 pcm respectively, while that of $LG = 16 \,\&\, 32$ is 5 pcm. As observed in Figure 5-7, k_{inf} appears to be converged between $LG = 16 \;\&\, 32$.

In Figure 5-8, it is seen that at $LG = 16$ the calculation time is less compared to $LG = 32$, thus the local grid of $LG = 16$ was selected.

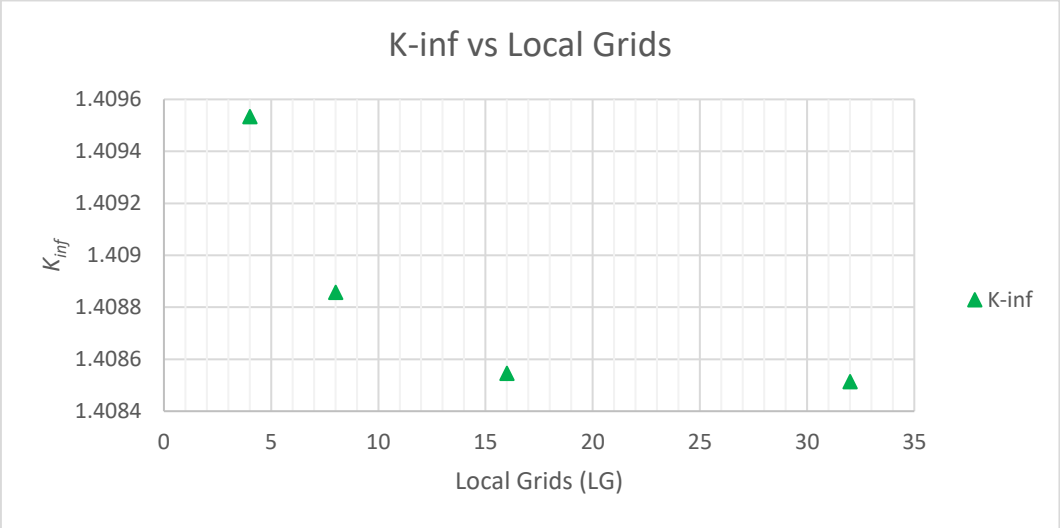

Figure 5-7: Effects of K_{eff} on LG

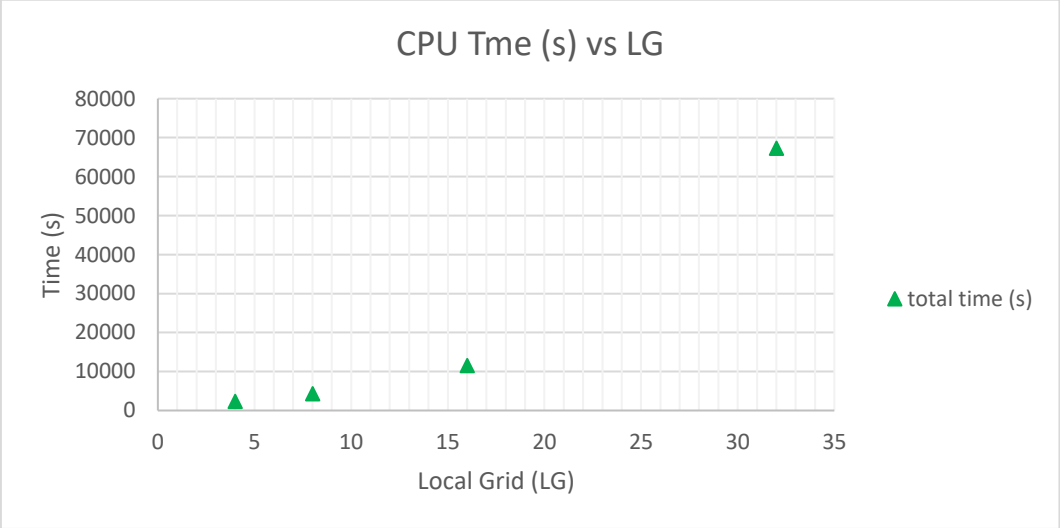

Figure 5-8: LG CPU time (s)

Through the T-NEWT/XSProc convergence study, it was decided that a calculation of the following parameters will be used $[S_{N=12};\ GG = 24 \times 24,;\ LG = 16 \times 16]$. The results that are generated by T-NEWT/XSProc calculation are extracted by NWURCS to generate a NESTLE model with converged homogenised cross-sections.

An error in NWURCS was detected, as mentioned in section 4.6.5.1.4. When the defaulted GG, LG and S_N parameters (from calc1.input file) were changed for NWURCS to create a T-NEWT calculation with the new desired parameters, NWURCS would only accept changes done to S_N, and ignored the changes done to the LG and GG. The following table presents the desired changes made to the XSProc parameters and the error that was generated in the T-NEWT input file.

Table 5-6: Error in NWURCS in terms of | S_N | GG | LG |

Desired Input	**The error made by NWURS in FA with 2.1 wt %, 2.6 wt %, and 3.1 wt%**	**The error made by NWURS in FA with reflector node**
S_N | GG | LG	**S_N | GG | LG**	**S_N | GG | LG**
6 |24 × 24 | 4 × 4	6 | 8 × 8 | 4 × 4	6 | 48 × 24 | 4 × 4
6 | 8 × 8 | 6 × 6	6 | 8 × 8 | 4 × 4	6 | 16 × 8 | 4 × 4
12 | 24 × 24 | 16 × 16	12 | 8 × 8 | 4 × 4	12 | 48 × 24 | 4 × 4
12 | 24 × 24 | 12 × 12	12 | 8 × 8 | 4 × 4	12 | 48 × 24 | 4 × 4

Therefore, the input calculation had to be manually edited after being generated by NWURCS (for the FAs with 2.1 wt %, 2.6 wt %, and 3.1 wt %, as well as that of the 3.1 wt% water- node FA) to reflect the correct values.

Table 5-7 presents the $\%\ diff$ (using Eq.(4-7) from section 4.6.5.1.3) of the T-NEWT output parameters (such as the transport cross-sections, the absorption cross-sections, and scattering cross-sections) generated from the 3.1wt% FA BM with the output parameters generated by the 3.1 wt% FA model with the $S_{N=12};\ Gd = 24 \times 24;\ LG = 16 \times 16$ parameters.

Table 5-7: Effects by the Cross-sections

Parameters [Cross-section(XS)]	**Transport**	**% Diff**	**Absorption**	**% Diff**	**Fission**	**% Diff**	**Scatter-ing**	**% Diff**
$XS_{l\ group\ 1}$ (Sn = 6; GG = 8; LG = 4)	0.2499	-0.029	0.0091	0.218	0.0027	-0.105	0.0005	0.022
$XS_{f\ group\ 1}$ (Sn = 12; GG =24; LG= 16)	0.2498		0.0091		0.0027		0.0005	
$XS_{l\ group\ 2}$ (Sn = 6; GG = 8; LG = 4)	1.3045	-0.027	0.1030	-0.030	0.0701	-0.035	0.0235	-0.012
$XS_{f\ group\ 2}$ (Sn = 12; GG =24; LG= 16)	1.3041		0.1030		0.0701		0.0235	

From the results presented in Table 5-7, it can be seen that the overall difference obtained from the initial XS' (**$S_N = 6;\ Gd = 8 \times 8;\ LG = 4 \times 4$**) with the final XS' (**$S_N = 12;\ GG = 24 \times 24;\ LG = 16 \times 16$**) is less than 0.03.

The transport cross-sections, absorption cross-sections, fission cross-sections, and scattering cross-sections, were then manually entered into the NESTLE BM TT1.i file. The effects of the cross-sections on the k_{eff} are seen in Table 5-8.

Table 5-8: Effect of NEWT-convergence on NESTLE base-models output.

Model	k_{eff}	**NESTLE BM - T-NEWT\NESTLE convergence**	**pcm**	**% Diff**
NESTLES BM ($S_N = 6;\ Gd = 8 \times 8;\ LG = 4 \times 4$)	1.31715	0.00035	35	-0.02657
T-NEWT\NESTLE convergence ($S_N = 12;\ Gd = 24 \times 24;\ LG = 16 \times 16$)	1.31680			

The NESTLE model decreased by 35 pcm from the original NESTLE BM, as seen in Table 5-8. This difference is small and is therefore not the reason for the large difference between the MCNP BM and the T-NEWT\NESTLE Model.

With regards to the $\%\ diff$ between the NESTLE BM and the T-NEWT/NESTLE converged model, a $\%\ diff$ that was less than 0.03 was obtained. Consistency in the results between Table 5-7 and Table 5-8 (the T-NEWT and the NESTLE calculations) is observed (the $\%\ diff$ is of the same order), which leads to further verification of the NWURCS model. It is noted that the actual quantities in both tables are different, and therefore only the $\%\ diff$ is appropriate.

Therefore, the rest of the investigations is conducted and modified based on the T-NEWT/NESTLE BM input file (as presented in section 5.1) and not on the converged input as the first file was faster to run.

5.3.2 Investigation test 3 - Core barrel tests

Tests on the core barrel were also conducted to see whether the core barrel dimensions or materials, etc., contribute to the large difference that lies between the MCNP Base Model (BM) and the NESTLE BM given in Table 5-1. The core barrel in the MCNP model has a cylindrical

boundary, whereas the NESTLE model has no core barrel but the core is surrounded by water nodes in a cuboidal lattice arrangement. Therefore, tests were conducted to observe how much influence the core barrel has on the value of k_{eff}. The core barrel tests were divided into the following subsections:

A. Without a CB presents;
B. CB changed to that of a helium material;
C. Changing the thickness of the CB material; and
D. Water as a core barrel.

The following tables below show the effects of the core barrel on $k_{eff.}$

Table 5-9: MCNP-6.2 core barrel test results

MODEL	MCNP $K_{eff} \pm \sigma$ (std)	% DIFF	AVERAGE	RATIO	%	pcm
BM	1.32590 ± 0.00018					
No CB	1.32544 ± 0.00015	-0.00045	1.32567	-0.00034	-0.034	-45
HE CB	1.32590 ± 0.00017	0.00004	1.32591	0.00003	0.003	4
CB (180.18253 cm)	1.32580 ± 0.00015	-0.00008	1.32585	-0.00006	-0.006	-8
CB (220.18253 cm)	1.32590 ± 0.00018	-0.00003	1.32588	-0.00002	-0.002	-3
CB (171.18253 cm)	1.32560 ± 0.00017	-0.00026	1.32576	-0.00020	-0.020	-26
Water as CB	1.32620 ± 0.00017	0.00030	1.32604	0.00023	0.023	30

The NESTLE model does not contain a core barrel structure and only consists of water nodes serving as reflectors. Therefore, changes in the CB material and the CB thickness only affected the MCNP calculations while the NESTLE calculations were not affected by the change. By removing the core barrel from the MCNP BM, k_{eff} was reduced by 45 pcm, as seen in Table 5-9.

Replacing the SS-304 CB material with that of a helium (He) composition in the MCNP model, caused the void boundary condition that existed at the core barrel to be moved from the outer surface of the CB to the inner surface of the CB. Having He as the CB resulted in k_{eff} to decrease by a factor of 4 pcm from the MCNP BM, in Table 5-9.

The results indicate that the treatment of the He as the CB does not influence the value of k_{eff} significantly, based on Table 5-9, also when the thickness of the CB is increased or decreased. The difference is smaller than the statistical error given by the MCNP BM, and therefore the statistics of the calculations essentially make all these results equal.

The last CB test that was conducted, was to replace the CB SS-304 material with water. From Table 5-9, a change in k_{eff} of 30 pcm can be seen from the MCNP BM and the MCNP model with water as the CB.

5.3.3 Investigation test 4: Square boundary and water node tests

In the MCNP model, the reactor core was modelled using a 17×17 lattice, which is enclosed in a cylindrical volume. This means that a cylindrical boundary condition was applied to the core in MCNP. Therefore, the nodes at the boundary were cut by the boundary, resulting in different volumes for these nodes, as mentioned in section 4.6.5.2. It should be noted that MCNP uses exact geometry modelling. Therefore, the nodes at the boundary were cut by the boundary, and only the volume inside the boundary for the node were considered.

In the NESTLE model, the reactor core was also modelled using a 17×17 square lattice, and rectangular lattice boundary conditions were applied. However, the nodes which are outside the boundary were set to have void material. Further, the complete full volumes of the node were modelled at the boundaries, as the boundary was set at the lattice edges.

Hence, this meant that the modelling of the nodes at the boundary was not the same for the NESTLE and MCNP models, thus an investigation was conducted to test whether this difference in modelling is important.

To make both models to have the same boundaries, a 13 x 13 square lattice was modelled, with rectangular boundaries for both MCNP and NESTLE.

This allows the MCNP model to treat the nodes at the boundary the same way that the NESTLE models the nodes (all the nodes at the boundary are complete). As mentioned in section 4.6.5.2, the 13×13 core array has 169 FAs, of which 12 FAs are considered as water nodes, to have 157 FAs in the core. Therefore, tests were conducted that tested how the nodes at the edges contribute to the multiplication factor.

5.3.3.1 Test A: Square model with different number of water nodes

Models with 0, 4 and 12 water nodes along the edges of the core were created and the effect on the k_{eff} was analysed as seen in Figure 5-9.

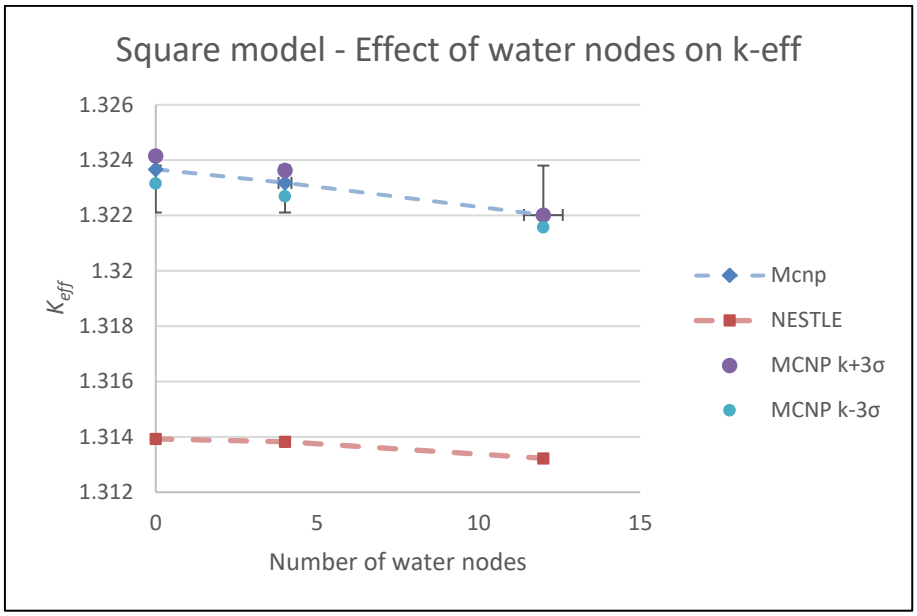

Figure 5-9: Effect of water nodes on k_{eff}

When the core is surrounded by a reflector, the neutron economy is improved (Lamarsh & Baratta, 2001), as the neutrons are reflected into the core, resulting in the fission neutron collisions increasing, which leads to an increase in the reactivity. Therefore, an increase in the number of water nodes would increase the moderation of the system, which would increase the k_{eff}.

However, when the water nodes are increased, then the FA nodes which contain fissile isotopes ^{235}U are removed. The number of fissile isotopes will decrease and thus k_{eff} would decrease. There are thus two competing effects, and Figure 5-9 shows that k_{eff} decreases as the number of water nodes increases (the number of fuel assemblies is correspondingly decreased).

5.3.3.2 Test B - Square model with increasing water densities

To isolate one of the two competing effects mentioned in the previous section, a test was conducted on models with four and 12 water nodes. In this test, the water density of the NESTLE model was decreased [starting from 1; 0.74058; 0.37029 to 0.185145 g/cm^3. By

decreasing the density of water, the k_{eff} is expected to decrease due to lesser moderation (although the neutron absorption of water can also decrease, giving rise to an increase in k_{eff}).

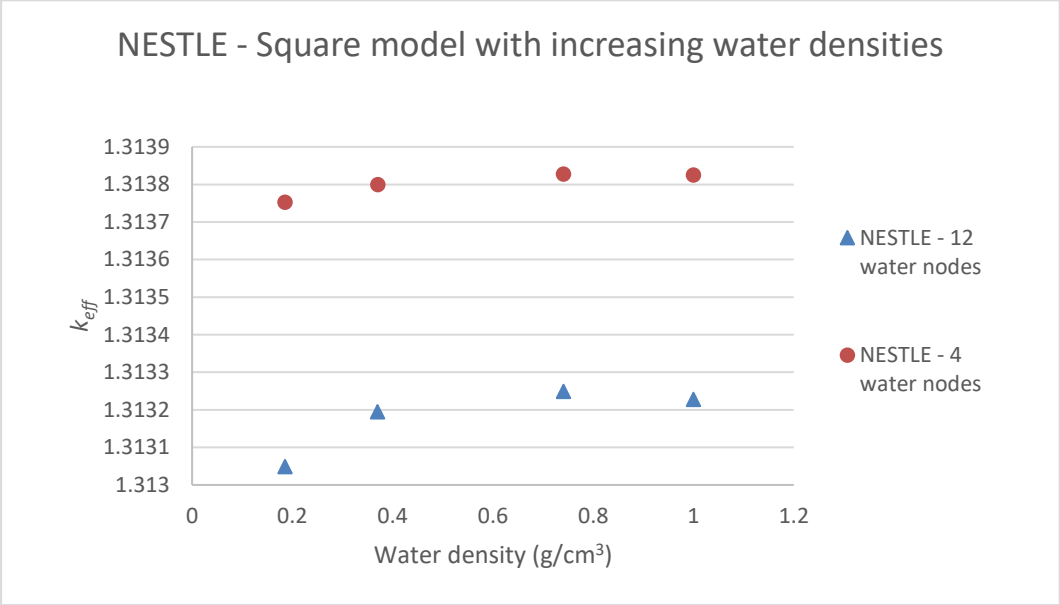

Figure 5-10: NESTLE - Square model water density test

From Figure 5-10, it can be seen that with the decrease in density, k_{eff} first increases very slightly, and then decreases. The slight increase could be due to lowering of the neutron absorption in water, allowing for more neutrons to be available for the fission process. The later decreasing effect then shows that the moderating ability of the water is decreasing with decreasing density, showing that the moderation phenomenon is stronger than the absorption phenomenon in this region.

Coding error in NWURCS

From the results generated by MCNP, a coding error (bug) in NWURCS was detected. NWURCS was generating the wrong water densities in the MCNP and KENO input files. It changes the number density of water for both the MCNP and KENO inputs, by automatically decreasing the values. Manual insertion of the desired densities was required, and this error has been reported to the code developer. However, since this applied only to the square model, this was not the cause for the difference between the MCNP and T-NEWT/NESTLE calculations.

5.3.3.3 Test C – Square model with decreasing fuel densities

Parallel to the test on the water density, a test was conducted on models with four & 12 water nodes. In this test, the fuel density of the models was decreased from 10.412; to 5.206 ending with 2.603 g/cm^3. By decreasing the density of the fuel, the k_{eff} is expected to decrease.

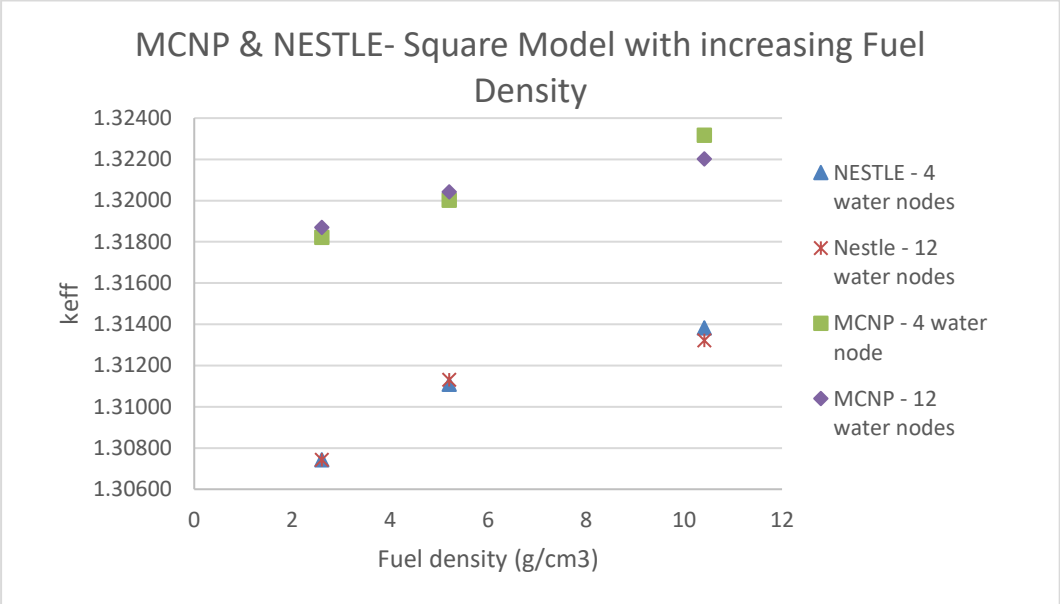

Figure 5-11: NESTLE & MCNP square model fuel density

Lowering the density of the fuel, as seen in Figure 5-11, lowers the k_{eff}. The effect of decreasing the fuel density lowers the ^{235}U neutrons, and therefore as a first-order estimate, a decrease lowers k_{eff}.

Although the MCNP and NESTLE models now have identical boundary conditions, the analysis based on Tests A, B & C, still shows a difference of around 800 pcm between MCNP and NESTLE square boundary model. The large difference was therefore not due to the nodes being cut by the boundary. The tests also show consistency in the trends and therefore leading to further verification of the NWURCS generated input since non-physical results did not arise, rather results arose as expected. The only test that showed an error was Test B. As stated previously, a coding error (bug) was detected in the code, regarding the density definitions and this illustrates the need for verification of computer codes.

5.3.4 Investigation test 5: Neutron flux distribution

In the tt1.i file, there are 10 axial sets of 17×17 radial positions assigned for the flux calculations. Once the calculations are completed, the flux data was obtained from the NESTLE BM output file located in '.C:\0_tr\iter01\relapxxx\outdta.', where the fluxes are

grouped into the fast and the thermal flux groups under the 'MINOR EDIT card'. In Figure 5-12, the flux plots for groups A, B, and C are presented, where the plot in Group A shows the fast and thermal fluxes in the axial direction while the plots from group B shows the fast and thermal fluxes in the radial x-direction, and group C's plots shows the fast and thermal fluxes in the radial y-direction.

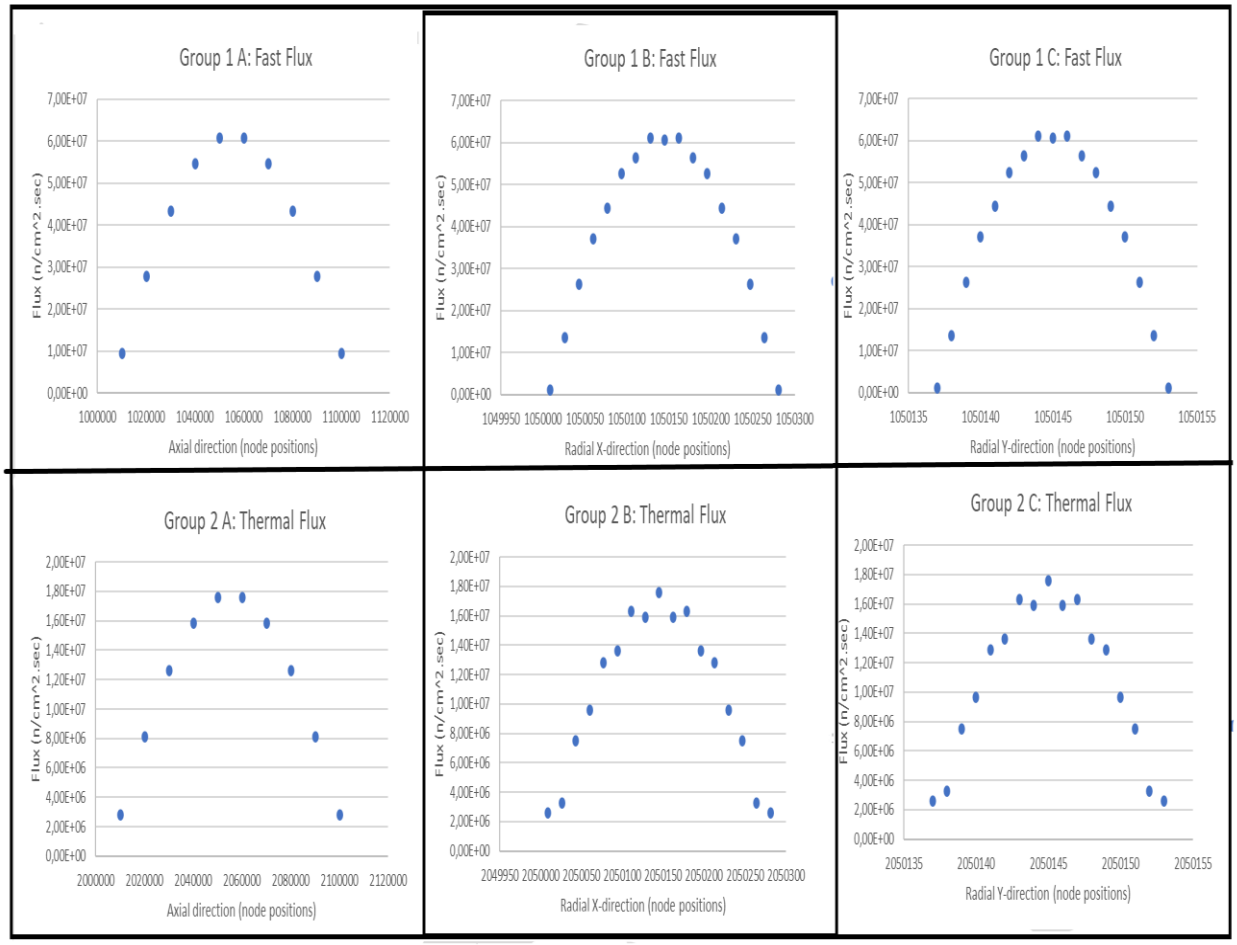

Figure 5-12: NESTLE's neutron fluxes plots

With regards to MCNP, the MCNP neutron flux data is generated when the tally switches in NWURCS are activated. It should be noted that the MCNP-6.2 tally results are not fully converged in the study due to computation time constraints, with the calculation run parameters set as 100000 source points, 245 inactive cycles and 1100 active cycles. To get the tallies to be fully converged, more active cycles would have been required. The neutron flux data was obtained from file '.C:\0_tr\flux_maps\gp00p00p00p00.', to be used for comparison with the fluxes generated from NESTLE. It is therefore noted that the flux comparison are not accurate but should show the trend.

In section 7.6 of the Appendix, the method on how the curves were fitted with sinusoidal curves is given. Figure 5-13 presents the least square fitted sinusoidal curves of the thermal and fast fluxes plotted with the calculated MCNP data points, respectively, while Figure 5-14 presents similar curves for the NESTLE data. For a homogenous reactor, a sinusoidal curve is expected, therefore, by using the 'least square fit', the sinusoidal curve is fitted along with the flux; similar calculations were conducted in Stacey (Stacey, 2007). Since both show agreement with the sinusoidal curve, it therefore means that the shape for both the MCNP and NESTLE plots are the same. Further comparisons were not made since the MCNP tallies were not fully converged and are reserved for further study.

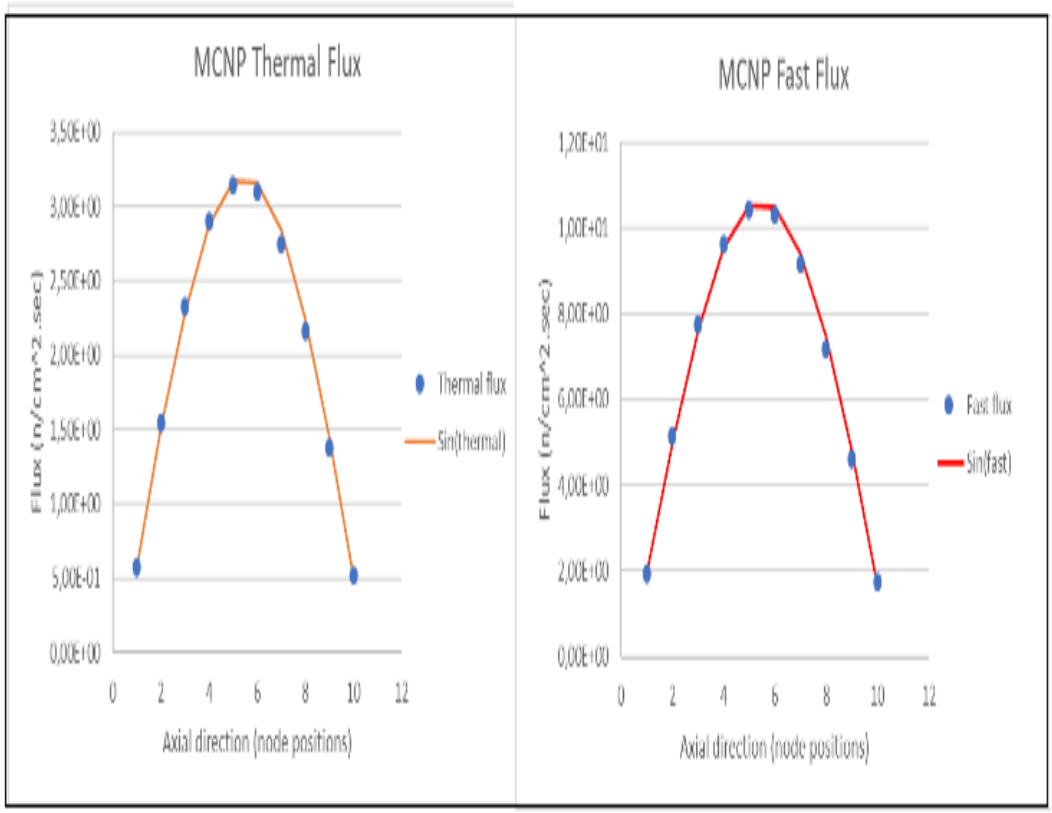

Figure 5-13: The MCNP thermal and fast sinusoidal flux curves

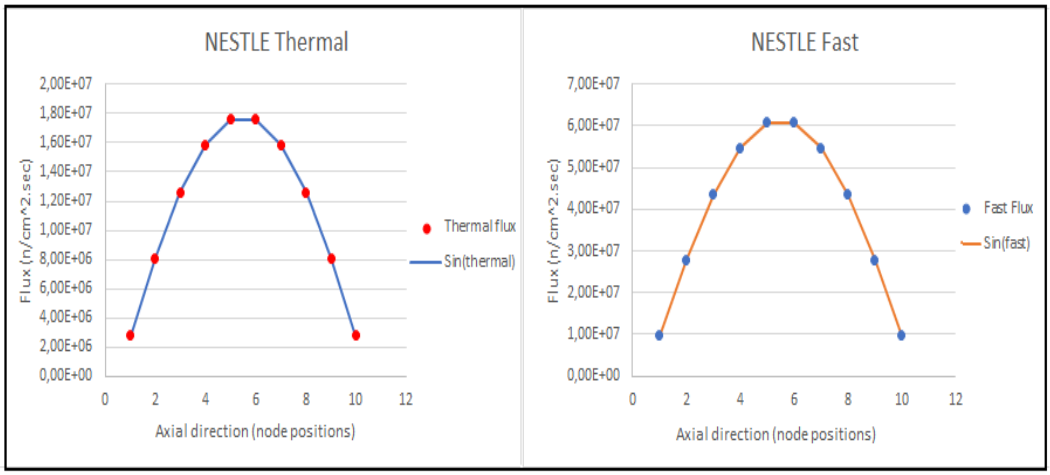

Figure 5-14: The NESTLE thermal and fast sinusoidal flux curves

5.3.5 Investigation test 6: ADF insertion in NESTLE tt1.i

The ADFs are generated in the T-NEWT output file. But the NWURCS does not extract the ADFs while creating the ttl.1. Therefore, the ADFs need to be manually inserted into the NESTLE input file. The ADF results are presented in Table 5-10.

Table 5-10: NESTLE ADF

Model	k_{eff}	BM- ADF	pcm
NESTLE ADF	1.316903		
NESTLES BM	1.317149	0.000246	24.6

By comparing the NESTLE BM with the model that has the ADFs inserted in the input, it can be observed that the value of k_{eff} decreased once the ADFs are inserted in the NESTLE input. The difference between the NESTLE BM and the NESTLE ADF model is 25 pcm.

To gain more insight into the influence of the ADFs, an uncomplicated core consisting of one enrichment (3.1wt%) was studied. This system resulted in k_{eff} = 1.38558. The ADFs were manually inserted (at various arbitrary values in a descending order) and the effects were analysed.

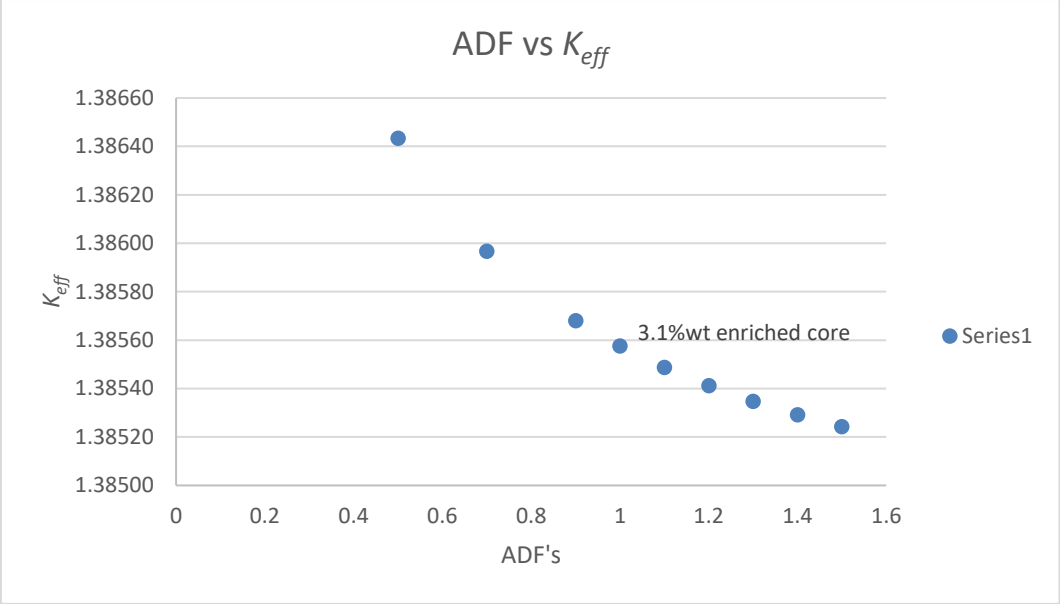

Figure 5-15: NESTLE ADF investigation

It can be seen from Figure 5-15, that as the ADF increases, the k_{eff} decreases. It can also be seen that the highest k_{eff} was obtained at ADF = 0.500 and the lowest at ADF = 1.5. The NESTLE system uses a default ADF value set to 1.000.

The difference in k_{eff} between ADF = 0.5 and 1.0 is 85 pcm and that between ADF = 0.5 and 1.5 is 119 pcm. Although these results are large (in terms of 50 pcm), it does not account for the large difference that exists between the MCNP and NESTLE models.

5.3.6 Investigation test 7: Boric acid at different concentrations

In section 5.1, it was stated that the BM models are calculated at BOC, with all rods out and with no boron in the coolant and with the temperatures of all the reactor components set at 300 K. Therefore, the system is expected to be supercritical as it contains only fresh fuel.

This test was conducted to obtain the critical (where the k_{eff} approaches unity) H_3BO_3 concentration of the NA PWR system at BOC for the NESTLE and MCNP models, by using the linear interpolation method in the vicinity of k_{eff} = 1 (plotting the H_3BO_3 concentration), as presented in Figure 5-16. It is noted that in a real reactor, the control rods and burnable poisons are also used to suppress the excess reactivity.

In Figure 5-16 the concentration of the boric acid was increased by increments of 300, starting from 0 to 2100 ppm (parts per million). This is done to anticipate the critical H_3BO_3 by linear interpolation.

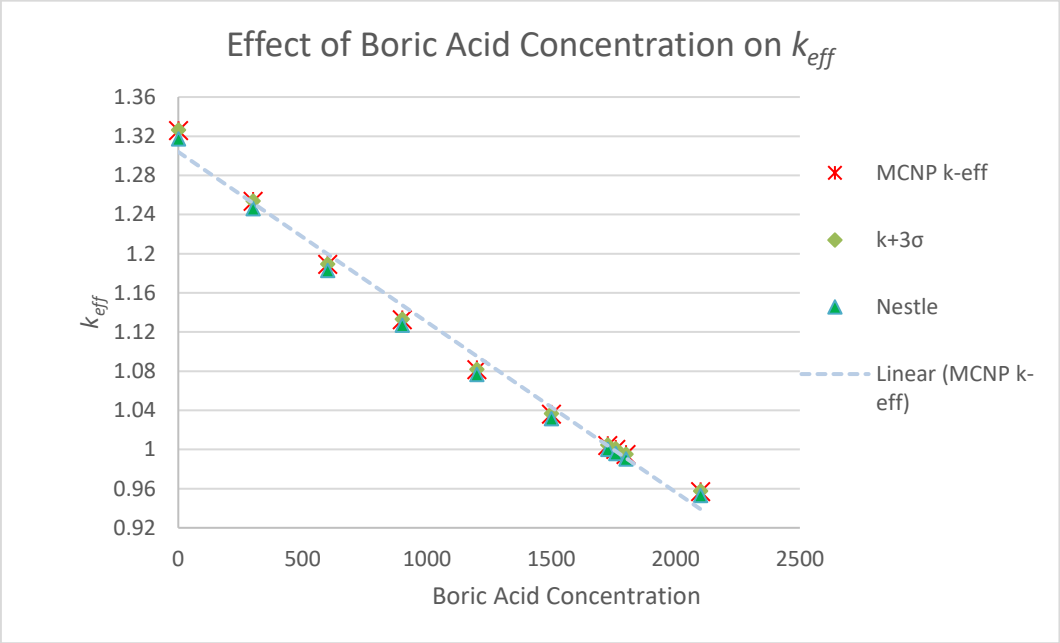

Figure 5-16: Effect of the boric acid concentration of k_{eff}

In Figure 5-16, it is observed that the larger the H_3BO_3 concentration, the smaller the value for k_{eff}, due to boron being a strong absorber. It is also noted, that over the entire range tested, the curve is non-linear.

With analysis based on Eq.(3-39), where $k_{eff} = \frac{\nu \Sigma_f}{DB_g^2 - \Sigma_a}$, it can be seen that the k_{eff} is inversely proportional to the sum of the leakage and the absorption terms. Due to its large thermal neutron absorption cross-section, boron is an ideal isotope for lowering reactor reactivity (Rui et al., 2017), therefore the higher the concentration of boric acid in the reactor, the more neutrons get absorbed.

Table 5-11: Critical boron concentration

	Boron Concentration	MCNP K_{eff} ± σ (std)	Nestle	MCNP - NESTLES	pcm
1	**0**	1.32589 ± 0.00018	1.317149	0.00874	874.1
2	**300**	1.25346 ± 0.00017	1.245855	0.00761	760.51
3	**600**	1.18895 ± 0.0002	1.182899	0.00605	605.08
4	**900**	1.1327 ± 0.00019	1.126858	0.00584	584.16
5	**1200**	1.08138 ± 0.00019	1.07664	0.00474	473.96
6	**1500**	1.03607 ± 0.00021	1.031381	0.00469	468.92

7	**1726.987**	**1.00420 ± 0.00022**	**1.00000**	**0.00420**	**419.92**
8	**1759.029**	**1.00012 ± 0.00021**	**0.995749**	**0.00427**	**427.1**
9	**1800**	0.99474 ± 0.00019	0.990379	0.00436	436.06
10	**2100**	0.95689 ± 0.00021	0.953057	0.00383	383.326
11	**3000**	0.86222 ± 0.00019	0.858801	0.00342	341.945

The critical H_3BO_3 concentration for the NESTLE FC model was obtained at 1726.987 ppm at 300K, with no burnable poisons (where k_{eff} = 1.00008 with the additional 8 pcm considered negligible), while at this concentration of 1726.987 ppm, the k_{eff} of the MCNP was k_{eff} = 1.00420 ± 0.00021 σ. The difference between the NESTLE and MCNP6 was 419.92 pcm and this was found to be a great improvement from the BM models with zero boron.

The critical H_3BO_3 concentration for the MCNP FC model was obtained at 1759.029 ppm which was equal to k_{eff} = 1.00012 ± 0.00021 σ (where the 12 pcm difference from 1.0000 was also considered negligible), while at this concentration of 1759.029 ppm, the NESTLE model obtains a subcritical result of k_{eff} = 0.995749, being 427 pcm below the MCNP value.

By comparing the critical boron concentrations required in both models; 1726.987 for NESTLE and 1759.029 for MCNP, the difference in concentrations is 32 ppm, which expressed as % $diff$ is 1.84%, of which is considered to be small. In this regard, there is good agreement between NESTLE and MCNP-6.2 models.

In Table 5-11 it was observed that the MCNP and NESTLE results have a closer agreement as the boron concentration increases. Although according to (Terradas, 2009); “The boron concentration at the beginning of life for a three-loop Westinghouse design is around 1700ppm” it was nonetheless decided to test the boron concentration for even larger values, to see how close the MCNP and NESTLE results could approach each other. It is noted that this is not intended as a true state of the reactor, since high boron concentrations are not allowed due to criticality safety reasons. As can be seen from the table, with the boron concentration set at 3000, the difference between the two codes reduces to 341.495 pcm.

The SBLOCA with boron dilution study (Terradas, 2009), obtained a steady boron concentration of 1728 ppm at the beginning of life period of a PWR, using RELAP5. This result is similar to the NESTLE result obtained in this study and this thus gives confidence in the present results.

The boron worth can be determined using Table 5-12.

Table 5-12: Boron worth

Boron Concentration	MCNP k_{eff} ± σ (std)	ρ (pcm)	Δρ (pcm)	Δ Bppm	Δρ/Δ Bppm
0	1.32589 ± 0.00018	0.2457896			
300	1.25346 ± 0.00017	0.2022083	-4358.1	300	-14.53
600	1.18895 ± 0.0002	0.1589217	-4328.7	300	-14.43
900	1.1327 ± 0.00019	0.1171537	-4176.8	300	-13.92
1200	1.08138 ± 0.00019	0.752557	-4189.8	300	-13.97
1500	1.03607 ± 0.00021	0.348143	-4044.1	300	-13.48
1800	0.99474 ± 0.00019	-0.52878	-4010.2	300	-13.37
2100	0.95689 ± 0.00021	-0.450522	-3976.4	300	-13.25
					Average = -13,85

By determining the slope of the graph at the two-points $(1200; 1.08138)$ and $(1500; 1.03607)$, the differential boron worth at midpoint (1350 ppm) can be approximated, using the Eq.(4-8) presented in section 4.6.5.4.

$$w_b = \frac{d\rho}{dc_b} = \frac{k_2 - k_1}{c_{b2} - c_{b1}}$$

$$w_b = (\Delta\,\rho/\Delta\,c_b) = \frac{1.03607 - 1.08138}{1500 - 1200} \times 10^5 = -15.1033\ pcm/ppm$$

According to (VEPCO, 2016), the boron coefficient (boron worth) in the primary coolant is -16 to -8 pcm/ppm. Therefore, in this regard, there is good agreement with the obtained result, as it is within the limit set by the NA FSAR report by (VEPCO, 2016).

From the obtained results, the tests are within the boron concentration limit, because the boron concentration in a PWR rarely reaches 3000ppm, although some PWR designs have boron concentrations of 2000ppm or even 2500ppm (Terradas, 2009).

The purpose of the boron tests was to show that the MNCP and NESTLE models behave as predicted. Even though the values are not close to each other, they did improve as the boron concentration increased. Also, the linear trend in the vicinity of k_{eff} = 1.0 was the same and consistent for both the MCNP and NESTLE models, as seen in Figure 5-16.

It should be noted that the use of the H_3BO_3 alone to reduce excess reactivity at BOC could result in a positive moderator coefficient at the beginning of the cycle (Lamarsh & Baratta, 2001; Nuclear Power Contributors, 2022), therefore more tests were conducted to obtain additional means to reduce the reactivity in the system, as shown in section 5.4.

Of all the tests performed to gain insight into why the NESTLE k_{eff} differed from the MCNP results by over 900 pcm, the introduction of boron in the water showed the most promising results.

5.4 Sensitivity studies

5.4.1 Investigation Test 8: Temperature variations of the fuel and moderator

The change in reactivity per degree change in temperature is called the temperature coefficient of reactivity. The fuel temperature coefficient is the change in reactivity per degree change in fuel temperature. An increase in reactor power causes an immediate change in fuel temperature hence a negative fuel temperature coefficient is favourable.

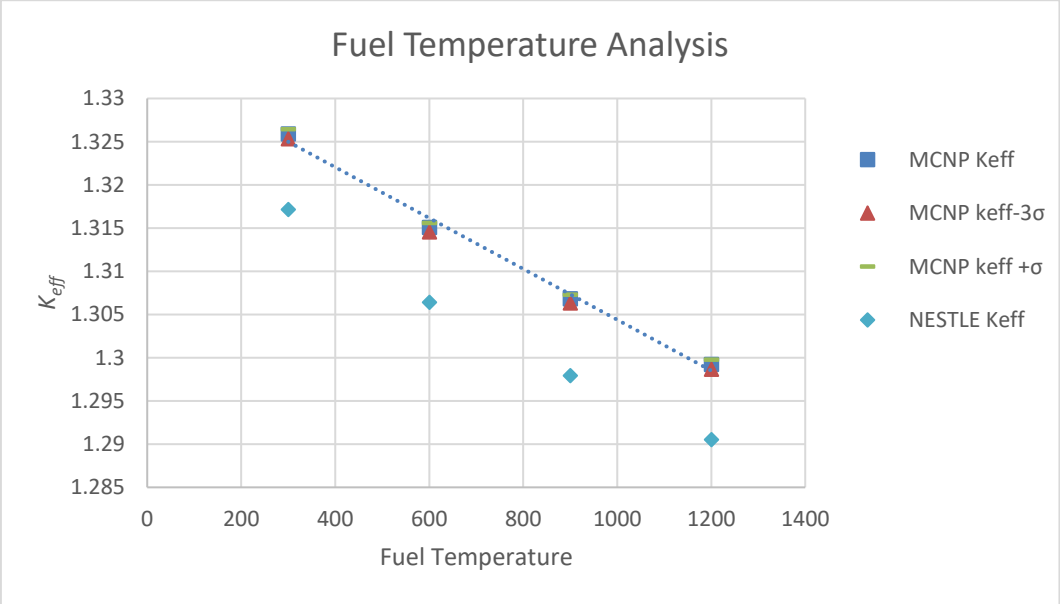

Figure 5-17: Fuel temperature analysis

As shown in Figure 5-17, as the temperatures increase, the k_{eff} of the system decreases. The decrease of k_{eff} with increasing temperature is expected, mainly due to the Doppler broadening of the resonance capture cross-sections of the ^{238}U (Sihlangu, et al., 2019). An increase in the fuel temperature increases the thermal motion of the target nuclei, resulting in the broadening of the lines due to the Doppler Effect. This causes more neutrons to be absorbed in the fuel

(which have absorption cross-section resonances) as they are being slowed down, which results in a reduction in the resonance escape probability (p) (Sihlangu, et al., 2019). This, therefore, causes a reduction in the k_{eff}.

The temperature effects on the moderator are presented in Figure 5-18 for MCNP and NESTLE. It is observed that the k_{eff} decreases as the temperature increases.

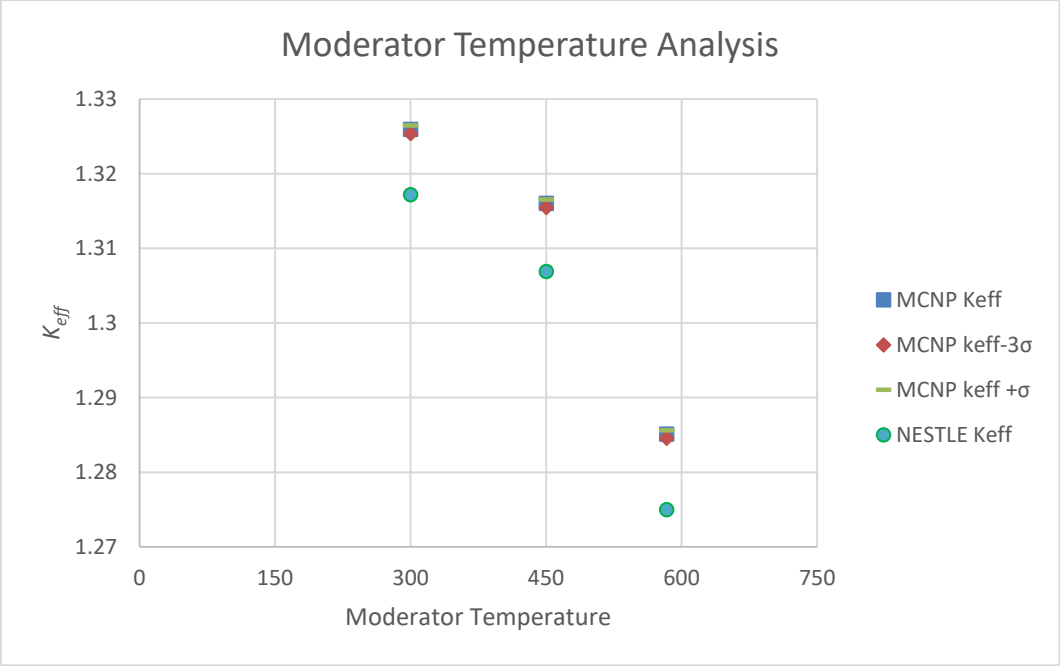

Figure 5-18: Moderator temperature analysis

As the temperature increases, the separation of the water molecules increases due to the thermal expansion, resulting in a decrease in the water density (at high temperatures, the water density is more sensitive). Therefore, there is a lesser moderator per unit volume, resulting in more neutrons having energies above the thermal range. The neutron spectrum in the reactor hardens, resulting in two effects. First, the fission cross-sections decrease in magnitude with increasing neutron energy. Therefore, the fission rate, given as the product of the macroscopic fission cross-section with the flux, decreases when there is a hardening of the neutron spectrum. Second, with the hardening of the neutron spectrum, there is a higher resonance absorption. Therefore, the reactivity (k_{eff}) is lower.

Table 5-13: Moderator temperature analysis

moderator temp	MCNP $k_{eff} \pm \sigma$	ρ (pcm)	Δρ (pcm)	Δ Bppm	Δρ/Δ Bppm
300	1.32589 ± 0.00018	24578.96			
450	1.316 ± 0.00018	24012.16	-566.80	150	-3.78

583.4	1.28507 ± 0.00018	22183.23	-1828.93	133.4	-13.71
				Average	-8.74

The moderating temperature coefficient (MTC) was calculated as shown in Table 5-13, and it can be seen that the system has a negative MTC. A negative temperature coefficient ($\alpha_T < 0$) is desirable because of the following: An increase in temperature leads to a decrease in k_{eff} and hence a decrease in power. This then leads to a decrease in reactor temperature, which then returns the reactor back to its original state before the temperature increases. Both the Doppler and moderator temperature coefficients were shown to be negative above.

5.4.2 Oak Ridge National Laboratory temperatures

The system was set to be modelled using the temperature based on the Oak Ridge National Laboratory (ORNL) report as provided in Table 5-14.

Table 5-14: ORNL parameters (Bowman & Suto, 1996)

ORNL Parameters	Data
System temperature	559 K
Fuel temperature	901 K
Clad Temperature	629 K
Water temperature	583.4 K
Water density	0.7041 g/cm^3

It should be noted that the temperature for helium was not provided, and so it was calculated by taking the average of the fuel and cladding temperatures. Therefore, the helium temperature was set to be 765 K.

With the use of the temperatures provided, a large decrease in the k_{eff} of the system is observed as shown in Table 5-15.

Table 5-15: Ideal system

Model type	Mcnp-k_{eff} ± σ	BM MCNP - MCNP	pcm	Nestle k_{eff}	Mcnp - NESTLE	pcm
Base modal,300k	1.3259 ± 0.00018	0	0	1.3171	0.00874	874.1

ORNL temperatures	1.2628 ± 0.00018	0.06306	6306	1.2520	0.01081	1080.5

The difference between the MCNP Base Model (BM) and the MCNP model with the ORNL temperatures is 6306 pcm, (k_{eff} decreased by 6306 pcm), while the difference between the MCNP and NESTLE model with the ORNL temperatures is 1081 pcm. This is greater than the difference of 874 pcm between the MCNP and NESTLE BMs for the cold model.

The effect of changing the fuel temperature and the moderator temperature has been discussed in the section 5.4.1 and the behaviour is as expected.

5.4.3 Investigation test 7: Insertion of burnable poisons

According to section 5.3.6, it was observed that as the boron concentration was increased, the k_{eff} decreased, but the use of H_3BO_3 alone to reduce excess reactivity at BOC could result in a positive moderator coefficient at the beginning of the cycle (Lamarsh & Baratta, 2001; Nuclear Power Contributors, 2022). Therefore, as per the design in the Safety Analysis Report, it was seen fit to insert the burnable poisons of borosilicate glass material in the core so that a lower H_3BO_3 concentration can be used, to ensure a negative moderator temperature coefficient in the system at BOC.

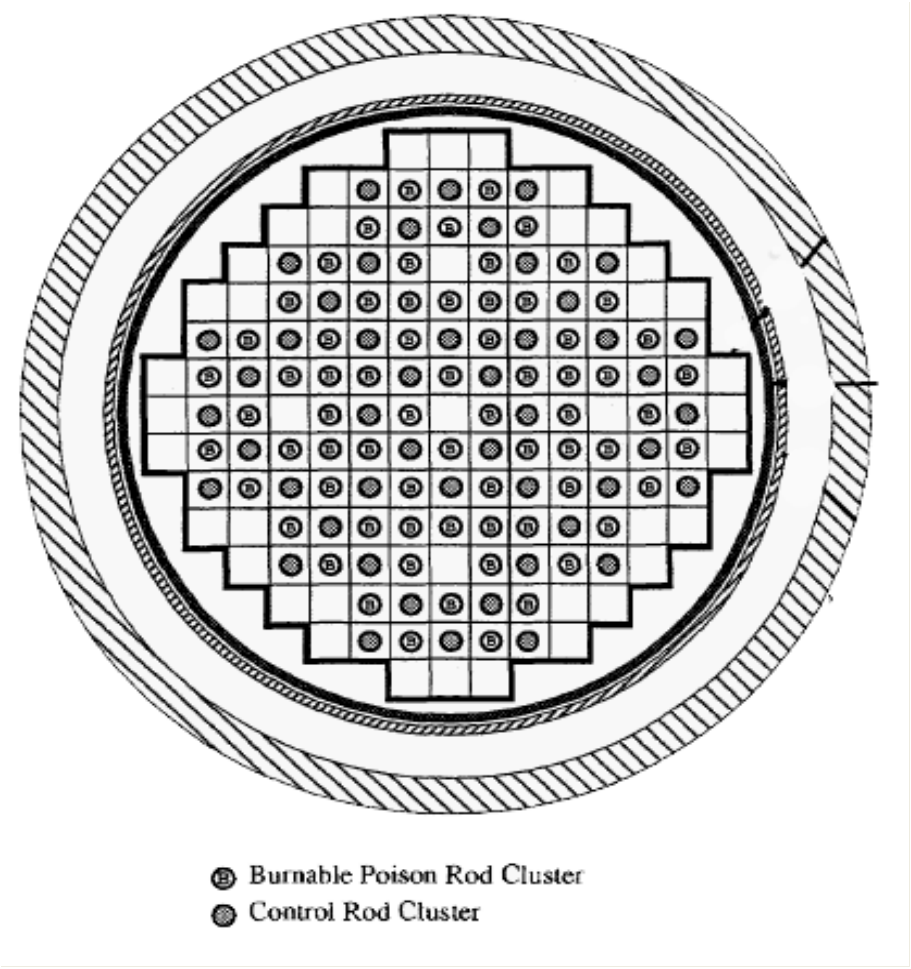

Figure 5-19: NA PWR burnable ooison rod cluster and control rod cluster core configuration (Bowman & Suto, 1996)

The system was tested with burnable poisons (BPs) inserted in the FAs at distinctive locations, according to Figure 5-19. To observe the maximum effect of the BPs in the system, 20 BPs were inserted in the FAs. The FAs that contain the BPs were inserted into the core, according to Figure 5-20.

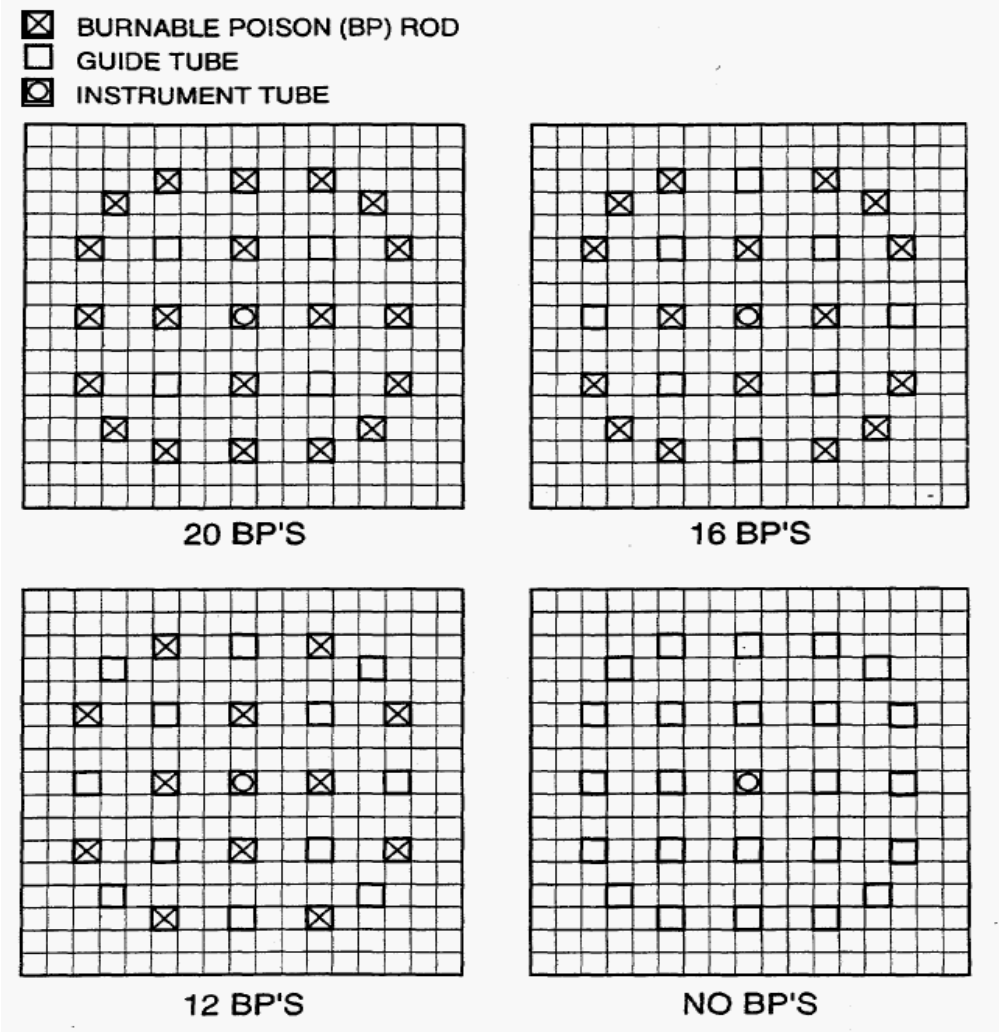

Figure 5-20: FA lattice arrangements in NA PWR (Bowman & Suto, 1996)

It should be noted that the burnable poison test is only conducted for the MCNP-6.2 models. The borosilicate glass material composition within the T-NEWT code is not yet modelled in NWURCS, since this requires self-shielding modelling in XSProc. This was unlike, in section 5.3.6, where the boron was part of the moderator mixture, and it, therefore, gets the correct self-shielding treatment. The control rods, or the burnable poisons, such as the borosilicate glass, must be treated as separate materials in the self-shielding calculations or be included in the other materials with appropriate homogenisation as done by (Sihlangu, et al., 2019; Sihlangu, 2019).

Modelling the BPs in XSProc in terms of the self-shielding was beyond the scope of this study. Therefore, the BP modelling is not conducted using NESTLE, as NWURCS extracts NESTLEs input parameters from the T-NEWT output, which cause the BP calculations within NESTLE to be incompatible due to the borosilicate glass content not being properly self-shielded.

Table 5-16: Borosilicate glass burnable poison analysis

	Model	MCNP k_{eff} ± σ	BM - BP	Average	Ratio	%	pcm
A	**BM (0 B, 300 K, ARO)**	1.32589 ± 0.00018					
B	**12 BP at 0 B, 300 K**	1.26524 ± 0.00018	0.0607	1.2956	0.0468	4.681	6065
C	**16 BP at 0 B, 300 K**	1.24868 ± 0.00017	0.0772	1.2873	0.0600	5.998	7721
D	**20 BP, 0 B, 300K**	1.23266 ± 0.00019	0.09323	1.2793	0.0729	7.288	9323

In Table 5-16, it can be seen that the BPs decreases the value of k_{eff} compared to the reference calculation listed as model D in Table 5-16 and Table 5-17 with the difference being 9323 pcm from the MCNP BM.

Table 5-17: 20 Borosilicated Glass Rods Analysis

	Model	MCNP k_{eff} ± σ	D - BP	Average	Ratio	%	pcm
D	**20 BP, 0 B, 300K**	1.23266 ± 0.00019					
E	**20 BP, 1285.687 ppm, 300K**	1.00004 ± 0.00020	0.2326	1.1164	0.2084	20.8	23262
F	**20 BP, ORNL temp**	1.15512 ± 0.00019	0.0775	1.1939	0.0649	6.5	7754
G	**20 BP, ORNL temp, 300 B**	1.00026 ± 0.00022	0.2324	1.1165	0.2082	20.8	23240

In Table 5-17, the model with 20 BPs at 0 Boron, at an isothermal temperature of 300 K, was used for comparison with later models and is called model D. Comparing model D with the model that has 20 BPs at the FAs, and H_3BO_3 concentration of 1285.687 ppm (model E), it is observed that the value of k_{eff} decreases even further by 23262 pcm. Therefore, a new critical system for MCNP-6.2 is obtained at 1.00004 ± 0.00020, by adding both the H_3BO_3 to the moderator, as well as inserting all 20 BPs at an isothermal temperature of 300 K, thus reduced the reactivity in the core.

With regards to the model (G) using '20 BPs inside the core but with the ORNL temperatures', a critical H_3BO_3 concentration of 300 ppm yields k_{eff} = 1.00026 ± 0.00022 ppm, as compared to the isothermal model (D) at 300K with 20 BP and at 0 ppm, which yielded k_{eff} = 1.23266 ± 0.00019. The increase of fuel temperature and the decrease in moderator density, leads to a decrease in reactivity.

The burnable poison tests, therefore, provides further verification for the NWURCS generated MCNP 6.2 models, and also provides a reference for the T-NEWT/NESTLE calculations when

the BPs are included in the XSProc modelling. It is noted however, that actual core layout incorporating these burnable poisons were not tested.

CHAPTER 6: CONCLUSION AND RECOMMENDATIONS

This chapter presents the conclusions that were reached, as well as recommendations for future studies.

6.1 Conclusion

In this study, the first step was to develop a FA model of the NA reactor using T-NEWT. The T-NEWT model that was manually generated by the user was compared with the T-NEWT model generated by the NWURCS model. Reactor parameters, such as the composition, densities and geometry specification from the input files, as well at the k_{inf} from the output files were compared, to verify the NWURCS input generation capability. The verification tests conducted in section 5.2, proved that the models (both input and output file calculations) to be in good agreement with each other as the % $diff$ between the manually generated T-NEWT model by the user with the NWURCS T-NEWT model was less than 0.5%.

The second step was to develop FC models using MCNP-6.2 and a T-NEWT/NESTLE combination. In section 4.6.1, it was assumed that the NA PWR system would be modelled without spacer grids; without the presence of a reactor vessel and without top and bottom reflectors in the FAs. Unlike the study by (Novak, et al., 2019), which used different temperatures for both the MCNP and NESTLE models, in this study, both the MCNP and the T-NEWT/NESTLE Base-Models (BM) were set to use an isothermal temperature of 300 K for all the core and structural components. The difference obtained between the codes was 874 pcm.

The computational methodology employed in this study could have caused a level of inaccuracies in the calculations, as the T-NEWT/NESTLE combination used deterministic nodal diffusion methods and the Monte Carlo methods were used in MCNP. This resulted in several tests being conducted for further verification.

Therefore, the third step was to verify the FC models, through the sections of 5.2. The NESTLE model was verified to see if the nuclear data taken from T-NEWT was accurately placed into the NESTLE input file through the use of NWURCS. Although certain errors in the models were detected, the NWURCS code was successfully verified. The error reported in section 5.2.2, was subsequently fixed, while the errors that were reported in sections 5.3.1.1 and 5.3.1.2, were minor and manual insertion was permitted. These will be fixed by the developer in further releases of NWURCS.

The MCNP model was verified through visual inspection of MCNP-6.2 and KENO-VI FC plots. The verification proved to be successful as the plots were identical in structure, and also reflected the geometry accurately.

To verify the T-NEWT/NESTLE model with MCNP 6.2 model, several tests were performed, given in section 5.3. First, the models were converged in section 5.3.1 both in terms of the source and the multiplication factor. The MCNP 6.2 model was converged to obtain a model with low statistical uncertainty. The convergence of the MCNP 6.2 FC model was successfully reached with 100000 neutron source points, with 245 inactive and 1100 active cycles for the FC model.

The NESTLE model decrease by 35 pcm when the following parameters $S_{N=12}$; $GG = 24 \times 24$; $LG = 16 \times 16$, were used to converge the k_{inf} in the XSPRoc/NEWT calculation, prior to the output extraction which was used in the NESTLE tt1.i.

The second analysis was based on the core barrel and the boundary conditions presented in sections 5.3.2 and 5.3.3. Although the MCNP-6.2 model was modified to have identical lattice boundary conditions to the NESTLE model (where there were no nodes intersected by the boundary at the edges), a difference of around 800 pcm was still obtained between the models. Although the testing demonstrated that the discrepancy was not caused by the boundary cutting through the nodes, the tests did reveal that the trends are consistent, implying that the NWURCS was working correctly.

With the control rods not modelled, and the structural temperature kept isothermally at 300K, the system's criticality was achieved utilizing H_3BO_3 at a concentration of 1726.987 ppm for the MCNP-6.2 model, with a differential boron worth -13.4 pcm/ppm.

While,1726.59 ppm was required for the NESTLE model to be critical. The readings in the literature study by (Terradas, 2009), which were 1728 ppm for the NESTLE model, were in good agreement with the critical boron concentration obtained in this study.

Finally, the T-NEWT/NESTLE code combination and MCNP provided results which were in good agreement with the nuclear engineering principles and graphic trends. When both the soluble boron and burnable poison rods are inserted into the modelled system, a critical state

is achieved. This research shows that the T-NEWT/NESTLE code combination can perform efficient and complete core computations for NA PWR.

6.2 Recommendations

T-NEWT/NESTLE

The first recommendation is with regards to the XSPRroc self-shielding calculation data. In the T-NEWT calculation, XSProc self-shields cells that contain fissile and fissionable material, such as a fuel pin, with the boron in the coolant. The unit cell that is not considered in the self-shielding process is the burnable poison rods.

To self-shield the borosilicate glass burnable poison rods, the rod materials have to be treated as separate materials in self-shielding calculations within T-NEWT, or they must be included in other materials with appropriate homogenization. A similar study was conducted by (Sihlangu, et al., 2019) for the prismatic gas cooled reactor. Once the burnable poison rods are self-shielded, this means that the multigroup cross-sections for fuel assemblies containing BPs will be available, and the NESTLE calculations can be extended. The NESTLE borosilicate glass analysis was not considered previously in section 5.4.3, therefore, it is recommended that further investigation should be taken in terms of NESTLE burnable poison analyses.

As an alternative, the cross-sections for the borosilicate glass burnable poison rods can be generated using the Monte Carlo code, SERPENT, and therefore the cross-sections from SERPENT could be used for the NESTLE calculations. However, due to the scope of the current work, and since the use of SERPENT means using a different code to those used in this study, this study is recommended for future work.

NWURCS

Recommendations are required to be carried out in NWURCS in terms of the extraction capability option of ADFs. The data must be extracted from the T-NEWT output and input into the collapsed cross-section file C:\0_tr\xscoll\xs_collapsed_00001 to _00004 for it to be included in the NESTLE input file.

The coding error found in NWURCS regarding the '*Sn*, the local grids and the global grids' insertion, needs to be fixed.

MCNP 6.2 model

With regards to the MCNP input file [C:\0_tr\iter01\runmcnp6\inputs\inp01], a coding error was detected with the KCODE section. Changes to the KCODE (increasing or decreasing the number of source points and the number of the active and inactive cycles) are done in C:\0_tr\ixxxxx\f005.i file, but the changes were overwritten and assigned default values. Therefore, a manual insertion was required. This coding error needs attention. These will be fixed by the developer in further releases of NWURCS.

REFERENCES

ATI, 2015. *Zirconium Alloys -Technical Data Sheet,* Pittsburgh, PA 15222-5479 U.S.A.: Allegheny Technologies Incorporated.

Bandini, B. R., 1990. *A THREE-DIMENSIONAL TRANSIENT NEUTRONICS ROUTINE FOR THE TRAC-PFl REACTOR THERMAL HYDRAULIC COMPUTER CODE.* Pennsylvania: The Pennsylvania State University, The Graduate School College of Engineering.

Bornstein, I. & Martin, W., 2016. *Britannica_Nuclear engineering.* [Online] Available at: https://www.britannica.com/technology/nuclear-engineering

Bowman, S. M. & Suto, T., 1996. *SCALE-4 Analysis of Pressurized Water Reactor Critical Configurations: Volume - North Anna Unit 1 Cycle 5.* ORNL/TM-12294/V5 ed. Oak Ridge, TN 3783, United States: Oak Ridge National Laboratory, Computational Physics and Engineering Division.

Brown, F. B., Mosteller, R. D. & Sood, A., 2003. Verification of MCNP5. Nuclear Mathematical and Computational Sciences. *Century in Review, A Century Anew.*

Carter, L. L. & Schwarz, R., 1995. *MCNP visual Editor computer code manual,* Washington, DC, United States: United States Department of Energy.

Cho, B. O., 1999. *MASTER-2.0: Multi-purpose Analyzer for Static and Transient Effects of Reactors.* KAERITR-121199 ed. s.l.:Korea Atomic Energy Research Institute.

du Toit, M. H., 2017. *Analysis of specific design aspects of a thorium-uranium fuelled European Pressurised Reactor.* PhD in Nuclear Engineering ed. North-West: North-West University.

du Toit, M. & Naicker, V. V., 2018a. Developing a Full-Core MCNP6 and RELAP5 Model of the European Pressurized Reactor Using NWURCS. *Nuclear Science and Engineering,* 191(3), pp. 291-304.

du Toit, M. & Naicker, V. V., 2018b. Neutronic design of homogeneous thorium/uranium fuel for 24 month fuel cycles in the European pressurized reactor using MCNP6. *Nuclear Engineering and Design,* 337(May), pp. 394-405.

Electric Power Research Center, 2003. *NESTLE Version 5.2.1. Few-Group Neutron Diffusion Equation Solver Utilizing The Nodal Expansion Method for Eigenvalue, Adjoint, Fixed- Source Steady-State and Transient Problems,* United States: Electric Power Research Center.

Eskom, 2020. *Eskom Holdings Limited.* [Online]
Available at: https://loadshedding.eskom.co.za/LoadShedding/Description
[Accessed 2020].

ESKOM, 2021. *ESKOM.* [Online]
Available at:
https://www.eskom.co.za/Whatweredoing/ElectricityGeneration/KoebergNuclearPowerStation/Pages/Operating_Method.aspx
[Accessed 20 June 2021].

Framatome, 2019. *Framatome.* [Online]
Available at: https://www.framatome.com/EN/businessnews-93/our-organization-evolves.html
[Accessed 20 June 2020].

Hollenbach, D. F., 2011. KENO-VI: A General Quadratic Version of the KENO Program. In: O. R. N. Laboratory, ed. U.S. Department of Energy. Oak Ridge, Tennessee: s.n.

Horelik, N. et al., 2018. *Benchmark for Evaluation And Validation of Reactor Simulations (BEAVRS).* v2.0.2 ed. Sun Valley, Idaho: MIT Computational Reactor Physics Group.

IAEA, 1999. *Assessment and management of ageing of major nuclear power plant components important to safety: PWR vessel internals.* IAEA-TECDOC-1119 ed. Wagramer Strasse 5, Wagramer Strasse 5, A-1400 Vienna: International Atomic Energy Agency.

IRP, 2019. *Integrated Resource Plan,* Republic of South Africa: Department of Minerals Resources and Energy.

Jessee, M. A. & DeHart, M. D., 2018. NEWT: A New Trabsport Algorithm for Two-Dimensional Discrete-Orfinates Analysis in Non-Orthogonal Geometries. In: B. T. Rearden & M. A. Jessee, eds. *SCALE Code System, ORNL/TM-2005/39, Version 6.2.3.* Oak Ridge, Tennessee: Oak Ridge National Laboratory, pp. 9-79 to 9-196.

Jessee, M. A. et al., 2018. TRITON: A Multipurpose Transport, Depletion, and Sensitivity and Uncertainty Analysis Module. In: B. T. Rearden & M. A. Jessee, eds. *SCALE Code System, ORNL/TM-2005/39, Version 6.2.3.* Oak Ridge, Tennessee: Oak Ridge National Laboratory, pp. 3-3 to 3-116.

Kirkland, W. M., 2017. *"Improvements to NESTLE: Cross-Section Interpolation and N-Group Extension".* Master's Thesis ed. Teennesse, USA: University of Tennessee, Knoxville.

Lamarsh, J. R. & Baratta, A. J., 2001. *Introduction to Nuclear Engineering.* Third Edition ed. Upper Saddle River, New Jersey 07458: Prentice Hall.

Lathrop, K. D., 1969. Spatial Difference of the Transport Equation: Positivity vs. Accuracy. Volume 4, 475.

Leppänen, . J., 2015. *Serpent - a Continuous-energy Monte Carlo Reactor Physics Burnup Calculation Code User Manual.* Finland: VTT Technical Research Centre of Finland.

Lewis, E. E. & Miller, W. J., 1993. *Computational methods of neutron transport.* La Grange Park, Illinois: American Nuclear Society.

Luciano, N. P. & Maldonado, I. G., 2017. *Two-dimensional hexagonal geometry discontinuity factors at the core periphery.* 107 ed. The University of Tennessee, Department of Nuclear Engineering, 311 Pasqua Engineering Building, Knoxville, TN 37996-2300, United States: Annals of Nuclear Energy.

Manassah, J. T., 1981. *Alternative Energy Sources.* London: Academic Press, Inc.

Maretele, D. A., 2016. *Uncertainty analysis of the fuel compact of the prismatic high temperature gas-cooled reactor test problem using SCALE6.1.* Potchefstroom: North-West University.

Mertyurek, U. & Williams, M. L., 2018. BONAMI: Resonance Self-Shielding by the BONDARENKO Method. In: B. T. Rearden & M. A. Jessee, eds. *SCALE Code System, ORNL/TM-2005/39, Version 6.2.3.* Oak Ridge, Tennessee: Oak Ridge National Laboratory, pp. 7-194 to 7-221.

Montwedi, O., 2014. *Neutonic simulation of a European Pressurised Reactor.* Potchefstroom North-West: Potchefstroom Campus of North West University.

Mulasi, C., 2021. *Criticality study of a spent fuel pool using SCALE-6.2.3 and MCNP6.2.* Master ed. North-West: North-West University.

Naicker, V. V., 2021, December. *NWURCS User Manual.* Version 3.1, Beta ed. North-West University, Potchefstroom, South Africa: North-West University.

Naicker, V. V., 2022. *NWURCS User Manual.* Version 3.1, Beta ed. North-West University, Potchefstroom, South Africa: North-West University.

Naicker, V. V., Sihlangu, S. F., Hou, J. & Reitsma, f., 2021. *Uncertainty Propagation for the HTTR in terms of the IAEA CRP on HTGR Uncertainty Analysis in Modelling.* INDONESIA, Proceedings of HTR 2021, Paper HTR 2021-097.

Novak, O. et al., 2019. Benchmark evaluation of zero-power critical parameters for the Temelin VVER nuclear reactor using SERPENT & NESTLE and MCNP. *Nuclear Engineering and Design,* 110243(353).

NRF, 2022. *National Research Foundation.* [Online]
Available at: https://www.nrf.ac.za/core-mandate-business-divisions/risa-directorates/research-chairs-and-centres-of-excellence-rcce/south-african-research-chairs-initiative/
[Accessed August 2022].

Nuclear Power Contributors, 2022. *Nuclear Power.* [Online]
Available at: https://www.nuclear-power.com/nuclear-power/reactor-physics/nuclear-fission-chain-reaction/operational-factors/
[Accessed 23 April 2022].

nuclear-power.net, 2021. *nuclear-power.net.* [Online]
Available at: (https://www.nuclear-power.net/nuclear-power/reactor-physics/nuclear-fission-chain-reaction/reactivity/
[Accessed 04 06 2021].

Nyalunga, . G., Naicker, V. & du Toit, M., 2016. Developing skills for neutronic modelling of nuclear power reactors in South Africa. *Journal of Energy in Southern Africa,* 27(4), pp. 64-76.

Nyalunga, G. P., 2016. *Developing a fresh core neutronic model at 300K for a VVER-1000 reactor type using MCNP6. 25449753.* Potchefstroom Campus of the North-West University: North-West University.

Nyalunga, G. P., 2019. *Quantifying uncertainties of aspects of the neutronics modelling of the Kozloduy-6 system using SCALE 6.2.1.* Potchefstroom Campus, North-West University: North-West University, Thesis.

Nyalunga, G. P., Naicker, V. V. & Ivanov, K., 2019. Quantification and propagation of neutronics uncertainties of the Kozloduy-6 VVER-1000 fuel assembly using SCALE 6.2.1 within the NEA/OECD benchmark for uncertainty analysis in modelling of LWRs. *Annals of Nuclear Energy,* Volume 133, pp. 723-749.

ORNL, 2021. *OAK RIDGE National Laboratory.* [Online]
Available at: https://www.ornl.gov/directorate/reactor-neutronics
[Accessed 14 October 2021].

Osusky, F. et al., 2018. Coupled Simulation of Gas Cooled Fast Reactor Fuel Assembly With Nestle Code System. *Acta Polytechnica CTU Proceedings,* 14(1), p. 34.

Oxford, U. P., 2020. *Oxford Reference.* [Online]
Available at:
https://www.oxfordreference.com/view/10.1093/oi/authority.20110803100533771
[Accessed 23 Nobember 2020].

Pelo, H. L., 2013. *Evaluation of an advanced fault detection system using Koeberg nuclear power plant data.* Potchefstroom Campus of the North-West University: North-West University; Master of Science in Nuclear Engineering - 21970386.

Perko, Z., 2015. *Sensitivity and uncertainty analysis of coupled reactor physics problems - Method development for multi-physics in reactor.* Delft, The Netherlands: Delft Universit of Technology, Thesis..

Petrie, L. M. et al., 2018. KENO: A Monte Carlo Criticality Program. In: ORNL/TM-2005/39, ed. *SCALE-6.2.3 Code System.* Oak Ridge, TN 37831-6283: Oak Ridge National Laboratory, pp. 8-5 to 8-586.

Rearden, B. T. & Jessee, M. A., 2018. *SCALE Code System, ORNL/TM-2005/39.* Version 6.2.3 ed. Oak Ridge, Tennessee: Oak Ridge National Laboratory.

RELAP5-3D Team, 2014. *RELAP5-3D/4.2.* Volume II , Appendices II ed. P.O. Box 1625, Idaho Falls, ID 83415: Idaho National Laboratory,.

RELAP5-3D_Team, 2013. *RELAP5-3D.* Version 4.1.3 ed. Idaho Falls: Idaho National Laboratory, P.O. Box 1625.

Rui, L., LingYu, Z., Dunfu, S. & Li, D., 2017. Criticality search of soluble boron iteration in MC code JMCT. *Science Direct,* Issue 127, pp. 329-334.

Sanchez, R., Mao, L. & Santandrea, S., 2002. *Treatment of boundary conditions in trajectory-based deterministic.* s.l.:Nuclear science and engineering.

Schultz, R. R., 2014. *RELAP5-3D Code Manual, Volume V: User's Guidelines.* Version 4.2 ed. Idaho Falls, Idaho 83415, United States: Idaho National Laboratory.

Shim, H. J. & Kim, C. H., 2016. *McCARD User's Manual ver 1.1.* s.l.:Seoul National University.

Shultis, J. K. & Faw, R. E., 2011. *An MCNP Primer.* Manhattan, KS 66506: Dept. of Mechanical and Nuclear Engineering, Kansas State University.

Sihlangu, S. F., 2016. *A neutronic model of the PMR200 prismatic modular reactor using MCNP5.* Master's in Nuclear Engineering ed. North-West: North-West University.

Sihlangu, S. F., 2019. *Uncertainty and sensitivity analysis of aspects of the neutronics of a prismatic block-type HTGR.* PhD ed. North-West: North-West University.

Sihlangu, S. F., Naicker, V. V., Hou, J. & Reitsma, S. F., 2019. Further development of methodology to model TRISO fuel and BISO absorber particles and related uncertainty quantification using SCALE 6. *Journal of Nuclear Science and Technology,* 56:8(DOI: 10.1080/00223131.2019.1617204), pp. 690-709.

Stacey, W. M., 2007. *Nucleaar Reactor Physics.* Second Edition, Completely Revised and Enlarged ed. Georgia Institute of Technology, Nuclear & Radiological Engineering, 900 Atlantic Drive, NW(Atlanta, GA 30332-0425): WILEY-VCH Verlag GmbH & Co. KGaA, Weinheim.

Taavitsainen, A., 2016. *CFENSS-SRS method for he uncertainty analysis of nuclear fuel and neutronics.* Thesis ed. Espoo, Finland: Aalto University.

Terradas, J. F., 2009. *SBLOCA with boron dilution in pressurized water reactors. Impact on operation and safety.* s.l.:s.n.

Thokwane, K. M., 2020. *Initial Implementation of the neutrinics codes DRAGON and DONJON at the North-West University.* Potchefstroom Campus at the North- West University(North-West): s.n.

Turinsky, P. J., Al-Chalabi, R. M. k., Engrand, P. & SarSour, H. N., 1994. *NESTLE. Few-Group Neutron Diffusion Equation Solver Utilizing the Nodal Expansion Method (NEM) for Eigenvalue, Adjoint, and Fixed-Source Steady-State and Transient Problems,* United States: Electric Power Research Center.

VEPCO, 2016. *North Anna Power Station Updated Final Safety Analysis Report Chapter 4,* Virginia Electric and Power Company Richmond, Virginia 2361: United States Nuclear Regulatory Commission.

VEPCO, 2016. *North Anna Power Station Updated Final Safety Analysis Report. Chapter 1.* NAPS UFSAR ed. Virginia Electric and Power Company Richmond, Virginia 2361: s.n.

Werner, C. J., 20217. *MCNP user's Manual Code Version 6.2..* LA-UR-17-29981 ed. Los Alamos: Los Alamos National Laboratory.

Wikipedia Contributors, 2021. *wikipedia.org.* [Online]
Available at: https://en.wikipedia.org/wiki/Framatome
[Accessed 18 October 2021].

Williams, M. L., 2018. CENTRM: A Neutron Transport Code for Computing Continuos-Energy Spectra in General One-Dimensional Geometries and Two-Dimensional Lattice Cells. In: B. T. Rearden & M. A. Jessee, eds. *SCALE Code System, ORNL/TM-2005/39, Version 6.2.3.* SCALE Code System, ORNL/TM-2005/39, Version 6.2.3: Oak Ridge National Laboratory, pp. 7-222 to 7-282.

Williams, M. L. et al., 2018. XSPROC: The Material and Cross-Section Processing Module for SCALE. In: B. T. Rearden & M. A. Jessee, eds. *SCALE Code System, ORNL/TM-2005/39, Version 6.2.3.* Oak Ridge, Tennessee: Oak Ridge National Laboratory, pp. 7-5 to 7-111.

Wu, Y., 2017. Fusion Neutronics. In: *Chapter 2: Neutron Transport Theory and Simulation.* 1 ed. Hefei: Springer Singapore, pp. XX, 392, p. 192.

X-5 Monte Carlo Team., 2003. *MCNP Version 5, Vol 1: Overview and Theory.* s.l.:s.n.

APPENDIX

7.1 Appendix A: T-NEWT input file

An input file example for T-NEWT is presented. The input file demonstrates the input for the fuel assembly with an instrumentation pin and 24 guide tubes for the North-Anna Reactor criticality calculations. The explanations shown in the second column include direct phrases from (Jessee & DeHart, 2018; Rearden & Jessee, 2018). This was done to maintain the specific meaning, and the reader is referred to the source for further clarification.

Table 7-1: T-Newt Input File

=t-newt parm=centrm input generated using NWURCS: gc_apr2020 v7-252	The type of code is specified together with the title of the calculation and the nuclear data library.
read composition ' Water_01_____ ' | SC | MX | VF | ADEN | TEMP | END | → Material Composition definition h-1 1 0 6.71153E-02 300.0 end h-2 1 0 7.71914E-06 300.0 end o-16 1 0 3.35487E-02 300.0 end o-17 1 0 1.27534E-05 300.0 end ' Water_02_____ h-1 2 0 6.71153E-02 300.0 end h-2 2 0 7.71914E-06 300.0 end o-16 2 0 3.35487E-02 300.0 end o-17 2 0 1.27534E-05 300.0 end ' fuel_3.1%_____ o-16 3 0 4.64444E-02 300.0 end o-17 3 0 1.76556E-05 300.0 end u-235 3 0 7.29086E-04 300.0 end u-238 3 0 2.25020E-02 300.0 end ' He_____ he-3 4 0 2.42905E-10 300.0 end he-4 4 0 2.40500E-04 300.0 end ' zircaloy_____ cr-50 5 0 3.30232E-06 300.0 end cr-52 5 0 6.36820E-05 300.0 end cr-53 5 0 7.22102E-06 300.0 end cr-54 5 0 1.79747E-06 300.0 end fe-54 5 0 8.25371E-06 300.0 end fe-56 5 0 1.29566E-04 300.0 end fe-57 5 0 2.99223E-06 300.0 end fe-58 5 0 3.98211E-07 300.0 end zr-90 5 0 2.18497E-02 300.0 end zr-91 5 0 4.76489E-03 300.0 end zr-92 5 0 7.28323E-03 300.0 end zr-94 5 0 7.38091E-03 300.0 end zr-96 5 0 1.18910E-03 300.0 end sn-112 5 0 4.83386E-06 300.0 end sn-114 5 0 3.28902E-06 300.0 end sn-115 5 0 1.69434E-06 300.0 end sn-116 5 0 7.24581E-05 300.0 end sn-117 5 0 3.82722E-05 300.0 end sn-118 5 0 1.20697E-04 300.0 end sn-119 5 0 4.28071E-05 300.0 end sn-120 5 0 1.62358E-04 300.0 end sn-122 5 0 2.30730E-05 300.0 end sn-124 5 0 2.88537E-05 300.0 end end composition	In this block, the compositions of the materials of the NA PWR are defined, such as the fuel, water zircaloy cladding and helium.
' ---------- read celldata latticecell squarepitch	This block shows the XSProc parameter definition for the cross-section processing.

fuelr = 0.40957 3 gapr = 0.41783 4 cladr = 0.47498 5 hpitch= 0.62992 2 end end celldata	
' ---------- read model read parm prtflux= yes prtxsec= yes prtmxsec= yes prtbroad= yes prtmxtab= no drawit= yes collapse= yes echo= yes solntype= b1 timed= yes inners= 2 outers= 200 epsilon= 5.00000E-05 epseigen= 5.00000E-05 sn = 6 cmfd = 2 xycmfd= 2 end parm	In the Parameter Block, the parameters that will be used to enable the printing of parameters such as cross-sections, convergence, and fluxes are specified and are given a set of instructions.
' ---------- read materials ' | M | N | Com | END | Mix = 1 pn= 2 end Mix = 1 pn= 2 end mix = 3 pn= 1 end mix = 4 pn= 1 end mix = 5 pn= 1 end end materials	Material Block is specified for the NEWT calculation.
' ---------- read collapse 213r1 39r2 end collapse	The collapse block is defined.
' ---------- read homog 122 node22 1 end 121 node21 2 3 4 5 end end homog	The homogenised block is defined.
' ---------- read adf 2 121 122 w= 21.503640 end adf	The Assembly Discontinuity Factors block is defined.
' ---------- read geom global unit 1 cuboid 10 43.00728 0.00000 21.50364 0.00000 cuboid 20 21.46046 0.04318 21.46046 0.04318 cuboid 30 21.50364 0.00000 21.50364 0.00000 media 1 1 10 -30 array 2 20 place 1 1 0.04318 0.04318 media 2 1 -20 30 boundary 10 16 8 unit 3 cylinder 10 0.40957 origin x= 0.62992 y= 0.62992 cylinder 20 0.41783 origin x= 0.62992 y= 0.62992 cylinder 30 0.47498 origin x= 0.62992 y= 0.62992 cuboid 40 1.25984 0.00000 1.25984 0.00000 media 3 1 10 media 4 1 -10 20 media 5 1 -20 30 media 1 1 -30 40 boundary 40 4 4 unit 4 cylinder 10 0.57150 origin x= 0.62992 y= 0.62992 cylinder 20 0.61214 origin x= 0.62992 y= 0.62992 cuboid 30 1.25984 0.00000 1.25984 0.00000 media 1 1 10 media 5 1 -10 20 media 1 1 -20 30 boundary 30 4 4 unit 5 cylinder 10 0.57150 origin x= 0.62992 y= 0.62992 cylinder 20 0.61214 origin x= 0.62992 y= 0.62992 cuboid 30 1.25984 0.00000 1.25984 0.00000 media 1 1 10 media 5 1 -10 20 media 1 1 -20 30 boundary 30 4 4 end geom	In the geometry block, a 3D geometry and a 2D geometry are defined for the NEWT calculation. The global unit defines the assembly pitch and assembly gap parameters. The local unit defined the fuel pin, instrumentation pin and guide tube parameters.

' ---------- read bounds all=refl end bounds	The boundary condition is defined in this block.
' ---------- read array ' ---------- ara= 2 typ=cuboidal nux=17 nuy=17 fill 3 3 3 3 3 3 3 3 3 3 3 3 3 3 3 3 3 3 3 3 3 3 3 3 3 3 3 3 3 3 3 3 3 3 3 3 3 3 3 4 3 3 4 3 3 4 3 3 3 3 3 3 3 3 4 3 3 3 3 3 3 3 3 3 4 3 3 3 3 3 3 3 3 3 3 3 3 3 3 3 3 3 3 3 3 3 3 4 3 3 4 3 3 4 3 3 4 3 3 4 3 3 3 3 3 3 3 3 3 3 3 3 3 3 3 3 3 3 3 3 3 3 3 3 3 3 3 3 3 3 3 3 3 3 3 3 3 3 4 3 3 4 3 3 5 3 3 4 3 3 4 3 3 3 3 3 3 3 3 3 3 3 3 3 3 3 3 3 3 3 3 3 3 3 3 3 3 3 3 3 3 3 3 3 3 3 3 3 3 4 3 3 4 3 3 4 3 3 4 3 3 4 3 3 3 3 3 3 3 3 3 3 3 3 3 3 3 3 3 3 3 3 3 3 4 3 3 3 3 3 3 3 3 3 4 3 3 3 3 3 3 3 3 4 3 3 4 3 3 4 3 3 3 3 3 3 3 3 3 3 3 3 3 3 3 3 3 3 3 3 3 3 3 3 3 3 3 3 3 3 3 3 3 3 3 3 3 3 3 end fill end array end model end	The array block is defined.

7.2 Appendix B: T-NEWT model development

Table 7-2 presents all the FA model developments for T-NEWT.

Table 7-2: T-NEWT model development

Model	Modification of the Model
	Fuel assembly to Fuel Pin
Lily_01 - 07 from NEWT4-sample 4 (Rearden & Jessee, 2018).	Lily_01: Using the NEWT4 sample, the collapsed block, homogenisation and ADF blocks were deleted. Lily_02: The array card was modified to cater for only one Fuel Pin FP. Lily_03-04: The material was modified to suit a fuel pin material. Lily_05-07: The array card was removed. As only one unit remained - unit1, the global unit was changed to 1 and a boundary was resigned.
Lily_07-08 from Lily_06	Using data from Table 2-2 and Table 2-3, the correct dimensions and materials were used for the pellet, clad and pitch, in the composition, material and celldata block. 2.1 w/o % enrichment was used. Temperatures were set to 300K.
	Fuel pin with Helium Gap
Tulip_01-04 from Lily_08	The helium gap was added. Tulip_01: The helium composition with the temperature set to 300K was inserted into the composition card. Tulip_02-03: The gap was specified in the latticecell of the 'celldata' block as 'gapd = 0.83566 4'. This included the addition of the gap material definition in the material card. Tulip_04: A cylindrical unit statement was Table 2-3 defined in the geometry block with the gap dimensions from Table 2-3.
Tulip_05-06 from Tulip_04	Tulip_05: This is carried out with the 2.6 w/t% composition, using tulip_04. Tulip_06: This is carried out with the 3.1 w/t% composition, using tulip_04.
	Fuel Pin to Fuel Assembly
Sunflower_01-03 from Tulip_04	Using tulip_04, a 17x17 fuel assembly was constructed with the only fuel pins in the array block. The NEWT4 sample was used as a template for the input syntax.

	The global unit and the lattice array had to be defined accordingly, based on the assembly pitch dimensions from Table 2-2
Fuel Assembly with Instrumental Pin and Guide Tube	
Gardenia_01-03 from Sunflower_03	A unit '5' is defined in the geometry block, for the instrumental, which has a cuboid unit statement and two cylindrical unit statements. These unit statements are assigned with the correct instrumental pin dimensions given in Table 2-3, and they use 'mix=1' and 'mix=5' in the material block are used for the instrumental pin, as seen in Table 7-1 The instrumental pin is defined in the centre of the 17x17 lattice in the array block.
Gardenia_04_05 from Gardenia_03	Since the guide tube and instrumental pin have the same dimensions, a 'unit 4' was defined in the geometry block with the same structural layout and dimensions as 'unit 5'. Therefore, 24 guide tubes were added to the array block. Note that no control rods were inserted into the guide thimbles.
Models with Gap Between the Assembly	
Daffodil_04 from Gardenia_05	Using Table 2-2, a gap around the assembly is added. The total assembly pitch with gap material included was 21.50364 cm and thus the actual gap dimension is 0.04318 cm. In the global unit, a cuboid definition of the assembly gap and its associated lattice array definition within the global unit were defined, along with the dimensions mentioned above. The assembly pitch and the gap can be seen in 'global unit 1' in Figure 4-2. .
Gardenia_06-07 from Gardenia_05	Gardenia_05 was repeated for a calculation that had 2.6wt % enrichment (Gardenia_06), and for the 3.1 wt% enrichment (Gardenia_07)
Base-Model	
BaseModel_01 from Gardenia_05	Gardenia_07, which consisted of 3.1 wt % enrichment was used for this calculation. The ENDF library was changed from v7- 238 to v7- 252.
BaseModel_02	The global unit grid boundary was changed from 30 30 to 8 8.
BaseModel_03	A homogenising block was added just below the params card.
BaseModel_04	The collapse block was added to the input.
BaseModel_05	The ADF Block was added.
BaseModel_06-07 from Basemodel_05	Calculations based on BaseModel_05 are repeated for enrichments 2.6 and 2.1 wt % respectively.
BaseModel_08 from Basemodel_05	BaseModel_05 is copied and renamed to BaseModel_08. A moderator material (material 1) in the composition card is added, and a mix = 1 in the material card was added, this serves as the reflector. Based on Newt5 from the SCALE manual, the assembly pitch with its gap is doubled to cater for the reflector. (21.50364 cm x 2= 43.00728 cm). The Homogenisation block and the ADF block were changed to: *"Read hmog* *500 fuelassm 2 3 4 5 end* ***501 reflassm 1** end* *end hmog"* *read adf* ***2 500 501 w= 21.50364*** *end adf*
BaseModel_09 from Basemodel_08	Basemodel_08 did not run to completion. The global definition was not defined correctly, in the geometry block. In 'global unit 1', three cuboids had to be defined. One for the fuel assembly, the other for the gap of the assembly pitch and lastly one for the reflector. Reflector: cuboid 13 (10) 43.00728 0.0 21.50364 0.0 FA with gap: cuboid 40(20) 21.50364 0.00000 21.50364 0.00000 FA without gap: cuboid 50(30) 21.46046 0.04318 21.46046 0.04318 Therefore, the reflector is indicated by a material indication number '1', which is inside cuboid 10 but outside the fuel assembly indicated by number 40. The following shows the syntax in the global unit of the geometry block: media 16 1 13 -40 array 101 13 place 1 1 0.04318 0.04318 media 3 1 40 -50 An example, of the fuel assembly with the reflector is shown in Figure 4-3.
Basemodel_10	The global grid boundary has to be redefined, due to the fuel assembly region and the reflective region. Therefore, the boundary in 'global unit 1' within the geometry block, is defined as the following: 'boundary 10 16 8'.
BaseModel_11-12 from BaseModel_10	Calculations based on BaseModel_11 were repeated for enrichments 2.1 and 2.6 wt % respectively.

7.3 Appendix C: NESTLE tt1.i input file

The input file tt1.i consists of several data cards that contain all the reactor parameters. After the card identification number has been entered, sets of data which are identified as 'words' W1, W2… W5 are written after the card identification number. Depending on the functionality and purpose of the card, one or more words can be defined which usually gives specifications of parameters or control features (RELAP5-3D Team, 2014). An example is shown below illustrating these concepts:

$$\underbrace{\text{card identification number}}_{7100000} \quad \underbrace{W1}_{0.728147} \quad \underbrace{W2}_{0.20000} \quad \ldots . W5$$

It should be noted that 'comments' are identified either as an asterisk (*) or a dollar sign ($). The explanations shown in the second column include direct phrases from (RELAP5-3D Team, 2014; Schultz, 2014). This was done to maintain the specific meaning, and the reader is referred to the source for further clarification.

Table 7-3 presents the NESTLE tt1.iinput file layout.

Table 7-3: NESTLE Tt1.i file (RELAP5-3D Team, 2014; Schultz, 2014)

***Title Card** = Input generated by NWURCS: lr_jul2020 1,33 50	
$ Problem Type and Option cards ***Problem Type** 100 new transnt *Unit selection card 102 si si * Restart and Plot Output File Control card 104 ascii * CPU Time Remaining and Diagnostic Edit/Dump card 105 5.0 6.0 1000000.0 *110 nitrogen ********** ********** * * **Time step cards** * * * 201 100.0 1.0e-6 0.05 3 1 50 2000 * * ********** * **Hydrodynamic components** * * * Time-Dependent Name and Type card 7100000 source tmdpvol * * * * *	(RELAP5-3D Team, 2014; Schultz, 2014): ***Problem Type** *In card 100, W1 is the problem type and W2 is the problem option. *Card 102, Indicates that SI units are used. *in card 104, the 'ascii' option indicates that a plot or strip file will be written in ASCII format. *In card 105, the termination time controls are provided. ********** *In card 201, W1 is the end time (s), W2 is the minimum time steps, W3 is the maximum time step, W4 is the control option, W5 is the minor edit and plot frequency, W6 is the major edit frequency, W7 is the restart frequency, and which is the number of maximum time-advances per write of restart information to the restart file. ********** *In card 7100000, W1 is the component name, which is defined as SOURCE. It describes the component's use in the system. W2 is the Component Type, which is defined as Tmdpvol. A volume-related boundary condition can be imposed on a model using the TMDPVOL component (Schultz, 2014). Pressure boundaries, such as where the fluid exits a model, can be specified using TMDPVOLs.

* **Time-Dependent Volume Geometry card** 7100101 0.728417 0.200000 0.0 0.0 90.0 0.200000 1.5E-06 0.0 0 * * * * * * * **Time-Dependent Volume Data Control Word card** 7100200 3 * ***Time-Dependent Volume Data card** 7100201 0.0 1.590E+07 566.5 * * *----------	*Card 7100101 is required for a time-dependent volume component. Where W1 is the volume flow area, W2 is the length of volume, W3 is the volume of volume, W4 is the azimuthal angle, W5 is the inclination angle, W6 is the elevation change, W7 Wall roughness, W8 is the hydraulic diameter and W9 is the volume control flags. *Card 7100201 is required for a time-dependent volume. * Card 7100201 is required for a time-dependent volume component. Where W1 is the search variable, W2 is the Initial Time Value and W3 is the user-Controlled Time Step. ----------
* **Single-Junction Component** 7200000 sngljun sngljun * * **Single-Junction Geometry card** 7200101 710010002 311010001 0.00 0.00 0.00 1110100 * * * * * * *** Single-Junction Initial Conditions** 7200201 1 1.0 0.0 0.0 * * *----------	*In card 7200000, the term 'sngljun' in W1, describes the component's use in the system. W2 is the Component Type. *In card 7200101, W1 refers to the origin of junction coordinate direction. W2 refers to the end of the junction coordinate direction. W3 is the Junction flow area. W4 is the Reynolds number (forward flow energy loss coefficient). W5 is the Reynolds number (reverse flow energy loss coefficient). W6 is the Junction control flags. *In card 7200201, W1 is the Control word, W2 is the initial liquid mass flow rate, W3 is the initial vapour/gas mass flow rate and W4 is the Interface velocity. ----------
* **Pipe, Annulus, or Pressurizer Component cards** *- * Pipe, Annulus, or Pressurizer Name and Type 3110000 pipe pipe * * **Pipe, Annulus, or Pressurizer Information** 3110001 10 * **Pipe, Annulus, or Pressurizer X-Coordinate Volume Flow Areas** 3110101 4.962 10 * ***Pipe, Annulus, or Pressurizer X-Coordinate Volume Lengths** 3110301 0.300000 10 * ***Pipe, Annulus, or Pressurizer Volume Azimuthal** Angles 3110501 0.000000 10 * * **Pipe, Annulus, or Pressurizer Volume Inclination Angles** 3110601 90.000000 10 * *** Pipe, Annulus, or Pressurizer Volume X-Coordinate Friction Data** 3110801 1.500E-06 0.010957 10 * ***Annulus, or Pressurizer Junction Loss Coefficients** 3110901 0.000000 0.000000 9 * *** Pipe, Annulus, or Pressurizer Volume X-Coordinate Control Flags** 3111001 0 10 * *** Pipe, Annulus, or Pressurizer Junction Control Flags** 3111101 0 9 * *** Pipe, Annulus, or Pressurizer Volume Initial Conditions** 3111201 3 1.590E+07 566.5 0.0 0.0 0.0 10 * *** Pipe, Annulus, or Pressurizer Junction Conditions Control Words** 3111300 0 * ***Pipe, Annulus, or Pressurizer Junction Initial Conditions** 3111301 0.0 0.0 0.0 9 * * *----------	*The pipe component is simply a series combination of single-volume and single-junction components. *In card 3110000, 'Pipe' is selected to be the Component name in W1 and the component type is W2. *In card 3110001, W1 is the Number of volumes. *In card 3110101, W1 is the volume area in the x-direction, and W2 is the Volume number. *In card 3110301, W1 is the volume area in the x-direction, and W2 is the Volume number. *In card 3110501, W1 is the azimuthal angles and W2 is the Volume number. *In card 3110601, W1 is the inclination angle and W2 is the Volume number. *In card 3110801, W1 is the wall roughness in the x-direction, W2 is the Hydraulic diameter in the x-direction, and W3 is the volume number. *In card 3110901, W1 is the Reynolds number (forward flow energy loss coefficient). W2 is the Reynolds number (reverse flow energy loss coefficient). W3 is the Junction number. *In card 3111001, W1 is the volume control flags and W2 is the Volume number. *In card 3111101, W1 is the Junction control flags and W2 is the Junction number. *In card 3111201, W1 is the control word, W2 to W6 are Quantities as described under Word 1, and W7 is the Volume number. *In card 3111300, W1 is the control word. *In card 3111301, W1 is the initial liquid mass flow rate, W2 is the initial vapour/gas mass flow rate, W3 is the Interface velocity, and W4 is the Junction number. ----------

*** Time-dependent junction component** ***** 8300000 tmpdjun tmdpjun * 8300101 311100002 840010001 0.0 * 8300200 1 * 8300201 0.0000 8.0655E+01 0.0 0.0 * 8300202 250.0000 8.0655E+01 0.0 0.0 * * ----------	* In the time- dependent junction card, the flow boundary condition may be imposed on a model using the TMDPJUN component (RELAP5-3D Team, 2014; Schultz, 2014) *In this card, the component name and the component type are defined as tmpdjun, which describes the component's use in the system and indicates the time-dependent junction component. The mass flow rate, the Search variable, the vapour/gas mass flow rate, and the Interface velocity (m/s) are defined. ----------
*** Time-Dependent Junction Name and Type** 8400000 sink tmdpvol * *** Time-Dependent Junction Geometry** 8400101 0.728417 0.200000 0.0 0.0 90.0 0.200000 1.5E-06 0.0 0 * *** Time-Dependent Junction Data Control Word** 8400200 3 * * **Time-Dependent Junction Data** 8400201 0.0 1.590E+07 566. * ----------	*In card 8400000, W1 is the Component name and W2 is the Component type. *In card 8400101, W1 refers to the origin of junction coordinate direction. W2 refers to the end of the junction coordinate direction. W3 is the Junction flow area. W4 is the junction control card. *In card 8400200, W1 is the control word. ----------
*** Core Heat Structures** * ---------- * Node 4 1 $ n-axial/ n-radial/ geom/ flags/ left position *** General Heat Structure Data card** 13110000 10 9 2 1 0.0000 ***Heat Structure Mesh Flags** 13110100 0 1 *** Heat Structure Mesh Point Location Data (Radial)** 13110101 5 0.0040958 13110102 1 0.0041783 13110103 2 0.0047498 *** Heat Structure Composition Data (Radial)** 13110201 1 5 13110202 2 6 13110203 3 8 *** Heat Structure Source Distribution Data (Radial)** 13110301 1.0000000 5 13110302 0.0000000 6 13110303 0.0000000 8 *** Initial Temperature Data** 13110401 566.50 6 13110402 566.50 7 13110403 566.50 9 ***Left Boundary Condition** 13110501 0 0 0 0 0.0000 10 **Right Boundary Condition** 13110601 311010000 10000 1 0 882.3 10 *	*In cards 13110000, W1 indicates the Number of axial heat structures, W2 is the Number of radial mesh points, W3 is the geometry type, W4 is the Steady-state initialization flag and W5 is the Left boundary coordinate. *In card 13110100, W1 is the mesh location flag. And W2 is the mesh format flag. *In cards 13110101 to 10110103, the mesh endpoint coordinates are provided, where W1 is the number of intervals and W2 is the right coordinate. *In cards 13110201 to 13110203, the composition numbers and the corresponding Interval numbers are defined. *In cards 13110301 to 13110303, the source fraction and corresponding mesh interval number. * In cards 13110401 to 13110403,, the initial temperature and the mesh point number are defined. *In card 13110501 and card 13110601, W1 is the boundary condition definition, W2 is the increment, W3 is the boundary condition type, W4 is the surface area code, W5 is the surface area\length, and W6 is the heat structure number.
* ---This section is written by subroutine lr_f50_50--- * ***Source Data** 13110701 100010 0.9733 0.0000 0.0267 1 13110702 100020 0.9733 0.0000 0.0267 2 13110703 100030 0.9733 0.0000 0.0267 3 13110704 100040 0.9733 0.0000 0.0267 4 13110705 100050 0.9733 0.0000 0.0267 5 13110706 100060 0.9733 0.0000 0.0267 6 13110707 100070 0.9733 0.0000 0.0267 7 13110708 100080 0.9733 0.0000 0.0267 8 13110709 100090 0.9733 0.0000 0.0267 9 13110710 100100 0.9733 0.0000 0.0267 10 *	*In this card 13110701 to 13110710, W1 is the Power source type, W2 is the Internal source multiplier, W3 is the Direct moderator heating multiplier for left boundary volume, W4 is the Direct moderator heating multiplier for right boundary volume, and W5 is the Heat structure number.
* ---This section is written by subroutine lr_f50_80 * ***Additional Left Boundary** 13110801 0.00 3.00 3.00 0.00 0.00 0.00 0.00 1.00 10 * *** Additional Right Boundary**	*In cards 13110801 and 13110802, The Heat transfer hydraulic diameter, the forward and the reverse Heated length, the forward and reverse Grid spacer length, the forward and reverse Grid loss coefficient, the Local boiling factor, and the Heat structure number are defined.

```
13110901 0.00   3.00   3.00   0.00   0.00   0.00   0.00   1.00 10
*
*=========================================================
*                  General tables
*Table power versus time
*        name  trip   factor
*Table Type and Multiplier Data
20201000  power
*          time      watts
*General Table Data
20201001     0.0000 1.0
20201002  2000.0000 1.0
*
*********************************************************************************************
* Heat structure thermal property data
*****************************************************
* Composition type and data format
*****************************************************
*
20100100       tbl/fctn       1       1    * core fuel
20100200       tbl/fctn       1       1    * core fuel gap
20100300       tbl/fctn       1       1    * core fuel cladding
20100400       tbl/fctn       1       1    * inconel
20100500       tbl/fctn       1       1    * stainless steel
*
*********************************************************************************************
* Thermal conductivity data (btu/sec-ft/deg f) and volumetric heat     *
* capacity  data (btu/ft**3-deg f) versus temperature for above        *
* composition                                                          *
* -------------------------------------------------------------------
20100101   271.2    3.3870E+00
20100102  3089.0    3.3870E+00
* -------------------------------------------------------------------
20100151   271.2    3.0649E+06
20100152  4701.4    3.0649E+06
* -------------------------------------------------------------------
20100201   271.2    1.5257E+00
20100202  3255.8    1.5257E+00
* -------------------------------------------------------------------
20100251   271.2    4.3593E+00
20100252  3255.8    4.3593E+00
* -------------------------------------------------------------------
20100301   271.2    7.7746E+00
20100302  2472.9    7.7746E+00
* -------------------------------------------------------------------
20100351   253.4    2.3792E+06
20100352  2199.4    2.3792E+06
* -------------------------------------------------------------------
20100401   271.2    2.5168E+01
20100402   837.2    2.5168E+01
* -------------------------------------------------------------------
20100451   271.2    4.1004E+06
20100452   698.2    4.1004E+06
* -------------------------------------------------------------------
20100501   271.2    2.5106E+01
20100502  1198.6    2.5106E+01
* -------------------------------------------------------------------
20100551   271.2    4.3344E+06
20100552  1365.4    4.3344E+06
*
*********************************************************************************************
* ---This section is written by subroutine lr_i50_04----
$              REACTOR KINETICS INPUT
$               (1 node/assembly)
* Reactor Kinetics Type
30000000  nodal  gen
* Reactor Kinetics Information
30000001  gamma-ac  3.600E+02 0.0076  6  1.0 0.48     $ reactor power at
100% power (3411 Mw)
* Fission Product Decay Information
30000002  ans79-1
*
$-------------------------------------------------------------------------------------------
$  nodal kinetics control (A.12.4)
```

*In card 20201000, the Table type and the table trip number are defined.
*In cards 20201001 to 20201002, the Argument valve and the function valve are defined.

*In cards 20100100 to 20100050, the material type, with the thermal conductivity flag and the Volumetric heat capacity format flag are defined.

*In cards 20100101 to 20100552, the temperature and the thermal conductivity are defined.

*Those ending with 01 and 02, define the temperature and the Thermal conductivity.

*Those ending with 51 and 52, Are the Volumetric Heat Capacity Data, which define the temperature and the Volumetric Heat Capacity.

*In card 30000000, the GEN option is a form of cross-section formulation.
*In card 30000001, the Reactor Kinetics Information for fission product decay is defined, such as the Total reactor power, the Initial reactivity and the fission product yield factor, and W6 is the ^{239}U yield factor.
*In card 30000002, theANS79-1 specifies the 1979 Standard data for 235U.

*The Nodal Kinetics Control Information card is used to define the core dimensions with

```
$-------------------------------------------------------
* Nodal Kinetics Control Information
*
30000003 10 17 17   2  1  1
+         1  0  1  1
+         1 500 10  5  0  0  0
*
$-------------------------------------------------------------------------------------------
$     Neutron Cross Section Data (Input Manual: 15.18.28.2)
$ composition data (A.12.13.11.1)
*Volume and Heat Structure Feedback Region Data Card
310000000  1 1       $ number of fdbk regions
*
*-------------------------------------------------------------------------------------------
*Volume Feedback Weighting Factors card
310001111  311010000  1.0 1.0 1.0
310002111  311020000  1.0 1.0 1.0
310003111  311030000  1.0 1.0 1.0
310004111  311040000  1.0 1.0 1.0
310005111  311050000  1.0 1.0 1.0
310006111  311060000  1.0 1.0 1.0
310007111  311070000  1.0 1.0 1.0
310008111  311080000  1.0 1.0 1.0
310009111  311090000  1.0 1.0 1.0
310010111  311100000  1.0 1.0 1.0
*
* Heat Structure Feedback Weighting Factors card
310001211    3110001  1.0
310002211    3110002  1.0
310003211    3110003  1.0
310004211    3110004  1.0
310005211    3110005  1.0
310006211    3110006  1.0
310007211    3110007  1.0
310008211    3110008  1.0
310009211    3110009  1.0
310010211    3110010  1.0
*
$   GEN options card
320000000  1  0  1  1  *SQRT(Tf)  15.18.27.4 Page A15-37
*
*
*
*320000001  9999        *15.18.27.5 Page A15-37
*
* Neutron Base Cross-Section Data card
*
$ Composition:     1
320001000    0.0000 0.0000
320001011   1.69952E-01  1.69952E-01  0.0000
320001012   3.77511E-04  3.77511E-04  0.0000
320001013    0.00000E+00   0.00000E+00   0.0000
320001014    0.00000E+00   0.00000E+00   0.0000
320001015    6.99368E-05    6.99368E-05    0.0000
320001021    1.59854E+00   1.59854E+00   0.0000
320001022    1.37422E-02    1.37422E-02    0.0000
320001023    0.00000E+00   0.00000E+00   0.0000
320001024    0.00000E+00   0.00000E+00   0.0000
320001025    4.26129E-02    4.26129E-02    0.0000
320001111    0.00000E+00   0.00000E+00   0.0000  579.7500
320001112    0.00000E+00   0.00000E+00   0.0000  579.7500
320001113    0.00000E+00   0.00000E+00   0.0000  579.7500
320001114    0.00000E+00   0.00000E+00   0.0000  579.7500
320001115    0.00000E+00   0.00000E+00   0.0000  579.7500
320001121    0.00000E+00   0.00000E+00   0.0000  579.7500
320001122    0.00000E+00   0.00000E+00   0.0000  579.7500
320001123    0.00000E+00   0.00000E+00   0.0000  579.7500
320001124    0.00000E+00   0.00000E+00   0.0000  579.7500
320001125    0.00000E+00   0.00000E+00   0.0000  579.7500
320001211    0.00000E+00   0.00000E+00   0.0000 1200.2000
320001212    0.00000E+00   0.00000E+00   0.0000 1200.2000
320001213    0.00000E+00   0.00000E+00   0.0000 1200.2000
320001214    0.00000E+00   0.00000E+00   0.0000 1200.2000
320001215    0.00000E+00   0.00000E+00   0.0000 1200.2000
```

regards to the Number of nodal axial mesh intervals in the z-direction, x-direction and y-direction on each mesh plane. The Number of neutron energy groups is specified. The Mesh symmetry flag is defined.

---

*In card 310000000, W1 is the Number of volume feedback regions, and W2 is the Number of heat structure feedback regions are defined.

---

*In cards 310001111 to 310010111, W1 is the Volume number, W2 is the Volume weighting factor for average fluid density, W3 is the Volume weighting factor for average fluid temperature and W4 is the Volume weighting factor for average poison density.

*In cards 310001211 to 310010211, W1 is the Heat structure number, and W2 is the Heat structure weighting factor for average structure temperature.

*Contains the temperature units code, the density or vapour/gas fraction variable flag, the structure temperature power flag, and the diffusion coefficient/transport cross-section flag.

*Nu fission ÷ fission from T-NEWT
*Transport XS Group 1 Group 1
*Absorption XS Group 1

*Scattering XS
*Transport XS Group 2
*Absorption XS Group 2

*Scattering XS

*This card is repeated for 3 more composition data blocks, as NWURCS sets T-1NEWt to calculate 4 calculations, the first begins a calculation with 3.1wt% enrichment that has a reflector. Its homogenized cross-sections make up the data for composition 1 of nestle input. The next is one with only the 3.1wt% enrichment, which will be used for composition 2. The other with 2.6wt% enrichment, which will be used for composition 3, and the last one for the 2.1wt% enrichment, which will be used for composition 4.

```
320001221   0.00000E+00   0.00000E+00   0.0000 1200.2000
320001222   0.00000E+00   0.00000E+00   0.0000 1200.2000
320001223   0.00000E+00   0.00000E+00   0.0000 1200.2000
320001224   0.00000E+00   0.00000E+00   0.0000 1200.2000
320001225   0.00000E+00   0.00000E+00   0.0000 1200.2000
320001311   0.0  0.0  0.0  0.0  0.0  0.0  712.5000
320001312   0.0  0.0  0.0  0.0  0.0  0.0  712.5000
320001313   0.0  0.0  0.0  0.0  0.0  0.0  712.5000
320001314   0.0  0.0  0.0  0.0  0.0  0.0  712.5000
320001315   0.0  0.0  0.0  0.0  0.0  0.0  712.5000
320001321   0.0  0.0  0.0  0.0  0.0  0.0  712.5000
320001322   0.0  0.0  0.0  0.0  0.0  0.0  712.5000
320001323   0.0  0.0  0.0  0.0  0.0  0.0  712.5000
320001324   0.0  0.0  0.0  0.0  0.0  0.0  712.5000
320001325   0.0  0.0  0.0  0.0  0.0  0.0  712.5000
320001411   0.0  0.0  0.0  891.4500
320001412   0.0  0.0  0.0  891.4500
320001413   0.0  0.0  0.0  891.4500
320001414   0.0  0.0  0.0  891.4500
320001415   0.0  0.0  0.0  891.4500
320001421   0.0  0.0  0.0  891.4500
320001422   0.0  0.0  0.0  891.4500
320001423   0.0  0.0  0.0  891.4500
320001424   0.0  0.0  0.0  891.4500
320001425   0.0  0.0  0.0  891.4500
*
```

*In cards 301 to 321, W1 is the Variable request code that is alphanumeric, and W2 is a Parameter

---

***Minor Edit Requests**

```
301  rkotpow 0
20800001 rkondfip -1
20800002 rkophi -1
*
*-------------------------------------------------------------------
302  rkophi  1010145        $ ijk    0  0  1
303  rkophi  1020145        $ ijk    0  0  2
304  rkophi  1030145        $ ijk    0  0  3
305  rkophi  1040145        $ ijk    0  0  4
306  rkophi  1050145        $ ijk    0  0  5
307  rkophi  1060145        $ ijk    0  0  6
308  rkophi  1070145        $ ijk    0  0  7
309  rkophi  1080145        $ ijk    0  0  8
310  rkophi  1090145        $ ijk    0  0  9
311  rkophi  1100145        $ ijk    0  0 10
*-------------------------------------------------------------------
312  rkophi  2010145        $ ijk    0  0  1
313  rkophi  2020145        $ ijk    0  0  2
314  rkophi  2030145        $ ijk    0  0  3
315  rkophi  2040145        $ ijk    0  0  4
316  rkophi  2050145        $ ijk    0  0  5
317  rkophi  2060145        $ ijk    0  0  6
318  rkophi  2070145        $ ijk    0  0  7
319  rkophi  2080145        $ ijk    0  0  8
320  rkophi  2090145        $ ijk    0  0  9
321  rkophi  2100145        $ ijk    0  0 10
*-------------------------------------------------------------------
. End of input.
```

*Rkotpow - Total Reactor Power.
* RKONDFIP - Fission power.
*RKOPHI - Neutron flux in neutron group g.

7.4 Appendix D: T-NEWT/NESTLE homogenized cross-sections and ADFs

Figure 7-1 presents the macroscopic cross-sections data of the 3.1 wt% FA with the water node generated from the T-NEWT output. Figure 7-2 presents the ADF data that was taken from the T-NEWT output file and inserted into the NESTLE tt1.i file.

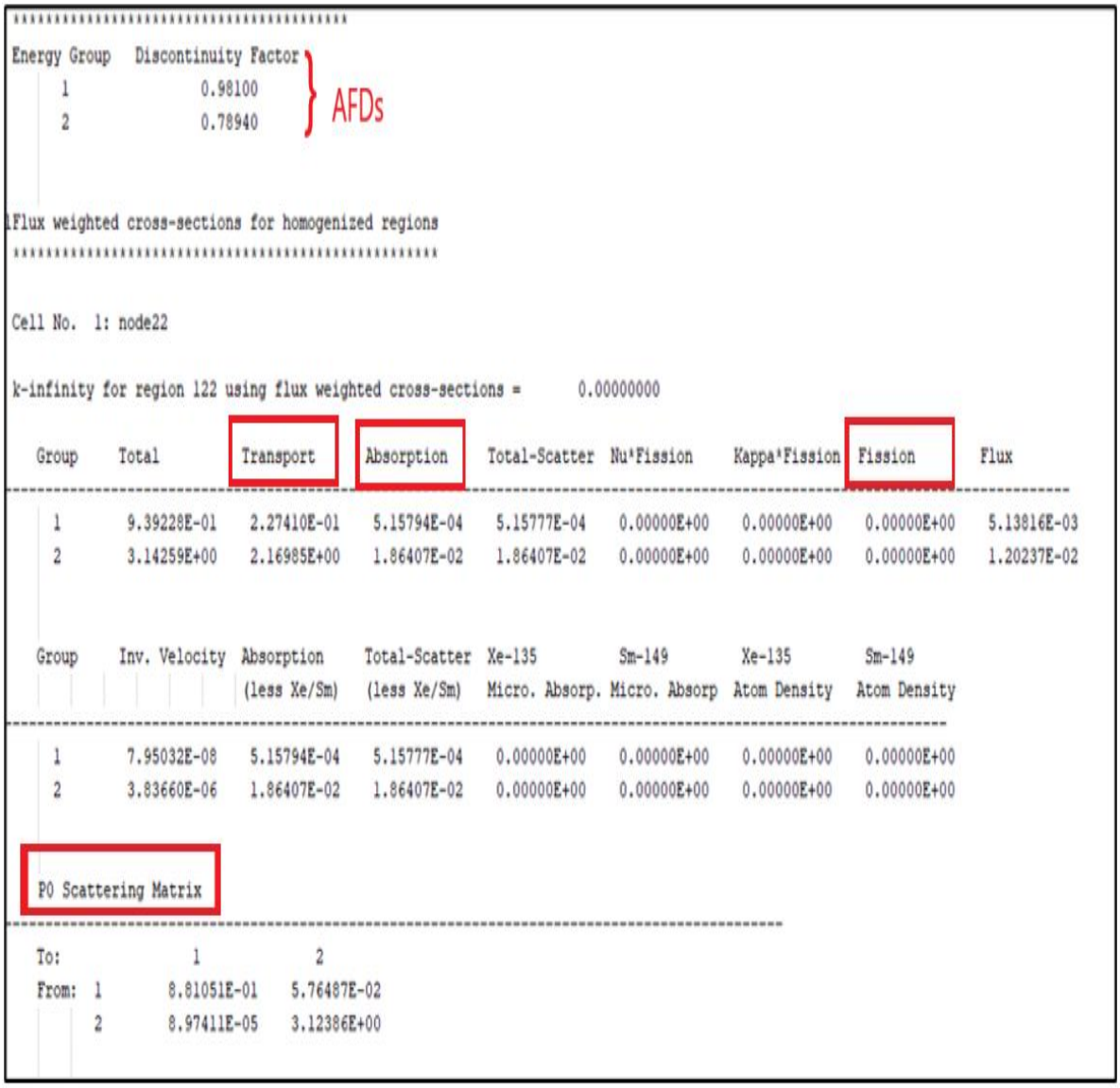

```
****************************************
Energy Group   Discontinuity Factor
     1              0.98100
     2              0.78940

1Flux weighted cross-sections for homogenized regions
****************************************************

Cell No.  1: node22

k-infinity for region 122 using flux weighted cross-sections =      0.00000000

  Group     Total         Transport     Absorption    Total-Scatter  Nu*Fission    Kappa*Fission  Fission       Flux
-------------------------------------------------------------------------------------------------------------------
    1       9.39228E-01   2.27410E-01   5.15794E-04   5.15777E-04   0.00000E+00   0.00000E+00   0.00000E+00   5.13816E-03
    2       3.14259E+00   2.16985E+00   1.86407E-02   1.86407E-02   0.00000E+00   0.00000E+00   0.00000E+00   1.20237E-02


  Group     Inv. Velocity  Absorption     Total-Scatter  Xe-135         Sm-149         Xe-135         Sm-149
                           (less Xe/Sm)   (less Xe/Sm)   Micro. Absorp. Micro. Absorp  Atom Density   Atom Density
-------------------------------------------------------------------------------------------------------------------
    1       7.95032E-08    5.15794E-04    5.15777E-04    0.00000E+00    0.00000E+00    0.00000E+00    0.00000E+00
    2       3.83660E-06    1.86407E-02    1.86407E-02    0.00000E+00    0.00000E+00    0.00000E+00    0.00000E+00

 P0 Scattering Matrix
-------------------------------------------------------------------------------------------
  To:              1              2
  From:  1      8.81051E-01    5.76487E-02
         2      8.97411E-05    3.12386E+00
```

AFDs

Figure 7-1: 3.1 wt % FA with reflector 'node 22' T-NEWT Output data for NESTLE BM

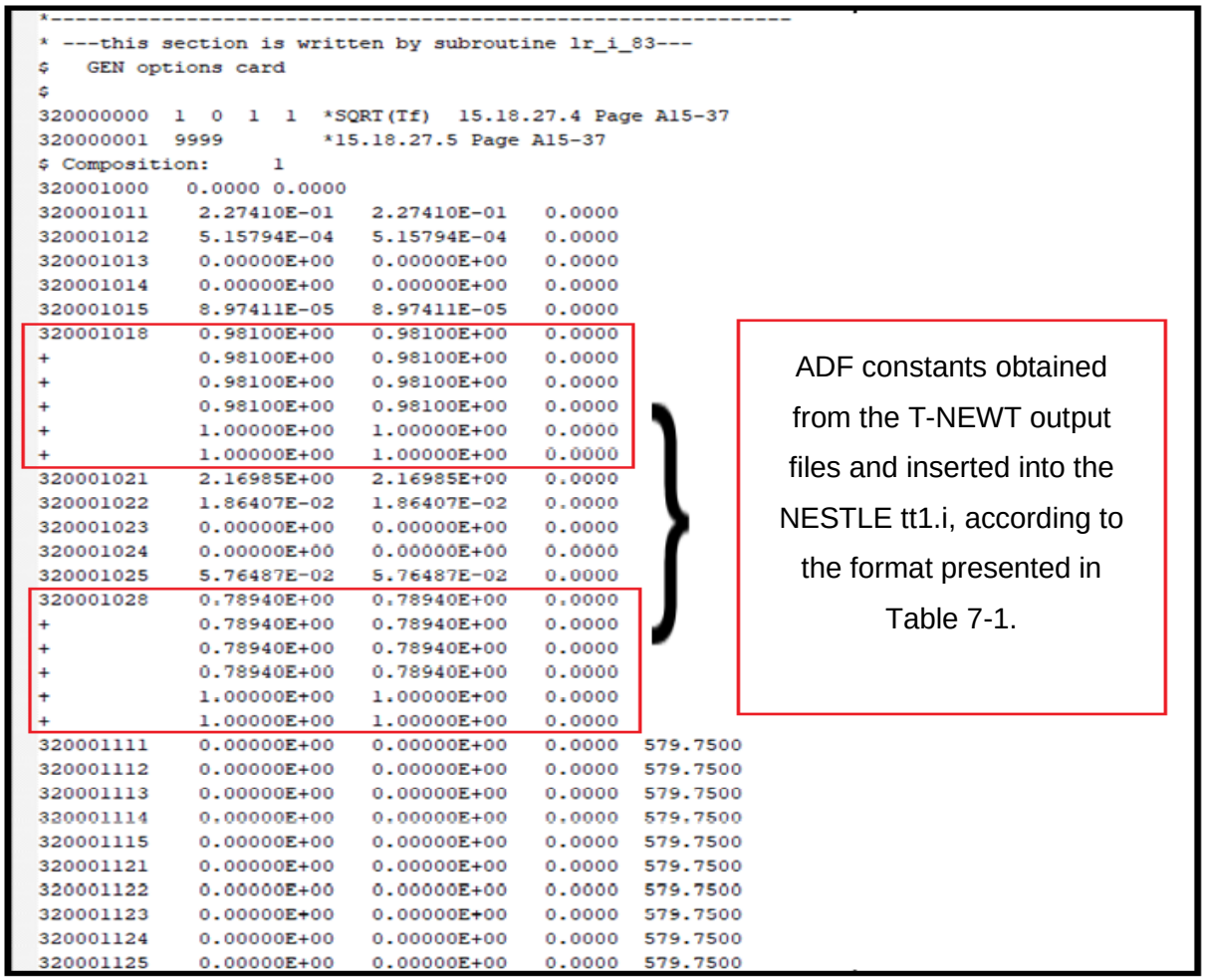

Figure 7-2: ADF insertion in NESTLE

7.5 Appendix E: MCNP-6.2 and NESTLE full core model development

Table 7-4, present all the FC model developments for MCNP-6.2 and NESTLE.

Table 7-4: MCNP-6.2 and NESTLE FC model developments

Model name	**NWURCS modification and Description**
	Base Model
F001 - MCNP F002- Nestle	This is the base model, which was modelled with zero boron, ARO, fresh fuel (2.1. 2.6 and 3.1 wt% FAs) and with all the system components set at 300K.
	Boron test
F003 to F0011 – MCNP F004 to F0012 - NESTLE	Various concentrations of H_3BO_3 were added to the system, to obtain the critical H_3BO_3 concentration in FC Model. In NWURCS, the H_3BO_3 changes were made in file C:\0_tr\folder_name \ixxxxx\f005.i.
	No Core Barrel (CB)
F0013 – MCNP F0014 – NESTLE	The core barrel was removed in the MCNP model. The NESTLE model does not have a core barrel, therefore the removal of the CB in the NWURCS file: '.\units_da1\unit00002.dat.', only affects the MCNP model and not the NESTLE model.
	Helium as CB
F0015 - MCNP & F0016 – NESTLE	The core barrel material was changed to helium. In file '.\ixxxxx\inputmat.dat.', a material definition for helium was created, which was also defined in file '.\units_da1\unit00002.da1.' as the CB material.
	CB diameter changes

F0021 - MCNP F0022 - NESTLE	The CB diameters are changed. The CB was increased to 180.18253 cm in file '.\units_da1\unit00002.da1.'.
F0023 -MCNP F0024 - NESTLE	The CB diameters are changed. The CB was increased to 220.18253 cm in file '.\units_da1\unit00002.da1.'.
F0025 - MCNP F0026 - NESTLE	The CB diameters are changed. The CB was decreased to 171,18253 cm in file '.\units_da1\unit00002.da1.'.
Water CB test	
F0027 – MCNP & KENO F0028 - NESTLE	The core barrel material was changed to water. In file '.\ixxxxx\inputmat.dat.', a material definition for water was created, which was also defined in file '.\units_da1\unit00002.da1.' as the CB material.

7.6 Appendix F: Least square fit of the fluxes

The normalization calculations were conducted in Excel, using the following steps below:

1) The MCNP flux data is obtained from the NWURCS file in 'C:\0_tr\folder_name\flux_maps\gp00p00p00p00'. This data provides fast and thermal fluxes in the axial-direction. the flux comparisons will only be based on the axial direction for both MCNP and NESTLE, since the core was homogenous only in this direction. The fast flux was analysed first, and the 'maximum' of the 10 nodes was calculated.
2) The values for the sine (sinusoidal) formula $[y = a \cdot \sin\big((fast\ flux\ /period) - X_0\big) + q]$, where the phase shift X_0, the background q (vertical shift), the a (amplitude), and the period are initially guessed. The equation was used to calculate the sinusoidal for all 10 nodes of the fast-flux.
3) A Fast flux versus sinusoidal (fast flux) graph was plotted. This enables the amplitude, the period as well as the q to be adjusted accordingly.
4) The 'least square fit' for all 10 nodes was calculated $[(Fast\ flux - \text{sinusoidal}\ formale\ for\ the\ fast\ flux)^2]$.
5) The minimum of the least square for all the 10 nodes was calculated using the sum function in Excel.
6) The Solver function in the Analyse tab within the Data tab was used to solve and accurately predict the $a, q, X_{0,}$ and the period values for the sine graph and formula.